

Surface Chemistry Study on the Pentlandite-Serpentine System

Mayeli Alvarez-Silva

Department of Mining and Materials Engineering

McGill University

Montreal, Quebec

A thesis submitted to the Faculty of Graduate Studies and research in partial fulfillment of the requirements for the degree of Doctor of Philosophy

© Mayeli Alvarez-Silva

February, 2011

To my parents.

Con todo mi amor, va por ustedes

Quamvis enim melius sit benefacere quam nosse, prius tamen est nosse quam facere.

Charlemagne

Abstract

Interaction with MgO-minerals is one mechanism suspected to reduce selectivity in flotation of pentlandite from ultramafic ore. Understanding the surface chemistry of the minerals involved will lead to improved flotation conditions that maximize flotation selectivity.

The first part of the thesis compares isoelectric point (i.e.p.) and point of zero charge (p.z.c.) determined using Mular-Roberts [M-R] titration technique of MgO-minerals chlorite, serpentine and talc. The M-R technique was unsuccessful with talc, attributed to Mg^{2+} acting as potential determining ion. For serpentine and chlorite, respectively, p.z.c. was pH 4.3 and 4.6 and i.e.p. pH 3.2 and <3. Dispersion index (DI) for chlorite suggested that aggregation/dispersion is controlled by both; serpentine remained dispersed, possibly due to hydration effects.

The second part determines surface properties of pentlandite and serpentine isolated from an ultramafic ore. Zeta potential measurements were made on minerals alone and as mixtures with either indifferent electrolyte or supernatant derived from an ore suspension as background. Individual mineral results anticipated interaction due to electrostatic attraction. This was confirmed in the mixed mineral case, with $Mg(OH)_2$ precipitate interaction as an additional factor. Scanning electron microscopy validated the findings.

Aggregation/dispersion was determined by turbidimetry using a light scattering technique and optical microscopy. The effect of selected factors on aggregation/dispersion of pentlandite and serpentine was investigated by a design of experiment (DOE). Concentration of carboxymethyl cellulose, CMC, and the interaction between CMC and pH were the important factors.

Contact angle measurements explored effects of several factors on pentlandite hydrophobicity and, using a DOE, small-scale flotation was used to investigate effects on pentlandite floatability. The pH was the most important factor, acidic pH increasing both hydrophobicity and floatability. Copper activation enhanced both properties, as well; magnesium affected hydrophobicity at alkaline pH, but it did not show significant effect on floatability; serpentine was detrimental to the process; and CMC was capable of partially restoring the hydrophobicity and floatability of pentlandite depressed with serpentine.

Résumé

L'interaction de la pentlandite avec des minéraux d'oxyde de magnésium (MgO-) est soupçonnée d'être à l'origine de la sélectivité réduite de la pentlandite dans les procédés de flottation de minerais ultrabasiques. Une meilleure compréhension de la chimie de surface des minéraux impliqués devrait mener à l'amélioration des conditions de flottation qui en maximisent la sélectivité.

La première partie de la thèse compare le point isoélectrique (p.i.e) et le point de charge nulle (p.c.n), déterminés à l'aide de la technique de titrage Mular-Roberts [M-R], de minéraux d'oxyde de magnésium tels que la chlorite, la serpentine et le talc. Dans le cas du talc, la technique M-R a échoué, probablement dû aux ions Mg^{2+} qui jouent le rôle d'ions déterminateurs de potentiel. Dans le cas de la serpentine et de la chlorite, les p.c.n. ont été déterminés à pH 4,3 et 4,6 respectivement et les p.i.e à pH 3,2 et <3 respectivement. Des tests de décantations ont suggéré que l'agrégation/dispersion observée pour la chlorite était contrôlée à la fois par le p.c.n et le p.i.e ; la serpentine au contraire est restée dispersée, possiblement dû à des effets d'hydratation.

La deuxième partie détermine les propriétés de surface de la pentlandite et de la serpentine isolées à partir d'un minerai ultrabasique. Des mesures du potentiel zêta ont été effectuées sur les minéraux seuls et mélangés en présence d'un électrolyte, indifférent dans un cas et surnageant dans l'autre cas, préparé à partir d'une suspension de minerai utilisée comme milieu d'étude. Les résultats relatifs aux minéraux individuels et en particulier les forces d'attraction électrostatique observables ont permis d'anticiper leur interaction. Cette hypothèse a été confirmée dans le cas des minéraux mélangés, étant après avoir pris en compte l'interaction de précipités de $Mg(OH)_2$ comme facteur additionnel. Des observations au microscope électronique à balayage ont permis de valider les résultats.

L'agrégation/dispersion a été déterminée par décantation en utilisant des techniques de lumière diffuse et de microscopie optique. L'effet de certains facteurs sur l'agrégation/dispersion de la pentlandite et de la serpentine a été étudié sur la base d'un plan d'expériences (PE). Entre autres, la concentration en carboxyméthyl cellulose (CMC) et l'interaction entre le CMC et le pH ont été considérés comme des facteurs importants.

Des mesures d'angle de contact ont permis d'explorer l'hydrophobicité de la pentlandite et, à l'aide d'un PE, une étude de flottation à petite échelle a été réalisée pour investiguer la flottabilité de la pentlandite. Les résultats ont montrés que le pH était le facteur le plus important, un pH acide ayant pour effet d'augmenter à la fois l'hydrophobicité et la flottabilité. L'ajout de cuivre a également permis de renforcer ces deux propriétés par un effet d'activation; la présence de magnésium au contraire a affecté l'hydrophobicité de la pentlandite à pH alcalin mais n'a pas eu d'effet significatif sur ses propriétés de flottabilité; la présence de serpentine s'est trouvée être préjudiciable au procédé mais l'utilisation de CMC a pu être utilisée afin de restaurer partiellement l'hydrophobicité et la flottabilité de la pentlandite diminuées par la présence de la serpentine.

Resumen

Durante el procesamiento de minerales ultramáficos, los silicatos de magnesio tienen un efecto nocivo en la flotación del mineral valioso, la pentlandita. Un posible mecanismo de la reducción de selectividad es la interacción de la pentlandita con los silicatos de magnesio. A fin de maximizar la flotación selectiva de estos minerales es preciso entender la química de superficie de los minerales involucrados.

La primera parte de la presente tesis está comprendida por la comparación de punto isoelectrico y punto de carga cero de los silicatos de magnesio: clorita, serpentina y talco, mediante la técnica de titulación Mular-Roberts. Dicha técnica no pudo aplicarse en el caso del talco, debido probable papel del magnesio como ión determinante del potencial. Para serpentina y clorita, el punto de carga cero se estableció a pH de 4.3 y 4.6, respectivamente, y el punto isoelectrico a pH 3.2 y <3. Mediante experimentos de sedimentación, se determinó que la agregación/dispersión de clorita fue controlada tanto por el punto de carga cero como por el punto isoelectrico. La serpentina, en cambio, permaneció dispersa en el rango de pH probado, posiblemente debido su tendencia a la hidratación.

La segunda parte del trabajo está constituida por la determinación de diversas propiedades de superficie de la pentlandita y serpentina aisladas de minerales ultramáficos. Se realizaron mediciones de potencial zeta a esos dos minerales por separado y a sus mezclas usando como solución base un electrólito indiferente o el sobrenadante de una suspensión de mineral ultramáfico. En el estudio de minerales individuales se concluyó que es posible la interacción entre las dos fases como consecuencia de la atracción electrostática. Esto se confirmó en el caso de mezclas de minerales, donde la precipitación de $Mg(OH)_2$ en la superficie de la pentlandita es un factor adicional. La inspección de los minerales mediante microscopía electrónica de barrido ayudó a validar los resultados.

La agregación/dispersión del sistema se estudió mediante experimentos de sedimentación, usando la técnica de dispersión de luz y observación directa en un microscopio óptico. Se investigó el efecto de diferentes factores en la agregación/dispersión de pentlandita y serpentina mediante un diseño experimental. Los factores más importantes fueron la concentración de carboximetilcelulosa (CMC) y la interacción entre ésta y el pH.

A fin de conocer el efecto de diferentes factores en la hidrofobicidad de la pentlandita, se realizó un estudio de ángulo de contacto. Para estudiar su flotabilidad, se realizó un diseño experimental de flotación en pequeña escala. El pH resultó el factor más importante: ambas propiedades se vieron favorecidas a pH ácidos. La activación con cobre también resultó beneficiosa para ambas propiedades. La presencia de magnesio a pH alcalino afectó negativamente la hidrofobicidad; sin embargo, la flotabilidad no pareció mostrar el mismo efecto. La serpentina afectó ambas propiedades. Finalmente, la carboximetilcelulosa remedió parcialmente los efectos negativos de la serpentina tanto en la hidrofobicidad como en la flotabilidad.

Contribution of authors

The following are manuscripts written by the author that were used in the preparation of this thesis. All the experiments were conducted by the authors or under the authors' directions. Manuscripts 1 and 2 comprise Chapter 4, and manuscripts 3, 4 and 5 make up Chapters 5, 6 and 7, respectively.

1. Alvarez-Silva M., Uribe-Salas A., Mirnezami M., Finch J.A. (2010) The point of zero charge of phyllosilicate mineral using the Mular-Roberts titration technique. *Minerals Engineering* 23: 383-389
2. Alvarez-Silva M., Uribe-Salas A., Mirnezami M., Finch J.A. (2010) Point of zero charge, isoelectric point and aggregation of phyllosilicate minerals. *Canadian Metallurgical Quarterly* 49: 405-410
3. Alvarez-Silva M., Uribe-Salas A., Mirnezami M., Finch J.A. Effect of presence of serpentine and dissolved mineral species on electrokinetic behaviour of pentlandite, to be submitted to the *International Journal of Mineral Processing*
4. Alvarez-Silva M., Uribe-Salas A., Mirnezami M., Finch J.A. Effect of flotation reagents on hetero-aggregation of pentlandite and serpentine, submitted for presentation at 49th Annual Conference of Metallurgists (COM 2010), Vancouver, BC, Canada
5. Alvarez-Silva M., Davila-Pulido G.I., Uribe-Salas A., Mirnezami M., Finch J.A. Contact angle measurements and flotation study in the pentlandite-serpentine system, to be submitted to *Minerals Engineering*.

All the manuscripts presented above are co-authored by Prof. James A. Finch in his capacity as research supervisor. Dr. M. Mirnezami and Dr. A. Uribe-Salas are also co-authors in recognition to their suggestions towards the experimental design and contribution to the discussions of results. Manuscript 5 also includes M.Sc. G.I. Dávila-Pulido for her contribution in performing part of the experiments. Beyond the contribution of the authors mentioned here, all the work presented in this dissertation was performed by the author.

Acknowledgements

First, I would like to thank my supervisor, Professor James A. Finch, for the guidance, suggestions and financial support that he has provided me during the course of my studies.

I would like to acknowledge Vale for the financial support of this project.

I would like to express my sincere gratitude to my master's supervisor, Dr. Alejandro Uribe-Salas, for believing in me, for his guidance and, foremost, for his friendship. Without his encouragement, it would not have happened.

I want to express my appreciation to all the people that helped me in one way or another during my studies, especially to my dear buddy Mr. Ray Langlois. Also, I would like to thank Dr. Ram Rao, Dr. Jan Nasset, Dr. César Gómez, Dr. Mitra Mirnezami, Ms. Helen Campbell, Mr. Ranjan Roy, Mr. Lang Shi, Prof. Kristian Waters, Ms. Monique Riendeau, Ms. Barbara Hanley and Dr. Manqiu Xu (Vale).

Special thanks go to my friends in the mineral processing group, in particular to Rebecca Payant, Rodrigo Araya, Yue (Hope) Tan and Patrick Blonde (my English editor among other things). Also, I would like to express my gratitude to Cécile Charbonneau for the translation of the abstract to French. Finally, I would like to thank the Mexican gang Paula M. Proa-Flores and Yaneth Aguilar-Díaz and my lab mates from Extractive Metallurgy in Cinvestav, Saltillo, especially Gloria Dávila-Pulido for her valuable help with the performance of contact angle and small-scale flotation experiments.

Table of contents

Chapter 1 Introduction.....	1
1.1. Objectives of the thesis.....	2
1.2. Structure of the Thesis.....	3
References.....	3
Chapter 2 Background.....	5
2.1. Uses of Nickel.....	5
2.2. Occurrence.....	6
2.3. Nickel deposits.....	7
2.4. Issues in ultramafic ore processing.....	8
2.5. The minerals.....	9
2.5.1. Sulphides.....	9
Pentlandite.....	9
Pyrrhotite.....	10
2.5.2. MgO-minerals.....	10
Serpentine.....	10
Amphibole.....	11
Chlorite.....	12
Olivine.....	12
Talc.....	12
2.6. Flotation reagents.....	13
2.6.1. Collectors.....	13
2.6.2. Dispersants.....	14
2.6.3. pH modifiers.....	16
Effect on the minerals.....	17
Effect on chemical species.....	18
2.7. Some other factors affecting flotation.....	18
2.7.1. Dissolved species.....	18
2.7.2. Process water.....	19
References.....	20
Chapter 3 Experimental techniques.....	25

3.1. Surface charge	26
3.1.1. Mechanisms of surface charge development	26
3.1.2. The electrical double layer	27
Helmholtz model	27
Gouy-Chapman model	28
Stern-Graham model	28
3.1.3. Ions in the double layer	28
3.1.4. Point of zero charge	29
3.1.5. Isoelectric point	32
3.1.6. Electrokinetic phenomena	32
Electro-osmosis	32
Streaming potential	32
Sedimentation potential	33
Electrophoresis	33
3.1.7. Calculation of zeta potential	33
3.1.8. Zeta potential apparatus	35
3.2. Aggregation/dispersion	36
3.2.1. Dispersion index	36
3.2.2. Light microscopy	37
3.3. Hydrophobicity and floatability	38
3.3.1. Contact angle	38
3.3.2. Small-scale flotation	39
3.4. Characterization instruments	40
3.4.1. Particle size distribution	40
3.4.2. Elemental analysis	41
3.4.3. Electron microprobe	41
3.4.4. X-ray diffraction	42
3.4.5. Scanning electron microscopy	42
References	42
Chapter 4 Point of zero charge and isoelectric point of phyllosilicate minerals	47
Abstract	47
4.1. Introduction	48
4.2. Experimental	50
4.2.1. Minerals	50
4.2.2. Determination of isoelectric point	50

4.2.3. Dissolution	51
4.2.4. Effect of Mg^{2+} concentration on zeta potential	51
4.2.5. Determination of point of zero charge	51
4.2.6. Aggregation/dispersion tests	52
4.3. Results	52
4.3.1. Mineralogical characterization.....	52
4.3.2. Validating M-R technique.....	53
4.4.3. Isoelectric point and effect of some experimental conditions.....	55
Effect of aging and solid/liquid ratio.....	55
Species dissolution.....	55
Effect of Mg^{2+}	58
4.4.4. Point of zero charge	60
4.4.5. Aggregation/dispersion tests.....	61
4.5. Discussion.....	62
4.6. Conclusions	66
References	66
Chapter 5 Effect of serpentine and dissolved mineral species on electrokinetic behaviour of pentlandite.....	70
Abstract.....	70
5.1. Introduction	71
5.2. Experimental.....	72
5.2.1. Minerals	72
5.2.2. Zeta potential	74
Serpentine	74
Pentlandite.....	74
Mixed mineral systems	75
5.2.3. Scanning electron microscopy	75
5.3. Results	76
5.3.1. Zeta potential	76
Individual minerals	76
In presence of indifferent electrolyte.....	76
In presence of supernatant.....	78
Mixed mineral systems.....	81
In presence of indiferent electrolyte.....	81
Pentlandite in presence of serpentine and supernatant	82

5.3.2. Scanning electron microscopy.....	84
5.4. Discussion.....	86
5.5. Conclusions	88
References	88
Chapter 6 Effect of flotation reagents on hetero-aggregation of pentlandite and serpentine.....	93
Abstract.....	93
6.1. Introduction	94
6.2. Experimental.....	95
6.2.1. Minerals	95
6.2.2. Reagents.....	95
6.2.3. Aggregation/dispersion tests	96
6.2.5. Optical microscopy	97
6.3. Results	97
6.3.1. Dispersion index	97
6.3.2. Optical microscopy.....	104
6.4. Discussion.....	105
6.5. Conclusions	106
References	107
Chapter 7 Contact angle measurements and flotation study in the pentlandite-serpentine.....	109
Abstract.....	109
7.1. Introduction	110
7.2. Experimental techniques.....	111
7.2.1. Minerals	111
Contact angle experiments	111
Flotation experiments.....	111
7.2.2. Reagents.....	112
7.2.3. Contact angle measurement	112
7.2.4. Flotation experiments.....	113
7.3. Results	114
7.3.1. Contact angle measurements.....	114
Effect of xanthate	114
Cu-activation	115
Effect of magnesium ions.....	116
Effect of serpentine	116
Effect of CMC.....	117

7.3.2. Flotation tests	119
7.4. Discussion	126
7.5. Conclusions	129
References	130
Chapter 8 Conclusions, contributions and future work	133
8.1. Conclusions	133
8.2. Contributions to the knowledge	136
8.3. Future work	136
Appendix 1: Characterization of phyllosilicates	138
Appendix 2: Isolation of mineral phases and characterization of samples	141
A-2.1. Product identification	143
A-2.1. Pentlandite for contact angle measurements	146
Appendix 3: Supernatant analysis	147
Appendix 4: Analysis of sulphate and chloride	149
A-4.1. Analysis of sulphate: turbidimetric method	149
Apparatus	149
Reagents	149
Procedure	149
A-4.2. Analysis of chloride: argentometric titration	150
Apparatus	150
Reagents	151
Procedure	151
Calculation	151
Reference	151
Appendix 5: Contact angle measurement	153

List of figures

Figure 2.1	Main industrial uses for nickel Source: Standard CIB Global Research http://www.standardbank.co.za	6
Figure 2.2	Major Nickel deposits. Modified from Elias (2002).....	7
Figure 2.3	Schematic representation of the (a) chrysotile and (b) lizardite structures. Modified from Klein and Hurlbut (1993).....	11
Figure 2.4	Scanning Microscope images of a chunk of lizardite (left) and fibers of chrysotile.....	12
Figure 2.5	Schematic diagram of xanthate structure.....	13
Figure 2.6	Carboxymethyl cellulose fragment.....	15
Figure 3.1	Representation of charge development in talc $[\text{Mg}_3\text{Si}_4\text{O}_{10}(\text{OH})_2]$ by the substitution of silicon by aluminum in the tetrahedral sheet and magnesium by iron in the octahedral sheet.....	27
Figure 3.2	Schema of a possible ions distribution on a surface and effect on the different potentials.....	29
Figure 3.3	Effect of a non-conductive particle on the applied field (a) $\kappa a \ll 1$; (b) $\kappa a \gg 1$. The broken line is at the distance of $1/\kappa$ from the particle surface (adapted from Hunter, 2001).....	34
Figure 3.4	Zeta potential apparatus.....	35
Figure 3.5	Schematic arrangement for dispersion index measurements.....	37
Figure 3.6	Top view of the platform for contact angle measurements (modified from Dávila- Pulido, 2010).....	39
Figure 3.7	Schematic of the Partridge/Smith cell.....	40
Figure 4.1	Sketch diagrams of serpentine $[\text{Mg}_3\text{Si}_2\text{O}_5(\text{OH})_4]$, talc $[\text{Mg}_3\text{Si}_4\text{O}_{10}(\text{OH})_2]$ and chlorite $[(\text{Mg},\text{Fe}^{2+})_5(\text{Al},\text{Fe}^{3+})_2\text{Si}_3\text{O}_{10}(\text{OH})_8]$. Structures viewed parallel to the sheets.....	49
Figure 4.2	Zeta potential of alumina (open squares) and silica (filled diamonds) as a function of pH. IS = 10^{-2} mol/L using KCl; i.e.p. occurs at ca. pH 7.9 and <3, respectively. The error bars represent the 95 % confidence interval from three observations.....	53

Figure 4.3	Δ pH as a function of pH_{IS2} for alumina. IS changed from 10^{-2} mol/L to 0.1 mol/L (circles), and from 0.1 mol/L to 1 mol/L (squares) using KCl; p.z.c. observed at ca. pH 8.1.....	54
Figure 4.4	Δ pH as a function of pH_{IS2} for silica. IS changed from 0.1 mol/L to 1 mol/L; p.z.c. observed at ca. pH 2.....	54
Figure 4.5	Zeta potential of chlorite as a function of pH for aged (24-hr) and fresh samples. IS = 10^{-2} mol/L using KCl. Solid-liquid ratio was 200 mg/L (filled squares and open diamonds) and 100 mg/L (filled triangles).....	56
Figure 4.6	Zeta potential of serpentine as a function of pH for aged (filled squares) and fresh (open diamonds) samples. IS = 10^{-2} mol/L using KCl.....	56
Figure 4.7	Zeta potential of talc as a function of pH for 24-hr aged (filled diamonds) and fresh (open diamonds) samples. IS = 10^{-2} mol/L using KCl.....	57
Figure 4.8	Zeta potential of serpentine (circles) and chlorite (squares) as a function of pH for 24-hr aged samples. IS = 10^{-2} (filled symbols) and 10^{-3} mol/L (open symbols) using KCl.....	57
Figure 4.9	Zeta potential of chlorite as a function of pH in 10^{-2} mol/L KCl for 0 mol/L (filled diamonds), 10^{-5} mol/L (open squares), 10^{-4} mol/L (filled triangles) and 10^{-3} mol/L (crosses) of magnesium.....	58
Figure 4.10	Zeta potential of serpentine as a function of pH in 10^{-2} mol/L KCl for 0 mol/L (filled diamonds), 10^{-5} mol/L (open squares), 10^{-4} mol/L (filled triangles) and 10^{-3} mol/L (crosses) of magnesium.....	59
Figure 4.11	Zeta potential of talc in 10^{-2} mol/L KCl for 0 mol/L (filled diamonds), 10^{-5} mol/L (open squares), 10^{-4} mol/L (filled triangles) and 10^{-3} mol/L (crosses) of magnesium.....	59
Figure 4.12	Δ pH as a function of pH_{IS2} for chlorite. IS changed from 10^{-2} mol/L to 0.1 mol/L (filled diamonds), and from 10^{-2} mol/L to 1 mol/L (open squares) using KCl. p.z.c. was observed at ca. pH 4.6.....	60
Figure 4.13	Δ pH as a function of pH_{IS2} for serpentine. IS change was from 10^{-2} mol/L to 0.1 mol/L using KCl. p.z.c. was observed at pH ca. 4.3.....	61
Figure 4.14	Dispersion index in absorbance increment per second as a function of pH for chlorite (open circles) and serpentine (filled squares).....	62
Figure 4.15	Interlayer bonding for different types of phyllosilicates.....	65
Figure 5.1	Zeta potential of pentlandite as a function of pH at two values of ionic strength: 10^{-2} mol/L (filled diamonds) and 5×10^{-3} mol/L (open squares) KNO_3 (Note, error bars are the 95 % confidence interval).....	77
Figure 5.2	Zeta potential of serpentine as a function of pH at two values of ionic strength: 10^{-2} mol/L (filled diamonds) and 5×10^{-3} mol/L (open squares) KNO_3	77

Figure 5.3	Zeta potential of pentlandite as a function of pH with supernatant as background electrolyte compared to 10^{-2} mol/L KNO_3 as background electrolyte.....	79
Figure 5.4	Zeta potential of serpentine as a function of pH with supernatant as background electrolyte compared to 10^{-2} mol/L KNO_3 as background electrolyte.....	79
Figure 5.5	Zeta potential of pentlandite as a function Mg^{2+} concentration at pH 10.....	80
Figure 5.6	Zeta potential of pentlandite as a function of pH in the presence of 50 mg/L Mg^{2+} compared to supernatant.....	81
Figure 5.7	Zeta potential of pentlandite conditioned with serpentine suspended in 10^{-2} mol/L KNO_3 (open squares) compared to result for pentlandite in 10^{-2} mol/L KNO_3 (filled diamonds).....	82
Figure 5.8	Zeta potential of serpentine conditioned with pentlandite suspended in 10^{-2} mol/L KNO_3 (open squares) compared to the result for pentlandite in 10^{-2} mol/L KNO_3 (filled diamonds).....	83
Figure 5.9	Zeta potential of pentlandite conditioned with serpentine suspended in supernatant compared to result for pentlandite conditioned with serpentine suspended in 10^{-2} mol/L KNO_3 (open squares).....	83
Figure 5.10	Scanning electron micrographs of the pentlandite conditioned in 10^{-2} mol/L KNO_3 solution alone at pH 10 [a]; conditioned in supernatant at pH 4 [b] and at pH 10 [c]; conditioned with serpentine at pH 10 [d] and a particle of fibrous serpentine [e].....	85
Figure 6.1	Representation of the experimental design in coded units; original units are displayed in the table on the right side.....	97
Figure 6.2	Pareto chart of regression coefficients.....	101
Figure 6.3	Comparison of modeled versus actual dispersion index.....	101
Figure 6.4	Contour plot of dispersion index (A/s) as a function of pH and CMC concentration (mg/L). PAX content was fixed at its centre level (3 mg/L).....	102
Figure 6.5	Dispersion index as a function of CMC concentration for pH 6, 8 and 10. (Note, symbols are to identify the trends).....	103
Figure 6.6	Optical micrographs of the pentlandite-serpentine systems (pH 10, 3 mg/L PAX, 10^{-2} mol/L KNO_3) (a) serpentine alone; (b) pentlandite alone; (c) serpentine and pentlandite; (d) serpentine and pentlandite with 50 mg/L CMC.....	104
Figure 7.1	Contact angle of pentlandite as a function of pH; PAX = 10^{-4} mol/L (filled diamonds) and no PAX (open squares), $\text{NaNO}_3 = 10^{-3}$ mol/L. Error bars indicate 95 % confidence interval.....	115
Figure 7.2	Contact angle of Cu-activated pentlandite as a function of pH (open squares). PAX = 10^{-4} mol/L, $\text{NaNO}_3 = 10^{-3}$ mol/L. For comparison the result for non-activated pentlandite is included (filled diamonds).....	116

Figure 7.3	Contact angle on Cu-activated pentlandite as a function of the pH in the presence of magnesium (50 mg/L) (open squares). PAX = 10^{-4} mol/L, $\text{NaNO}_3 = 10^{-3}$ mol/L. For comparison the curve for the Cu-activated pentlandite in absence of magnesium is included (filled circles).....	117
Figure 7.4	Contact angle on Cu-activated pentlandite as a function of the pH in the presence of magnesium (50 mg/L) (filled circles) when Na_2CO_3 pH is used as pH modifier. PAX = 10^{-4} mol/L, $\text{NaNO}_3 = 10^{-3}$ mol/L. For comparison the curves for the Cu-activated pentlandite in the presence of PAX (filled diamonds), and in the presence of PAX and magnesium (50 mg/L) (open squares) when NaOH is used as pH modifier are included.....	118
Figure 7.5	Contact angle on Cu-activated pentlandite as a function of the pH in the presence of CMC (50 mg/L) (open squares). PAX = 10^{-4} mol/L, $\text{NaNO}_3 = 10^{-3}$ mol/L. For comparison the curve for the Cu-activated pentlandite in absence of serpentine is included (filled diamonds).....	118
Figure 7.6	Contact angle on Cu-activated pentlandite as a function of the pH in the presence of serpentine (0.1 g/L) and CMC (50 mg/L) (open triangles). PAX = 10^{-4} mol/L, $\text{NaNO}_3 = 10^{-3}$ mol/L. For comparison, curves for Cu-activated pentlandite with PAX and CMC (open squares), and with PAX and serpentine (filled squares) are included.....	119
Figure 7.7	Comparison of modeled versus actual recoveries.....	123
Figure 7.8	Studentized residuals as a function of the predicted recovery.....	123
Figure 7.9	Pareto chart of regression coefficients.....	125
Figure 7.10	Contour plot of pentlandite recovery as a function of serpentine content and CMC concentration. pH, magnesium and copper concentrations were fixed at their centre level.....	125
Figure 7.11	Contour plot of pentlandite recovery as a function of pH and serpentine content. CMC, magnesium and copper concentrations were fixed at their centre level.....	126
Figure 7.12	Species distribution diagram of magnesium in concentration percentage as a function of pH. Mg species concentration equal to 50 mg/ (modified from Sui and Huang, 1998).....	128
Figure A-1.1	X-ray diffraction of serpentine identified as lizardite. The diffraction peaks for lizardite is shown.....	138
Figure A-1.2	X-ray diffraction of chlorite identified as clinocllore with minor serpentine-chlorite. The diffraction peaks for clinocllore (continuous line) and chlorite-serpentine (dashed line) are shown.....	139
Figure A-1.3	X-ray diffraction of talc identified as steatite. The diffraction peaks for steatite is shown.....	139
Figure A-1.4	Particle size distribution for serpentine, chlorite and talc. P80 ca. 40 μm for serpentine and 30 μm for chlorite and talc.....	140

Figure A-2.1	Schematic diagram of the ore processing.....	142
Figure A-2.2	Schematic diagram of the rougher concentrate processing.....	143
Figure A-2.3	X-ray diffraction of pentlandite used for small-scale flotation. The diffraction peaks for pentlandite (continuous line) and pyrrhotite (dashed line) are shown.....	144
Figure A-2.4	X-ray diffraction of serpentine used for small-scale flotation. The diffraction peaks for clinochrysotile (continuous line) and pyrrhotite (dashed line) are shown.....	144
Figure A-2.5	Particle size distribution for pentlandite used in the flotation tests. P80 ca. 120 μm	145
Figure A-2.6	Particle size distribution for serpentine used in the flotation and contact angle tests. P80 ca. 25 μm	145
Figure A-2.7	Optical micrographs of serpentine (left) and pentlandite (right).....	146
Figure A-2.8	X-ray diffraction pattern of pentlandite used for contact angle measurements compared to the standard diffraction pattern for pentlandite (thick lines).....	146
Figure A-3.1	Magnesium in solution as a function of time in supernatant.....	147
Figure A-4.1	Calibration curve for determining sulphate concentration.....	150
Figure A-5.1	Picture of a bubble on a hydrophobic surface.....	153

List of tables

Table 2.1	Main MgO-minerals in ultramafic ores at Thompson (Lee, 2006).....	9
Table 2.2	Dispersants classification (Kissa, 1999).....	14
Table 3.1	Detection limits and analytical sensitivity for some elements in inductively coupled plasma-optical emission spectrometry and atomic absorption spectroscopy	41
Table 4.1	Mineralogical characterization (XRD) of samples.....	52
Table 4.2	Comparison between i.e.p. and p.z.c. for samples tested.....	61
Table 5.1	Measured elemental composition of the sample determined by AAS compared to ideal pentlandite composition and composition determined by microprobe analysis on identified pentlandite grains.....	73
Table 5.2	Chemical species in the supernatant.....	78
Table 6.1	Dispersion index for the experimental design.....	98
Table 6.2	Coefficient and P values of the factors and interactions on the first regression model	99
Table 6.3	Coefficient and P values of the factors and interactions on the final regression model	100
Table 7.1	Elemental composition of pentlandite samples for contact angle and small-scale flotation tests. Theoretical composition of is also shown.....	111
Table 7.2	Conditioning of pentlandite for contact angle measurements.....	113
Table 7.3	Levels of the factors considered in the experimental design.....	114
Table 7.4	Recovery of pentlandite according to experimental design.....	121
Table 7.5	Coefficient of the first regression model.....	121
Table 7.6	Coefficients of the final regression model.....	122
Table A-2.1	Main mineral phases in the Thompson ultramafic ore.....	141
Table A-3.1	Metals in solution in supernatant.....	148
Table A-3.2	Sulphate concentration in supernatant calculated by turbidimetry.....	148
Table A-3.3	Chloride concentration in supernatant calculated by argentometric titration.....	148

Introduction

Pentlandite, typically given the formula $(\text{Ni,Fe})_9\text{S}_8$, is the most common sulphide nickel mineral and the source of much of the world's nickel. These sulphide ores are universally treated by flotation. In the case of ultramafic ores, the major gangue includes a host of MgO-minerals (Edwards et al., 1980). These minerals can reduce selectivity in flotation, causing loss of Ni-mineral to the tails and in some operations reporting in significant amount to the concentrate, diluting grade and increasing transport and smelting costs.

The mechanisms by which MgO-minerals degrade flotation performance include entrainment, physical entrapment, true flotation of naturally hydrophobic particles or through activation which promotes recovery to concentrate, and hetero-aggregation (e.g., slime coating) that may also induce loss of Ni-mineral to tails. Among these

mechanisms, slime coating is explored in this study.

Slime coating is believed to be primarily controlled by the magnitude and sign of the surface charge of the interacting particles as reflected by zeta potential measurements. Oppositely charged or near-neutral charged particles tend to aggregate. This electrostatic mechanism is suspected in the case of MgO-gangue slime coating of pentlandite (Dai et al., 2009; Xu and Wells, 2006).

Slime coating can be controlled using dispersants, which adsorb preferentially onto slimes, reversing and/or increasing the surface charge and preventing electrostatic attraction. In the case of pentlandite other remedial techniques such as salt addition and flotation at acidic pH which again influence surface charge have been shown to improve selectivity against MgO-minerals (Senior and Thomas, 2005; Mani et al., 1997; Wellham et al., 1992).

1.1. Objectives of the thesis

The general objective is to determine the surface characteristics of the minerals in an ultramafic ore in order to interpret and control particle-particle and particle-chemical species (reagents) interactions and improve flotation selectivity. As steps towards this goal, the following specific tasks were addressed:

- To determine whether isoelectric point or point of zero charge of two MgO-minerals, serpentine and chlorite, controlled the interactions.
- To determine the effect of the presence of dissolved species and serpentine (the most abundant MgO-gangue in ultramafic ore) on the electrokinetic behaviour of pentlandite.

- To determine the effect of flotation reagents on aggregation/dispersion in the pentlandite-serpentine system.
- To determine the effect of flotation reagents on the hydrophobicity of pentlandite.

1.2. Structure of the Thesis

The thesis consists of nine chapters. Objectives and scope of the research are given in Chapter 1. The background, which describes ultramafic ore mineralogy and problems related to mineral processing, is discussed in Chapter 2. Experimental techniques and theory are included in Chapter 3. Comparison of isoelectric point and point of zero charge of the specimen samples of MgO-minerals are presented in Chapter 4. A systematic study of electrokinetic behaviour of pentlandite and serpentine is found in Chapter 5. The aggregation/dispersion state of the pentlandite-serpentine system is presented in Chapter 6. The effect of flotation reagents and dissolved mineral species on hydrophobicity of pentlandite is discussed in Chapter 7. Although Chapters 4-7 contain conclusion sections, the overall conclusions are summarized in Chapter 8, which includes the intended contributions to the original knowledge and recommendations for future work. Following Chapter 8, five appendixes providing supporting material are included.

This thesis was prepared as a manuscript-based structure. Consequently, some repetition is expected, especially in the introduction sections of Chapters 4-7.

References

Edwards C.R., Kipkie W.B., Agar G.E. (1980) The effect of slime coatings of the serpentine minerals, chrysotile and lizardite, on pentlandite flotation. *International Journal of Mineral Processing* 7: 33-42

Dai Z., Bos J.A., Quinn P. Lee A., Xu M. Flowsheet development for Thompson ultramafic low-grade nickel ores. C.O. Gomez; J.E. Nasset, S.R. Rao (Eds.) *Advances in Mineral Processing Science and Technology. International Symposium of the Metallurgical Society of CIM*, 217-228. 2009

Mani H., Xu M., Quinn P. The effect of ultramafic mineralogy on pentlandite flotation. J.A. Finch, S.R. Rao, I. Holubec (Eds.) *Processing of Complex Ores, Mineral Processing, and the Environment. International Symposium of the Metallurgical Society of CIM*, 63-76. 1997

Senior G.D., Thomas S.A. (2005) Development and implementation of a new flowsheet for the flotation of a low grade nickel ore. *International Journal of Mineral Processing* 78: 49-61

Wellham E.J., Elber L., Yan D.S. (1992) The role of carboxy methyl cellulose in the flotation of a nickel sulphide transition ore. *Minerals Engineering* 5: 381-395

Xu M, Wells P.F. Effect of Slime Coating on Flotation of Nickel Sulphide Ores. *Proceedings of 23rd IMPC, Instambul, Vol. 2, 2006, 965-971*

Background

Nickel is a silvery-white transition metal. It was first isolated in 1751 by Baron Axel Fredrick Cronstedt, a Swedish chemist and mineralogist. Nickel is widely recognized because of its use in coinage and its many household and industrial applications that make it one of the most important metals (Encyclopædia Britannica, 2009).

2.1. Uses of Nickel

Nickel is seldom used in pure form. It is mostly used as an alloying element in stainless steel and other alloy steels. Nickel (in combination with other elements such as chromium and copper) is used to produce alloys with high strength and corrosion resistance including super-alloys used in aircraft turbines and other high temperature

applications (Encyclopædia Britannica, 2009; Bacon et al., 2002). A common application is electroplating. A layer of electrochemically deposited nickel provides a substrate with nickel's natural resistance to corrosion which is exploited, for example, in food and chemical-processing components. Electroplating is also used for decorative purposes (Encyclopædia Britannica, 2009). A small amount of nickel is used in nonmetallic form. Some nickel compounds are used as catalysts in processes such as petroleum refining or as pigments and mordants. A summary of uses is given in (Figure 2.1).

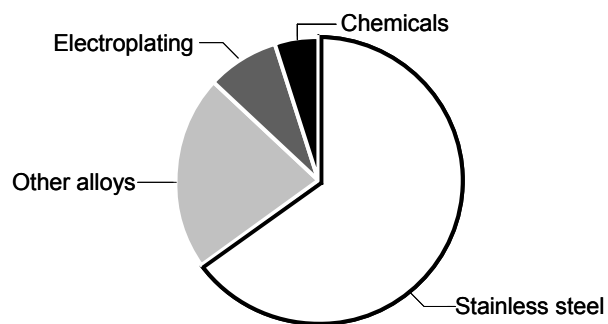


Figure 2.1 – Main industrial uses for nickel
Source: Standard CIB Global Research <http://www.standardbank.co.za>

2.2. Occurrence

Nickel accounts for about 0.007 % of the Earth's crust; however, a higher percentage lies at the planet's core. This segregation occurred when the Earth was young and hot, and denser elements like nickel sank (Encyclopædia Britannica, 2009).

2.3. Nickel deposits

Although nickel is a fairly common constituent of igneous rocks, few deposits qualify in concentration, size and accessibility for exploitation. Countries with “world-class” deposits are Russia, Canada, Australia, Indonesia and New Caledonia (France) (Figure 2.2).

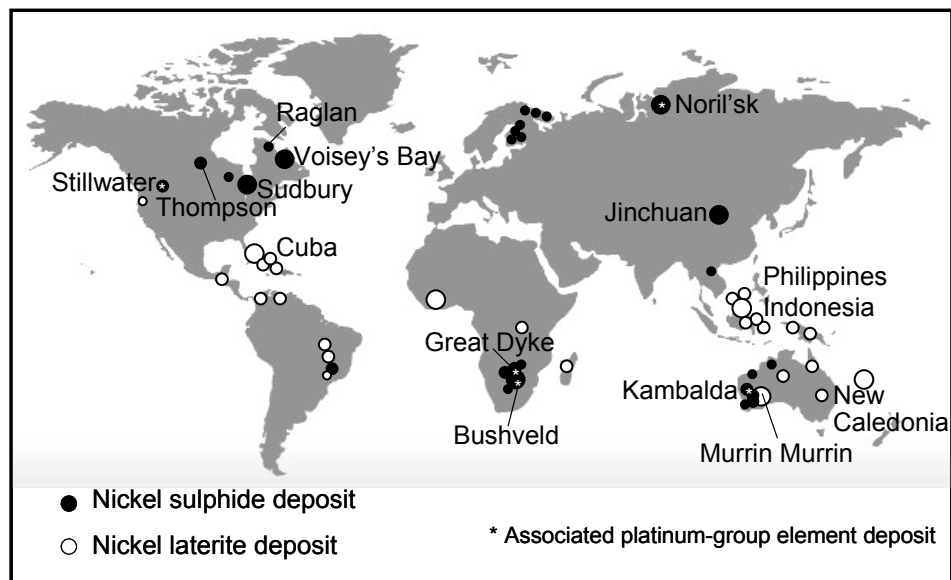


Figure 2.2 – Major Nickel deposits. Modified from Elias (2002)

Nickel deposits can be classified in two main groups: laterites and sulphides. Nickeliferous limonite, $(\text{Fe,Ni})\text{O}(\text{OH})$, and garnierite (a hydrous nickel silicate) are the main nickel phases in laterites while pentlandite $[(\text{Ni,Fe})_9\text{S}_8]$ is the most important nickel mineralization among sulphide ores. Even though nearly 70 % of nickel resources are contained in laterites, the bulk of production comes from sulphides due to the complex and high-cost processing required for laterites (Bacon et al., 2002).

Canada's major nickel deposits include Sudbury, Thompson, Voisey's Bay and Raglan. All are associated with pyrrhotite (Fe_{1-x}S) and MgO-minerals as the dominant gangue. These deposits usually depend on combinations of nickel, copper and cobalt to be profitable. However, low grade disseminated sulphide deposits like some ultramafic ores with complex mineralization from Thompson may be economic due of their significant size.

2.4. Issues in ultramafic ore processing

Ultramafic ores are more than 90 % composed of mafic rocks. Mafic is the term used to define igneous rocks rich in FeO and MgO characterized by the presence of dark-colored minerals such as olivine and pyroxene (Hurlbut and Sharp, 1998).

For sulphide deposits hosted in mafic-ultramafic rocks, the major gangue includes a variety of MgO-minerals, which must be rejected as their presence in the Ni-concentrate increases the slag melting point. The other common gangue, pyrrhotite, must be rejected to reduce SO_2 emissions.

The primary method for concentrating pentlandite is by froth flotation. This is usually performed using thiol collectors in an alkaline pulp, sometimes with polyamines (DETA, TETA) as pyrrhotite depressants, and polysaccharides (e.g., carboxymethyl cellulose, CMC) to depress MgO-gangue.

MgO-minerals (e.g., serpentines) break readily. Thus size reduction (liberation) produces fines or slimes, roughly particles less than ca. 10 μm . These gangue slimes can interfere with flotation by forming a coating on the pentlandite surface. This has two consequences: dilution of the concentrate when pentlandite partially coated remains floatable and loss of pentlandite recovery when extensively coated pentlandite becomes hydrophilic.

In the case under study here (Vale's ultramafic ores around Thompson, Manitoba), MgO-gangue of concern is mainly serpentine. Some other silicates present are amphibole, olivine, chlorite and minor talc (Table 2.1).

Table 2.1 – Main MgO-minerals in ultramafic ores at Thompson (Lee, 2006)

Name	General chemical formula ¹	Grade ²
Serpentine	$\text{Mg}_3\text{Si}_2\text{O}_5(\text{OH})_4$	63.29
Amphibole (hornblende)	$\text{Ca}_2(\text{Mg,Fe,Al})_5(\text{Al, Si})_8\text{O}_{22}(\text{OH})_2$	1.77
Olivine	$(\text{Mg,Fe})_2\text{SiO}_4$	11.99
Chlorite	$(\text{Mg,Fe}^{2+})_5(\text{Al,Fe}^{3+})_2\text{Si}_3\text{O}_{10}(\text{OH})_8$	3.46
Talc	$\text{Mg}_3\text{Si}_4\text{O}_{10}(\text{OH})_2$	0.08

2.5. The minerals

2.5.1. Sulphides

Pentlandite

Pentlandite is the main source of nickel worldwide. Usually, the Fe:Ni ratio is close to 1, but the mineral commonly contains small amount of cobalt. It is brassy yellow with a light bronze-brown streak, metallic, dense (4.6-5 g/cm³) and non-magnetic (Klein and Hurlbut, 1993; Dana and Ford, 1952). Pentlandite bears a resemblance to pyrrhotite but can be differentiated by the octahedral parting and its lack of magnetism (Klein and Hurlbut, 1993).

The structure of pentlandite is rather complex, with a face centered cubic arrangement and metal ions in tetrahedral and octahedral coordination with sulphur. Pentlandite commonly occurs as exsolution lamellae with pyrrhotite (Klein and Hurlbut, 1993).

¹ Dana and Ford, 1952

² Lee, 2006

Pyrrhotite

Pyrrhotite, general formula Fe_{1-x}S , is one of the most abundant iron sulphide minerals but has little commercial value. It often occurs as a gangue mineral in pentlandite deposits. To limit SO_2 emissions during smelting, the separation of pentlandite from pyrrhotite has been widely practiced and studied.

Pyrrhotite is a solid solution between two end members, pyrite and troilite. The non-stoichiometry of pyrrhotite is caused by a deficiency of iron atoms in the Fe-layers (as indicated by the formula: Fe_{1-x}S) and ordering of these vacancies leads to superstructure and non-stoichiometry of intermediate pyrrhotites (Morimoto et al., 1975). The non-stoichiometric structure helps this mineral to oxidize 20-100 times faster than pyrite (Shaw et al., 1988).

Pyrrhotite rarely exists as a single phase. Lamellae intergrowths of ferrimagnetic monoclinic and antiferromagnetic hexagonal phases are responsible for the variation in magnetic properties within single pyrrhotite grains (Miller et al., 2005; Pósfai et al., 2000).

2.5.2. MgO-minerals

Serpentine

The main MgO-mineral in ultramafic ores is serpentine. Serpentine minerals are formed through hydrothermal alteration of previously existing minerals, such as olivine and pyroxene (Azer and Khalil, 2005). The idealized formula is $\text{Mg}_3\text{Si}_2\text{O}_5(\text{OH})_4$, but frequently iron, nickel, aluminum and other cations can substitute into the Mg position (Tartaj et al., 2000). Chrysotile, lizardite and antigorite are the most common serpentine polymorphs found in nature.

Serpentine belongs to the phyllosilicate mineral class. These minerals are built of a silicon tetrahedral sheet bonded by a magnesium octahedral (“brucite-like”) sheet (Ciullo, 1996). In serpentine, the lateral dimension of the octahedral sheet is larger than that of the tetrahedral sheet, which forces the mineral to adopt various arrangements. In the case of chrysotile, the structure bends forming long hollow tubes while in lizardite the bending is not continuous but occurs as corrugations, which gives the minerals its characteristic platy morphology (Figure 2.3). Figure 2.4 shows scanning electron micrographs of lizardite and chrysotile.

Amphibole

Included in the amphibole group are several minerals closely related chemically and structurally, which crystallize in the monoclinic or prismatic systems (Hurlbut and Sharp, 1998; Dana and Ford, 1952). Tremolite and hornblende are the most common amphiboles. The former is usually produced during the metamorphosis of siliceous dolomites at intermediate metamorphic conditions, while hornblende is often formed by hydrous alteration of pyroxene (Hurlbut and Sharp, 1998; Klein and Hurlbut, 1993; Dana and Ford, 1952).

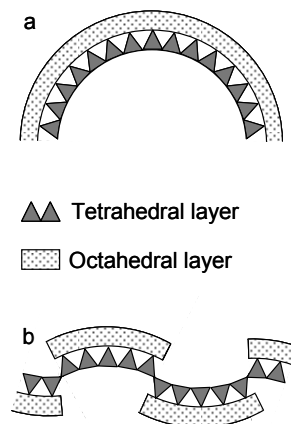


Figure 2.3 – Schematic representation of the (a) chrysotile and (b) lizardite structures. Modified from Klein and Hurlbut (1993)

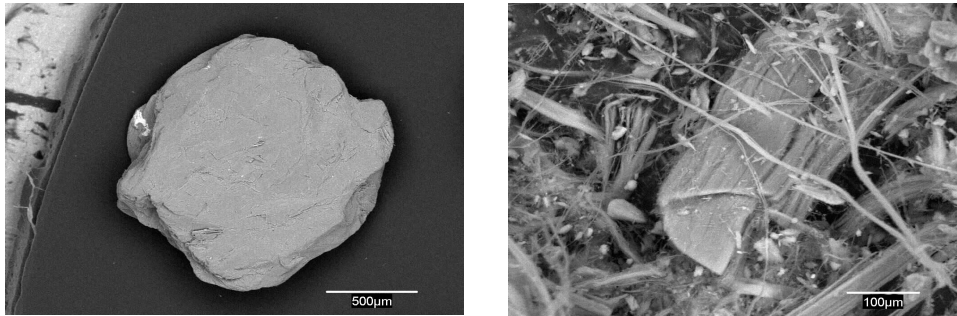


Figure 2.4 – Scanning micrographs of a chunk of lizardite (left) and fibers of chrysotile

Chlorite

Chlorite is a general term to designate a family of minerals with similar chemical and physical properties with the general formula $(\text{Mg}, \text{Fe}^{2+})_5(\text{Al}, \text{Fe}^{3+})_2\text{Si}_3\text{O}_{10}(\text{OH})_8$. Chlorite is made up of an octahedral sheet bonded on both sides by tetrahedral sheets interleaved with a “brucite-like” sheet in which one in two Mg^{2+} is replaced by Al^{3+} (Ciullo, 1996; Klein and Hurlbut, 1993; Dana and Ford, 1952).

Olivine

Olivine is a common rock-forming mineral abundant in mafic rocks. The general formula $(\text{Mg}, \text{Fe})_2\text{SiO}_4$ represents an intermediate member in a solid solution series between the magnesium-rich forsterite (Mg_2SiO_4) and the iron-rich fayalite (Fe_2SiO_4). Fayalite is much less common than forsterite (Klein and Hurlbut, 1993; Dana and Ford, 1952).

Talc

Talc is a secondary mineral formed by the alteration of magnesium silicates such as olivine, and amphiboles. Naturally hydrophobic, talc can be difficult to separate from valuable minerals via flotation. It is hydrophobic because of its structure and the way it

breaks. The atoms within the layers are held together by ionic bonds, while the interlayer atoms are linked by van der Waals forces. When ground, two kinds of surfaces are formed: one resulting from the easy cleavage of the layers (basal plane) and the other resulting from the rupture of chemical bonds (edge plane). The basal plane, which represents about 90 % of the surface, has a very low charge (ideally zero if the talc has no isomorphic substitution) and high hydrophobicity, unlike the edge plane, which has a relatively high electric charge and is strongly polar (Fuerstenau et al., 1988).

2.6. Flotation reagents

2.6.1. Collectors

A collector is the chemical reagent that makes a particle hydrophobic enabling it to be held at the water-air interface (Sutherland and Wark, 1955). Collectors generally comprise polar and non-polar groups. The polar group should have affinity with the desired mineral, which confers selectivity. The non-polar group is responsible for the hydrophobic properties.

The flotation of sulphide minerals such as pentlandite is often performed with xanthate type collectors (Figure 2.5)

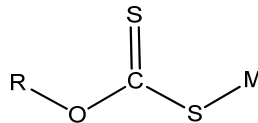


Figure 2.5 – Schematic diagram of xanthate structure. M represents metal and R a hydrocarbonated group

The hydrocarbon chain length and structure (i.e., whether it is straight or branched) introduces certain properties: in general, reagents with iso-structure are considered more selective collectors than the straight-chain ones (Somasundaran and Wang, 2006). The point of addition of collector (e.g. before or after pH adjustment) often has some effect (Wiese et al., 2006).

Bozkurt et al. (1998) studied interactions between pentlandite, pyrrhotite and sodium isobutyl xanthate by FTIR-ATR spectroscopy and open circuit potential measurements. It was demonstrated that dixanthogen formation on pentlandite was promoted when the two minerals were in direct contact.

2.6.2. Dispersants

Dispersants are reagents used to promote and keep particles dispersed in the slurry. They act through several mechanisms, such as: being a good wetting agent for the particles to be dispersed; lowering the viscosity of the dispersion; and stabilizing the dispersion by controlling surface charge (Kissa, 1999). Both the wetting and stabilizing mechanisms require adsorption of the dispersant onto the particle surface.

Dispersants may be classified as inorganic or organic, the latter being further sub-divided as either low molecular weight or polymeric (macromolecular) (Table 2.2). Since dispersion efficiency is related to adsorption of the dispersant, polymeric dispersants are preferred over low molecular weight dispersants (Kissa, 1999). Dispersants derived from natural sources are preferred to synthetic varieties because of environmental concerns.

Table 2.2 – Dispersants classification (Kissa, 1999)

Inorganic dispersants	Organic dispersants			
	Low molecular weight dispersants	Polymeric dispersants		
		Natural or derived from natural products	Synthetic	
			Homopolymers	Copolymers

Some macromolecular dispersants, especially those that belong to the polysaccharide family, are used to reduce the natural floatability of some MgO-minerals (e.g., talc) in pentlandite flotation. The most widely used are introduced below.

Carboxymethyl cellulose (CMC) type reagents have been used extensively. They are derivatives of cellulose with carboxymethyl groups bound to some of the hydroxyl groups of the glucopyranose monomers. A schematic CMC structure is shown in the Figure 2.6.

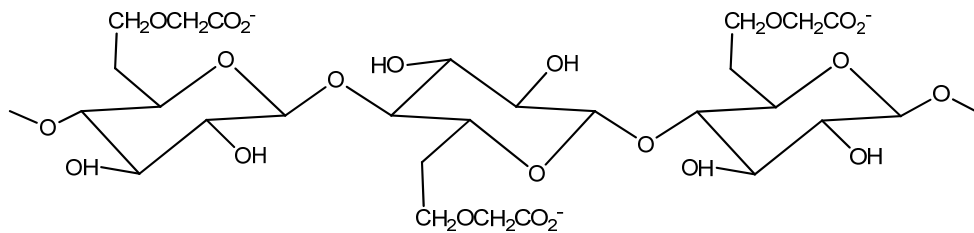


Figure 2.6 – Carboxymethyl cellulose fragment

Adsorption of CMC on serpentine apparently reverses its positive surface charge, so attraction forces between pentlandite and serpentine are eliminated (Bremmel et al., 2005). However, Wellham et al. (1992) reported that the CMC dosage to achieve satisfactory nickel selectivity is uneconomically high. They showed 10 % sodium chloride solution gave superior results, particularly in the flotation of fine material.

Gums are macromolecular substances containing polysaccharides extracted from plants. Guar gum is chemically modified from natural gums, which is used mainly as a dispersant for silicate mineral slimes. There are several studies on the application of this reagent for MgO-gangue (Shortridge et al., 2000; Kumar-Rath et al., 1997; Pugh, 1989). Kumar-Rath et al. (1997) found that guar gum gave excellent depression of talc and its effect was independent of pH. They proposed that the adsorption mechanisms are hydrogen bonding and chemical interaction.

Dextrin is a common dispersant made by the hydrolysis of natural starch with dilute acids. It can vary in chain length and configuration, molecular weight and in level and type of impurities. It has been widely used to depress hydrophobic minerals such as talc, coal and molybdenite by producing an adsorbed hydrophilic coating as a result of the polar groups of the macromolecule. Apparently, adsorption of dextrin on mineral surfaces takes place through hydrogen bonding (Kumar-Rath et al., 1997).

Belonging to the synthetic class of dispersant, block copolymers may have a place in the flotation of ultramafic ores. They are formed by two homopolymers joined at their edges. Consequently, block copolymers are adsorbed onto a surface if one of the polymers has an affinity for some surface sites while the other polymer remains in solution (Hadjichristidis et al., 2003). This arrangement confers block copolymers with properties that make them potential depressants/dispersants. Common monomers used to form copolymers are isobutylene, ethylene oxide and acrylamide.

2.6.3. pH modifiers

The pH of mineral pulps is critical for optimum flotation selectivity. In commercial practice, the majority of pH modifiers are alkalis with acids only used to achieve selectivity if alkaline conditions fail.

Alkalis are divided in two main groups: reagents that produce hydroxyl (OH^-) by dissociation (e.g., sodium hydroxide) and reagents which form OH^- by hydrolysis (e.g., sodium carbonate). Equations 2.1 and 2.2 show dissociation of sodium hydroxide and hydrolysis of carbonate, respectively.





The effects of pH on flotation systems are both on the mineral surfaces and on the solution chemical species. These effects are briefly discussed.

Effect on the minerals

Surface charge – For many minerals, OH^- and H^+ are potential determining ions, i.e., they determine the surface charge and the electrochemical potential of the double layer and thus hinder or promote chemical species adsorption.

Mineral dissolution – All solids dissolve to a different degree which can be controlled by the pH of the media. Some silicates, for example, demonstrate incongruent dissolution depending on the pH: alkaline conditions facilitate the detachment of silicon, while at low pH magnesium is preferentially released from the lattice (Pokrovsky and Schott, 2000 a, b; Brady and Walther, 1989).

Surface hydration – pH affects the hydration of the surface by the direct adsorption of hydroxyls and protons, which changes the stability of the hydrated layer surrounding the particle. Sometimes, the effect is indirect: in the case of some silicates, the variability in H^+/OH^- concentration can enhance or hinder the adsorption of other ions at sites that are otherwise occupied by water molecules (He et al., 1999; Goldberg et al., 1996; Ramachandran et al., 1993).

Effect on chemical species

Active form of chemical species – pH can change the degree of dissociation of compounds into ions and control the chemical species present by processes such as hydrolysis. For example, most metallic ions precipitate as hydroxides at alkaline pH.

Stability of reagents – For example, the xanthate ion can hydrolyse to form xanthic acid, which decomposes at acidic pH. In neutral and alkaline media, xanthates decompose by another mechanism known as hydrolytic decomposition (Rao, 1971).

Competition for surface sites – Hydroxyls and protons can compete with collectors and other reagents for adsorption sites on mineral surfaces.

2.7. Some other factors affecting flotation

2.7.1. Dissolved species

Most minerals dissolve to some extent in aqueous solution. The dissolved species can undergo further reactions such as hydrolysis, complexation, adsorption, and bulk precipitation. The nature of the equilibria involved in such reactions will determine the interfacial properties of the particle, and consequently its floatability.

For example, polyvalent metallic ions can adsorb specifically on minerals; this phenomenon occurs when the cation involved hydrolyses to its first hydroxy complex or it precipitates on the particle surface as a hydroxide. In general, adsorption of cations increases markedly at pH values just below that required for the precipitation of the corresponding metal hydroxide. Fuerstenau and Palmer (1976), in experiments with quartz, found that flotation arises only after metal ions are present in the system within a pH range in which hydrolysis to the first hydroxy complex occurs.

Not all metal ions have a flotation effect. Fuerstenau et al. (1965) observed that flotation of quartz in presence of amyl xanthate did occur with Pb^{2+} and Zn^{2+} ions, but not with copper or magnesium ions. If the first hydroxy complex of metal ions is the responsible for activation, Cu^{2+} will not be expected to act as a activator because in the presence of xanthate cupric ions are reduced to cuprous, thus there would not be a valence site for the collector ion. In the case of Mg^{2+} , since Mg-xanthate does not form (it is essentially completely soluble) flotation is not possible.

In some contrast, Fornasiero and Ralston (2005) studying inadvertent activation of silicate minerals noted that lizardite, chlorite and quartz can be activated with Cu^{2+} or Ni^{2+} and floated with xanthate in the pH region from 7 to 10, where copper and nickel form positively charged hydroxides that adsorb on the negatively charged silicate surface. It was observed that activation was much more pronounced for copper than for nickel. They concluded that the increased quartz flotation with Cu^{2+} was the result of xanthate adsorption and the formation of hydrophobic species of cuprous xanthate and dixanthogen. Nagaraj and Brinen (1996) studied the adsorption of sulphide collectors on apparently copper-activated pyroxene by SIMS (secondary ion mass spectroscopy) and XPS (X-ray photoelectron spectroscopy). They found that in the presence of thiol collectors, copper on pyroxene was in the Cu^+ form.

2.7.2. Process water

Process water always contains ions such as Ca^{2+} , Mg^{2+} , SO_4^{2-} , etc. The type of chemical species present in water is an essential factor in designing flotation conditions. It has been observed that Ca^{2+} activates pentlandite, and to a lesser extent pyrrhotite (Malysiak et al., 2002). Rao and Finch (1991) found that the presence of cations enhances uptake of xanthate-dixanthogen by pyrrhotite at pH 8.4. Thiosulphate ions are reported to increase pentlandite recovery (Kirjavainen et al., 2002).

References

- Azer M.K., Khalil A.E.S. (2005) Petrological and mineralogical studies of Pan-African serpentinites at Bir Al-Edeid area, central Eastern Desert, Egypt. *Journal of African Earth Sciences* 43: 525-536
- Bacon W.G., Dalvi A.D., Rochon B.A., Selby M. (2002) Nickel Outlook – 2000 to 2010. *CIM Bulletin* 95: 47-52
- Bozkurt V., Xu Z., Finch J.A. (1998) Pentlandite/pyrrhotite interaction and xanthate adsorption. *International Journal of Mineral Processing* 52: 203-214
- Brady P.V., Walther J.V. (1989) Controls on silicate dissolution rates in neutral and basic pH solutions at 25 °C. *Geochimica et Cosmochimica Acta* 53: 2823-2830
- Bremmell K.E., Fornasiero D., Ralston J. (2005) Pentlandite-lizardite interactions and implications for their separation by flotation. *Colloids and Surfaces A: Physicochemical and Engineering Aspects* 252: 207-212
- Ciullo P.A., “Silicate Structure”, *Industrial Minerals and their uses—A Handbook and Formulary*, PA Ciullo, Ed., William Andrew Publishing, 1996, Westwood, NJ, USA, 1-16
- Dana E.S., Ford W.E. (1952) *Manual of Mineralogy*. John Wiley & Sons: Cambridge
- Elias M., Nickel Laterite Deposits – Geological overview, Resources and Exploitation. In *Giant Ore Deposits: Characteristics, Genesis, and Exploration*, D.R. Cooke and J. Pongratz (Eds.), Centre for Ore Deposit Research Special Publication 4. University of Tasmania, 205-220. 2002

- Fornasiero D., Ralston J. (2005) Cu(II) and Ni(II) activation in the flotation of quartz, lizardite and chlorite. *International Journal of Mineral Processing* 76: 75-81
- Fuerstenau M.C., Lopez-Valdivieso A., Fuerstenau D.W. (1988) Role of hydrolyzed cations in the natural hydrophobicity of talc. *International Journal of Mineral Processing* 23: 161-170
- Fuerstenau M.C., Miller J.D., Pray R.E., Perinne B.F. (1965) Metal ion activation in xanthate flotation of quartz. *Transactions of the American Institute of Mining, Metallurgical and Petroleum Engineers* 232: 359-364
- Fuerstenau M.C., Palmer B.R. Anionic flotation of oxides and silicates. M.C. Fuerstenau (Ed). *Flotation A.M. Gaudin Memorial Volume 1*, 148-196. 1976. New York
- Goldberg S., Forster H. S., Lesch S. M., Heick E. L. (1996) Influence of anion competition on boron adsorption by clays and soils. *Soil Science* 161: 99-103
- Hadjichristidis N., Pispas S., Floudas G. (2003) *Block Copolymers: Synthetic Strategies, Physical Properties, and Applications*. John Wiley and Sons Inc.
- He J. Z., De Cristofaro A., Violante A. (1999) Comparison of adsorption of phosphate, tartrate, and oxalate on hydroxy aluminum montmorillonite complexes. *Clays and Clay Minerals* 47: 226-233
- Hurlbut C.S., Sharp W.E. (1998) *Dana's Minerals and how to study them*. John Wiley & Sons: New York
- Kirjavainen V., Schreithofer N., Heiskanen K. (2002) Effect of some process variables on flotability of sulfide nickel ores. *International Journal of Mineral Processing* 65: 59-72

- Kissa E. (1999) Dispersions. Characterization, Testing, and Measurements. At Hubbard (Ed). Surfactant Science Series. Marcel Dekker: New York
- Klein C., Hurlbut C.S., (1993) Manual of Mineralogy. John Wiley & Sons: New York
- Kumar-Rath R., Subramanian S., Laskowski J.S. (1997) Adsorption of dextrin and guar gum onto talc. A comparative study. *Langmuir* 13: 6260-6266
- Lee, A. (2006) Pipe Lake Mineralogy. Internal Communication
- Malysiak V., O'Connor C.T., Ralston J., Gerson A.R., Coetzer L.P., Bradshaw D.J. (2002) Pentlandite-feldspar interaction and its effect on separation by flotation. *International Journal of Mineral Processing* 66: 89-106
- Miller J.D., Li J., Davidtz J.C., Vos F. (2005) A review of pyrrhotite flotation chemistry in the processing of PGM ores. *Minerals Engineering* 18: 855-865
- Morimoto N., Gyobu A., Mukaiyama H., Izawa E. (1975) Crystallography and stability of pyrrhotites. *Economic Geology* 70: 824 -833
- Nagaraj D.R., Brinen J.S. (1996) SIMS and XPS study of the adsorption of sulfide collectors on pyroxene: a case for inadvertent metal ion activation. *Colloids and Surfaces A: Physicochemical and Engineering Aspects* 116: 241-249
- Nickel (2009). In *Encyclopædia Britannica*. Retrieved May 26, 2009, from *Encyclopædia Britannica Online*:
<http://www.britannica.com/EBchecked/topic/414238/nickel>
- Pokrovsky O.S., Schott J. (2000 a) Forsterite surface composition in aqueous solutions: a combined potentiometric, electrokinetic, and spectroscopic approach. *Geochimica et Cosmochimica Acta* 64: 3299-3312

- Pokrovsky O.S., Schott J. (2000 b) Kinetics and mechanism of forsterite dissolution at 25 °C and pH from 1 to 12. *Geochimica et Cosmochimica Acta* 64: 3313-3325
- Pósfai M., Sharp T.G., Kontny A. (2000) Pyrrhotite varieties from the 9.1 km deep borehole of the KTB project. *American Mineralogist* 85: 1406–1415
- Pugh R.J. (1989) Macromolecular organic depressants in sulphide flotation - A review, 1. Principles, types and applications. *International Journal of Mineral Processing* 25: 101-130
- Ramachandran A. R., Grutzeck M. W. (1993) Effect of pH on the hydration of tricalcium silicate. *Journal of the American Ceramic Society* 76: 72-80
- Rao S.R. (1971) *Xanthates and Related Compounds*, Marcel Dekker, Inc., New York
- Rao S.R., Finch J.A. (1991) Adsorption of amyl xanthate at pyrrhotite in the presence of nitrogen and implications in flotation. *Canadian Metallurgical Quarterly* 30: 1-6
- Shaw S.C., Groat L.A., Jambor J.L., Blowes D.W., Hanton-Fong C.J., Stuparyk R.A. (1998) Mineralogical study of base metal tailings with various sulfide contents, oxidized in laboratory columns and field lysimeters. *Environmental Geology* 33: 209-217
- Shortridge P.G., Harris P.J., Bradshaw D.J., Koopal L.K. (2000) The effect of chemical composition and molecular weight of polysaccharide depressants on the flotation of talc. *International Journal of Mineral Processing* 59: 215-224
- Somasundaran P., Wang D. (2006) *Solution Chemistry: Minerals and Reagents*. Elsevier: Amsterdam

Sutherland K.L., Wark I.W. (1955) Principles of Flotation. Australasian Institute of Mining and Metallurgy: Melbourne

Tartaj P., Cerpa A., Garcia-Gonzalez M.T., Serna C.J. (2000) Surface instability of serpentine in aqueous suspensions. Journal of Colloid and Interface Science 231: 176-181

Wiese J., Harris P., Bradshaw D. (2006) The role of the reagent suite in optimising pentlandite recoveries from the Merensky reef. Minerals Engineering 19: 1290-1300

Wellham E.J., Elber L., Yan D.S. (1992) The role of carboxy methyl cellulose in the flotation of a nickel sulphide transition ore. Minerals Engineering 5: 381-395

Experimental techniques

This chapter aims to determine the mechanisms of the interaction of pentlandite and MgO-minerals. This was achieved through a systematic characterization of the minerals, relating structure to relevant properties. This approach included a comparison of isoelectric point (obtained by zeta potential calculated from electrophoretic mobility) and point of zero charge (calculated using a titration technique) of some MgO-minerals relevant to ultramafic ore systems. This was followed by zeta potential measurements on samples of pentlandite and serpentine (main MgO-gangue) isolated from ultramafic ore from the Thompson area (Manitoba). These measurements were conducted on the individual minerals and on mixtures using different background solutions to progressively approach actual flotation conditions. To help interpret the findings, scanning electron microscopy with energy dispersive spectroscopy was used.

The effect of dispersant, collector, and other chemical species and pH on the state of aggregation/dispersion of the pentlandite-serpentine system was investigated by turbidimetry. Direct observations by light microscopy provided visual support for the aggregation/dispersion state of the systems.

Contact angle of pentlandite as a function of reagent dosage was measured using the captive bubble technique and small-scale flotation tests were performed in a Partridge/Smith cell. These techniques provided a guide to the effect of flotation reagents and other chemical species on pentlandite hydrophobicity and floatability.

3.1. Surface charge

3.1.1. Mechanisms of surface charge development

Surface charge determines the adsorption of chemical species and is an important factor in controlling particle-particle interactions (e.g., flocculation, coagulation, aggregation). All solids immersed in polar media (e.g., aqueous solutions) develop a charged surface. The main mechanisms of charging are described briefly below (Shaw, 1969).

- The ionization/dissociation of ionogenic groups can take place on the surface of a solid resulting in the development of surface charge. The ionization of these groups is pH dependant. This mechanism is responsible for the development of surface charge on oxides, metal hydroxides, silicates and polymers among others.
- Charge can develop by adsorption of ions. Surfaces in contact with aqueous media tend to acquire negative charge due to the fact that cations are more easily hydrated than anions.
- Unequal dissolution of ions in the case of certain ionic substances can lead to a net charge on the substrate.

- Lattice substitutions and defects which can, in many cases, lead to an exchange of one ion for another of similar ionic radius, which is known as isomorphic substitution (Figure 3.1).

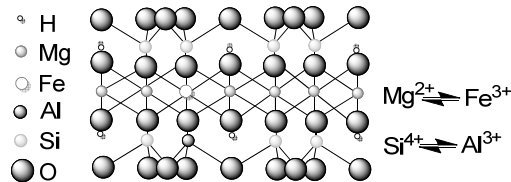


Figure 3.1 – Representation of charge development in talc $[Mg_3Si_4O_{10}(OH)_2]$ by the substitution of silicon by aluminum in the tetrahedral sheet and magnesium by iron in the octahedral sheet

3.1.2. The electrical double layer

The surface charge developed on a particle surface results in an unequal distribution of ions in the adjacent media: ions of opposite charge (counterions) are attracted to the surface, and ions of like charges (co-ions) are repelled from the surface.

As a consequence of this uneven distribution of ions in the vicinity of the particle, an increase in the potential across the interface occurs. The distribution of ions in the vicinity of the surface is important because it determines the rate of potential decay with distance into the bulk solution, which in turn influences phenomena occurring at the interface. Several models have been developed to describe the distribution (Hunter, 2001).

Helmholtz model

Helmholtz developed the earliest model of the electrical double layer over a century ago. The model considers the solution to be a plane layer with a charge opposite to that of the solid. The potential as a function of distance from the surface was solved and the model was able to explain some phenomena such the electrophoretic response (i.e., particle

motion in an electric field) but it did not account for some other phenomena such as adsorption from solution.

Gouy-Chapman model

Gouy and Chapman independently made improvements to the Helmholtz model by introducing a diffuse layer into the electrical double layer. They considered point charges whose concentration decreases exponentially from the surface into the bulk solution.

Stern-Graham model

The Stern-Graham model is commonly applied in many areas of flotation surface chemistry. The approach combined the Helmholtz and Gouy-Chapman models, giving an internal compact (Helmholtz) layer and an outer diffuse layer and replaced the point charges with ions of finite size. In addition, the concept of specific adsorption of ions within the Helmholtz layer was introduced. The plane in which specific adsorption of non-hydrated ions occurs is known as the inner Helmholtz plane (IHP), while that of the closest approach for more weakly adsorbed hydrated ions is known as outer Helmholtz plane (OHP) (Figure 3.2).

3.1.3. Ions in the double layer

The effect of chemical species on the surface charge and electric potentials determines their probable allocation at the solid-liquid interface. The potential determining ions (p.d.i.) are those species that have a fundamental control over the surface charge and the surface potential of the solid. The specifically adsorbed ions are those whose adsorption at the surface obeys forces other than electrostatic interactions. Specifically adsorbed ions can be recognized by their ability to change the iso-electric point (i.e.p.). On the other hand, the effect of non-specifically adsorbed ions is only apparent when the underlying surface is of the opposite sign. Finally, the indifferent ions are those species

that control the extent of the double layer but are not involved in any specific interaction with the surface (Hunter, 1981).

Electrokinetic (zeta) potential is the potential drop across the mobile part of the double layer, which can be assumed to be the outer Helmholtz plane (OHP). Figure 3.2 illustrates a possible ion arrangement at a negatively charged surface.

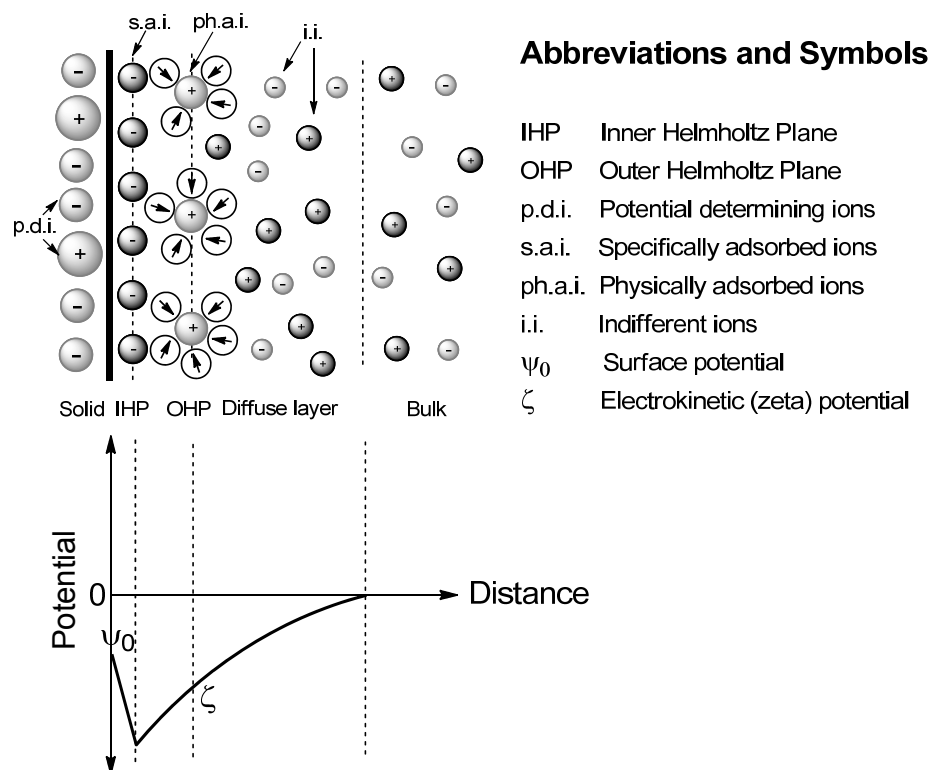


Figure 3.2 – Schema of a possible ions distribution on a surface and effect on the different potentials

3.1.4. Point of zero charge

Point of zero charge (p.z.c.) is defined as the condition at which the surface charge of a solid is zero. It is normally reported as the negative logarithm (base 10) of the molar

concentration of the potential determining ions. If the p.d.i.'s are H^+ and OH^- , the point of zero charge becomes the pH at which the surface charge is zero³.

Titration with each potential determining ion one by one is commonly used to determine p.z.c. (Ardizzone et al., 1981; Hunter, 1981; Breeuwsma and Lyklema, 1971). The technique depends on the fact that when a solid is prepared at its p.z.c. then dialyzed and dried, if it is placed in solution at the same pH as the p.z.c. at any ionic strength, the pH will not change. The procedure, described in detail by Hunter (1981), requires a precise measurement of the surface area of the sample, which is frequently difficult to obtain.

Mular and Roberts (1966) proposed a simplified titration. This technique exploits the effect on surface charge as the concentration of indifferent (background) electrolyte is changed. As with any titration method, it is only valid if there are no other competing processes.

The Mular-Robert (M-R) technique is also referred to as batch equilibration (Čerović et al., 2007; Milonjić et al., 2007). The procedure is as follows. Samples are prepared at different pH but the same ionic strength. At a given pH (pH_1) indifferent electrolyte is added to increase the ionic strength. When the new pH reading is stable, the reading is noted (pH_2). The point of zero charge is read from the plot of ΔpH (i.e., pH_2 minus pH_1) as a function of pH_2 as the pH at which ΔpH is zero.

In the M-R technique, the underlying principle is that the p.z.c. is based on the calculation of the net surface charge density, σ_0 , given by Equation 3.1 (Hunter, 1981):

³ From here on, all solids will be assumed to have H^+ and OH^- as the only potential determining ions.

$$\sigma_o = \sum_i z_i F \Gamma_i \quad 3.1$$

where F is the Faraday constant, Γ_i is the adsorption density of potential determining ion, and z_i is their corresponding valence. When p.d.i.'s are H^+/OH^- , Equation 3.1 becomes,

$$\sigma_o = F(\Gamma_{H^+} - \Gamma_{OH^-}) \quad 3.2$$

Indifferent electrolyte strongly influences the surface charge when surface potential is not zero. According to Equation 3.3 (Hunter, 1981):

$$\sigma_o = -\varepsilon \left(\frac{d\psi}{dx} \right)_{x=0} \quad 3.3$$

where ε is the permittivity of the dielectric, and $(d\psi/dx)$ the potential decay given by the Debye-Hückel approximation,

$$\frac{d\psi}{dx} = -\kappa\psi \quad 3.4$$

where the parameter κ is defined as,

$$\kappa = \left(\frac{e^2 \sum_i n_i^0 z_i^2}{\varepsilon k T} \right)^{1/2} \quad 3.5$$

and e is the elementary charge, n_i^0 the electrolyte concentration, k the Boltzmann constant, and T the absolute temperature.

In the M-R technique, ionic strength (given by indifferent electrolyte) is increased, and consequently more p.d.i.'s will be adsorbed at the surface in order to maintain a constant surface potential and κ is increased (Eq. 3.5). Thus, the rate of potential decay increases

(Eq. 3.4), which causes more p.d.i. to adsorb at the surface when $\psi \neq 0$ (Eq. 3.3). As a result, this phenomenon induces a change in pH. The p.z.c. is located where there is no change in pH.

3.1.5. Isoelectric point

The iso-electric point i.e.p. is defined as the negative logarithm (base 10) of the molar concentration of H^+ (i.e., pH) at which the zeta potential is zero (i.e., particles show no electrokinetic response).

3.1.6. Electrokinetic phenomena

Electrokinetic phenomena can be generally defined as all phenomena involving fluid motion adjacent to a charged surface. The most important electrokinetic phenomena are briefly described (Delgado et al., 2007; IUPAC, 1971).

Electro-osmosis

Electro-osmosis is the motion of a liquid through a membrane (or other porous) structure caused by the application of an electric field across the membrane. The electro-osmotic velocity, v_{eo} , is the uniform velocity of the liquid far from the charged interface. Usually, the measured quantity is the volume flow through the membrane per unit of field strength (electro-osmotic volume flow, J_v); v_{eo} and J_v are positive if the flow is in the direction of lower potential. The electro-osmotic pressure, Δp , is the pressure difference across the membrane needed to stop the electro-osmotic flow; Δp is positive if the higher pressure is on the high potential side.

Streaming potential

Streaming potential, E_{st} , is the potential difference at zero current caused by the flow of liquid under a pressure gradient through a membrane. This potential difference is created

by charge accumulation caused by the flow of counter-charges inside capillaries or pores; E_{st} is positive if the higher potential is on the high-pressure side.

Sedimentation potential

Sedimentation potential, E_{sed} , or Dorn effect, is the potential difference at zero current caused by the sedimentation of particles (or rise of bubbles) by gravitational forces (or another external force, e.g., in a centrifuge). Charge destabilization created by the fluid drag surrounding each particle induces numerous dipoles in the suspension. These individual dipoles add together to determine the macroscopic potential difference between two identical electrodes at different levels (or a different distances from the rotation axis). E_{sed} is positive if the lower (peripheral) electrode is negative.

Electrophoresis

Electrophoresis is the movement of particles in a liquid medium when a peripheral electric field (E) is applied. Electrophoretic velocity (v_e) is the velocity of the particle during electrophoresis and electrophoretic mobility (μ_e) is the velocity divided by the electric field strength. The mobility is counted as positive if the particles move toward the negative electrode and negative if they move in the opposite direction.

3.1.7. Calculation of zeta potential

Several models have been developed to calculate zeta potential from electrokinetic phenomena. In this study, zeta potential was calculated from the electrophoretic response. Thus, it is worth reviewing the models related to this phenomenon.

Experimentally, what is measured is the electrophoretic mobility, from which zeta potential is calculated. The relationship between zeta potential and electrophoretic mobility depends on the chosen model.

There are two classic models that result from two limiting conditions: the Smoluchowski and the Hückel equations. The limits are defined by the dimensionless product κa , where 'a' is the radius of the particle. If $\kappa a \ll 1$ (thick double layer case) the relationship between electrophoretic mobility and zeta potential is given by the Hückel equation; if $\kappa a \gg 1$ (thin double layer case) zeta potential can be calculated with the Smoluchowski equation. Figure 3.3 is a schematic of the two limits.

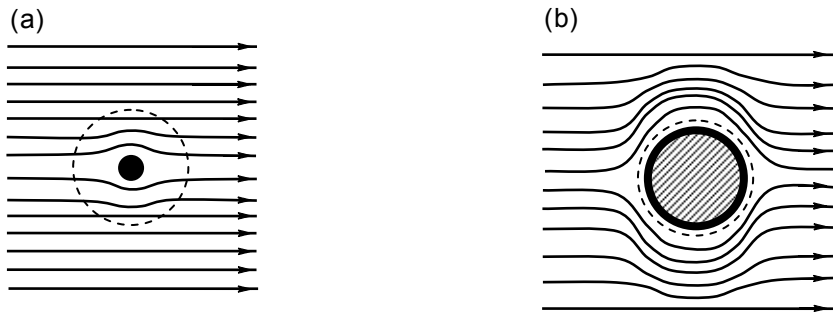


Figure 3.3 – Effect of a non-conductive particle on the applied field (a) $\kappa a \ll 1$; (b) $\kappa a \gg 1$. The broken line is at the distance of $1/\kappa$ from the particle surface (adapted from Hunter, 2001)

For nanoparticles suspended in a low concentrating electrolyte it is fairly easy to satisfy the Hückel limit. In this model Equation 3.6 defines the relationship between the electrophoretic mobility and zeta potential:

$$\mu_e = \frac{2e\zeta}{3\eta} \quad 3.6$$

For microparticles suspended in a moderate to highly concentration electrolyte the Smoluchowski limit is applicable and the equation is:

$$\mu_e = \frac{e\zeta}{\eta} \quad 3.7$$

The majority of flotation systems approach this case.

3.1.8. Zeta potential apparatus

Zeta potential measurements were performed using the micro-electrophoretic apparatus Zeta Plus (Brookhaven Instruments Corporation). This instrument determines the electrophoretic mobility and calculates zeta potential using the Smoluchowski model.

The apparatus detects particle motion using laser scattering. The laser beam passes through the sample in a cell that has two electrodes to provide the electric field. The frequency of light scattered by the particles is Doppler shifted by an amount proportional to the velocity of the particles. The scattered beam is compared to a portion of the incident beam at the detector (photomultiplier) and a frequency shift gives a signal from which both sign and magnitude of electrophoretic mobility are derived. Figure 3.4 shows a schema of the Zeta Plus instrument.

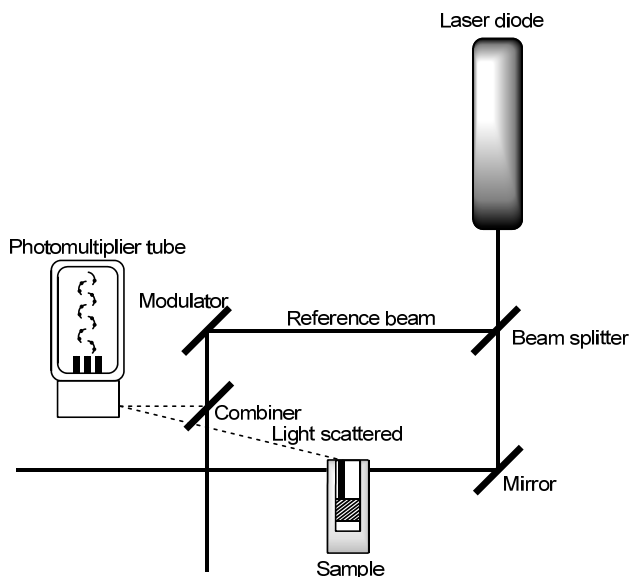


Figure 3.4 – Zeta potential apparatus

3.2. Aggregation/dispersion

Numerous methods to study the state of aggregation/dispersion have been developed. Generally, although several quantitative techniques are available, qualitative or semi-quantitative methods are frequently chosen to perform routine tests or to study complex (e.g. multi-component) systems.

The state of aggregation/dispersion can be studied by the examination of the whole system or its components (i.e., the suspended particles, the aggregates and supernatant). For studies monitoring the whole system, measures such as electrical conductance (Mirnezami et al., 2003; Vergow et al., 1997; Ecanow et al., 1982), light scattering (Moussa et al., 2007; Reinecke et al., 2000; Zentner et al., 1981) and rheological properties (Hicyilmaz et al., 2006; Shapovalov et al., 2006; Muster and Prestidge, 1995) have been used. For the inspection of an aggregated system by its components, techniques such as sedimentation (Reichert et al., 2009), microscopy (Liu et al., 2009; Zhang et al., 2008), particle size distribution (Atteia et al., 2001) and filtration (El Ouriaghly et al., 1992) have been used.

In this study a dispersion index (DI) calculated from light scatter light and optical microscopy was used to determine the state of aggregation/dispersion.

3.2.1. Dispersion index

Particles suspended in solution will aggregate or remain dispersed depending on the particle-particle interaction forces. Aggregates usually settle faster than individual particles, thus, dispersion index calculated from light scatter is a convenient, albeit indirect measure.

The tests were conducted in a quartz cell in a UV/Visible spectrophotometer (Helios) set at a wavelength of 550 nm. Dispersion index was reported as the slope of the absorbance-time curve within the linear section. The technique proved straightforward, and suited to the small amount of sample available. Figure 3.5 shows the experimental setup.

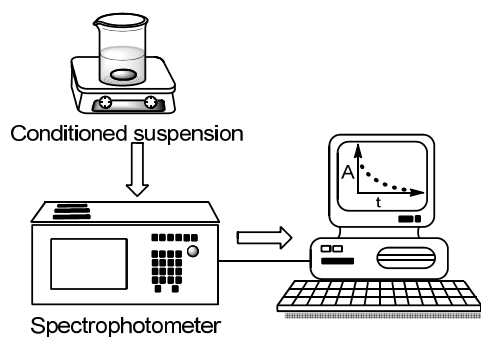


Figure 3.5 – Schematic arrangement for dispersion index measurements

3.2.2. Light microscopy

Optical (or light) microscopy is useful for visual examination of the state of aggregation/dispersion. It has the advantage that size and shape of aggregated and individual particles can be monitored *in-situ*, at least for particles larger than ca. 200 nm. Electronic microscopy can handle smaller particles, but the required sample preparation prior the inspection may distort the actual state of the aggregates (Kissa, 1999).

In this study, images of diluted suspension samples were taken rather than individual aggregates. After sample conditioning, a pipette was used to transfer the sample of the suspension to a beaker and the sample diluted several times with supernatant. A sub-sample was withdrawn and placed in a Petri dish and examined under a petrographic microscope (Leitz Laborluz 11POL) equipped with a video camera (Sony CCD Iris).

3.3. Hydrophobicity and floatability

Flotation relies on mineral particles suspended in water attaching to passing gas bubbles. The bubble must displace water from the surface and make an effective contact; in other words, the mineral must be hydrophobic (Rao and Leja, 2004). A measure of hydrophobicity is the contact angle.

The floatability can be defined as the response of minerals to the flotation process. Thus parameter is closely related to the hydrophobicity.

3.3.1. Contact angle

The methods that have been developed for measurement of contact angle applicable to mineral surfaces can be divided into two main groups: ones applicable to flat, smooth surfaces (e.g., captive bubble technique), and ones used for particles (e.g., capillary penetration method).

Measurement of contact angle using the captive bubble technique is popular due to its simplicity and small sample mass requirements. The technique is not universally accepted as providing a measure relevant to flotation processes. One argument is that real solid surfaces are heterogeneous, composed of hydrophobic micro-domains coexisting with hydrophilic areas (Rao and Leja, 2004).

In counterpoint, there are examples of successful description of flotation systems by contact angle measurements using the captive bubble technique. Contact angle measurements continue to show a correlation between hydrophobicity and flotation recovery and between hydrophobicity and adsorption of reagents (Dávila-Pulido, 2010; Beaussart et al., 2009; Holuszko et al., 2008; Mierczynska-Vasilev et al., 2008; Beattie et al., 2006; Osasere, 2000).

The main experimental challenge in this technique lies in obtaining a clean, flat mineral surface giving reproducible results. To address this problem, the experimental procedure proposed by Wark and Cox (1934) as reported by Chau (2009) was adopted. The technique consists of abrasion and/or polishing under distilled, deoxygenated water using a meticulously controlled environment. The specimen is then ultrasonicated (to remove particles of abrasive material and abraded mineral left on the surface after polishing) and dried in an oxygen-free environment. After conditioning, the sample was transferred to the experimental setup (Figure 3.6). A bubble of about 1 mm in diameter produced by a digital syringe was placed in contact with the sample. Finally, a picture was taken and processed with an image analyzer to determine the contact angle.

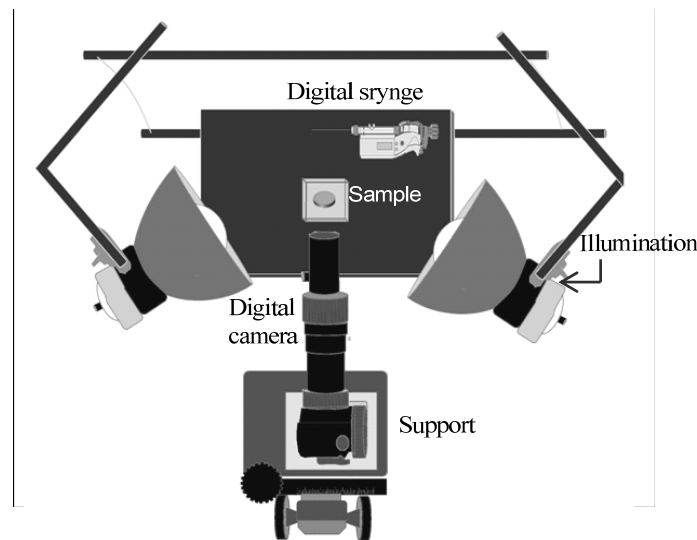


Figure 3.6 – Top view of the platform for contact angle measurements (modified from Dávila-Pulido, 2010)

3.3.2. Small-scale flotation

The flotation tests were carried out in the cell described by Partridge and Smith (1971). The device is made of glass closed with a fritted glass disc at the bottom of the cell where the gas is introduced. The cell had a transversal area of 5.3 cm² and a height of ca. 26 cm

(Figure 3.7). It proved easy to use on small (ca. 1 g) samples. The mineral was maintained in suspension with a magnetic stirring bar. Gas (nitrogen) rate was set at 23 mL/min, equivalent to a superficial velocity of 0.072 cm/s.

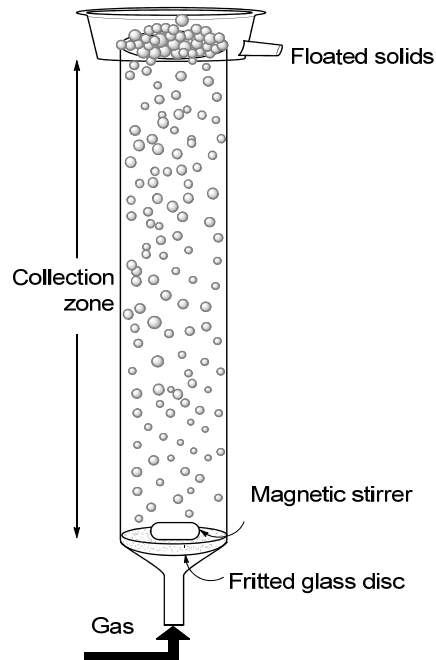


Figure 3.7 – Schematic of the Partridge/Smith cell

3.4. Characterization instruments

3.4.1. Particle size distribution

Laser particle size analyzers models LS100 (Coulter) and LA 920 (Horiba) was used for particle size distribution of the powdered samples. The instruments use an optical laser system.

3.4.2. Elemental analysis

Metal composition was determined by acid digestion followed by atomic absorption spectroscopy (AAS) model AA240FS (Varian). The analytical sensitivities of the elements are shown in Table 3.1.

An inductively coupled plasma-optical emission spectrometer (ICP-OES) model Trace Scan (Thermo Scientific) was also used for elemental analysis. The detection limits of the elements are shown in Table 3.1.

Table 3.1 – Detection limits and analytical sensitivity for some elements in inductively coupled plasma-optical emission spectrometry and atomic absorption spectroscopy

Element	Detection limit (ICP-OES), mg/L	Analytical sensitivity (AAS), mg/L
Sodium	0.21	0.0066
Magnesium	0.014	0.0033
Calcium	---	0.0176
Potassium	0.35	0.0088
Iron	0.0045	0.055
Cobalt	0.029	0.055
Nickel	0.008	0.0044
Copper	0.0076	0.0033
Zinc	0.0089	0.0066
Lead	0.051	0.11

3.4.3. Electron microprobe

The JEOL JXA-8900 Electron Microprobe with Wavelength Dispersive Spectrometer detector was used for spot chemical analysis at a scale of a few micrometers. This allowed the detection of elemental composition within an individual crystal of pentlandite. The operating conditions were: accelerating voltage 20 kV, beam current 30 nA.

3.4.4. X-ray diffraction

An X-Ray diffractometer Philips PW1710 with rotating Cu anode was used for mineral phase identification. The X-ray tube was set at 40 kV and 20 mA. X'pert Quantify and X'Pert High Score software were used for data acquisition and phase analysis, respectively.

3.4.5. Scanning electron microscopy

The Philips XL30 field emission gun system scanning electron microscope was used for the morphological characterization (secondary electrons) and elemental analysis of the samples (energy dispersive spectroscopy).

References

- Atteia O., Mondì C., Perret D. (2001) Aggregation rates of natural particle populations. *Water Research* 35: 2429-2434
- Ardizzone S., Siviglia P, Trasatti S. (1981) The point of zero charge of ruthenium dioxide. *Journal of Electroanalytical Chemistry* 122, 1981, 395-401
- Breeuwsma A., Lyklema J. (1971) Interfacial electrochemistry of haematite (α -Fe₂O₃). *Discussions of Faraday Society* 52: 325-333
- Beattie D.A., Huynh L. Kaggwa G.B., Ralston J. (2006) Influence of adsorbed polysaccharids and polyacrylamides on talc flotation. *International Journal of Mineral Processing* 78: 238-249
- Beaussart A., Mierczynska-Vasilev A., Beattie D. (2009) Adsorption of dextrine on hydrophobic minerals. *Langmuir* 25(17): 9913-9921

- Čerović L.S., Milonjić S.K., Todorović M.B., Trtanj M.I., Pogozhev Y.S., Blagoveschenskii Y. Levashov E.A. (2007) Point of zero charge of different carbides. *Colloids and Surfaces. Section A: Physicochemical and Engineering Aspects* 297: 1-6
- Chau T.T. (2009) A review of the techniques for measurement of contact angles and their applicability on mineral surfaces. *Minerals Engineering* 58: 67-65
- Dávila-Pulido G.I., (2010) Estudio Experimental sobre los Mecanismos de Activación y Depresión de Esfalerita (Experimental Study of Activation and Depression of Sphalerite) MSc Thesis, Centro de Investigación y Estudios Avanzados del IPN Unidad Saltillo
- Delgado A.V., Gonzalez-Caballero F., Hunter R.J., Koopal L.K., Lyklema J. (2007) Measurement and interpretation of electrokinetic phenomena. *Journal of Colloid and Interface Science* 309: 194-224
- Ecanow B., Webster J.M., Blake M.I. (1982) Conductivity studies of suspension systems in different states of aggregation. *Journal of Pharmaceutical Sciences* 71: 456-457
- El Ouriaghli T., Francois J., Sarazin D., Nguyen T. D. (1992) Influence of nonionic surfactant on aggregation state of scleroglucan in aqueous solution. *Carbohydrate Polymers* 17: 305-312
- Hicyilmaz, C., Oezuen S., Altun N. E. (2006) Rheological properties of asphaltite-water surries. *Energy and Fuels* 20: 2037-2045

Holuszko M.E., Franzidis J.P., Manlapig E.V., Hampton M.A., Donose B.C., Nguyen A.V. (2008) The effect of surface treatment and slime coating on ZnS hydrophobicity. *Minerals Engineering* 21: 958-966

Hunter R.J., *Zeta Potential in Colloid Science—Principles and Applications*, Academic Press, New York, NY, USA, 1981

Hunter R.J. *Foundations of Colloid Science*, Oxford University Press, Oxford, OXON, U.K., 2001

International Union of Pure and Applied Chemistry, Division of Physical Chemistry (1971) *Manual of symbols and terminology for physicochemical quantities and unites. Appendix II: Definitions, terminology and symbols in colloid and surface chemistry*. London Butter Worths

Kissa E. *Dispersions. Characterization, Testing, and Measurements*. Surfactant Science Series Vol. 84. Marcel Dekker. New York, NY, USA, 1999

Liu J., Aruguete D.M., Murayama M., Hochella M.F. (2009) Influence of size and aggregation on the reactivity of an environmentally and industrially relevant nanomaterial (PbS). *Environmental Science and Technology* 43: 8178-8183

Mierczynska-Vasilev A., Ralston J., Beattie D. (2008) Adsorption of modified dextrans in talc: effect of surface coverage and hydration water on hydrophobicity reduction. *Langmuir* 24: 6121-6127

Milonjić S.K., Čerović L.S., Čokeša D.M., Zec S. (2007) The influence of cationic impurities in silica on its crystallization and point of zero charge. *Journal of Colloid and Interface Science* 309: 155-159

Mirnezami M., Restrepo L., Finch, J.A. (2003) Aggregation of sphalerite: role of zinc ions. *Journal of Colloid and Interface Science* 259: 36-42

Moussa A.S., Soos M., Sefcik J., Morbidelli M. (2007) Effect of solid volume fraction on aggregation and breakage in colloidal suspensions in batch and continuous stirred tanks. *Langmuir* 23: 1664-1673

Mular A.L., Roberts R.B., (1966) A simplified method to determine isoelectric points of oxides. *Transactions of the Canadian Institute of Mining and Metallurgy*, 69, 438-439

Muster T.H., Prestidge C.A. (1995) Rheological investigations of sulfide mineral slurries. *Minerals Engineering* 8: 1541-55

Osasere O.F. (2000) Relation of contact angle data to Hallimond tube flotation of coal with coagulants and flocculants. *Fuel*, 79: 193-199

Partridge A.C., Smith G.W. (1971) Small-sample flotation testing: a new cell. *Institution of Mining and Metallurgy Transactions. Section C: Mineral Processing and Extractive Metallurgy* 80: C199-C200

Rao S.R., Leja J. *Surface Chemistry of Froth Flotation*, Kluwer Academic Publishers, New York, N.Y. USA, 2004

Reichert J.M., Norton L.D., Favaretto N., Huang C., Blume E. (2009) Settling velocity, aggregate stability, and interrill erodibility of soils varying in clay mineralogy. *Soil Science Society of America Journal* 73: 1369-1377

Reinecke H., Mijangos C., Lopez D. Guenet J.M. (2000) Light-scattering study of thermoreversible aggregates from chemically modified PVCs: outcomes for the gel state. *Macromolecules* 33: 2049-2054

Shapovalov N.A., Slyusar' A.A., Slyusar' O.A. (2006) The effect of oligomeric electrolytes on the aggregative stability and rheological properties of aqueous mineral suspensions. *Colloid Journal* 68: 350-356

Shaw D. J. (1969) *Electrophoresis*, Academic Press: New York, NY, USA

Vergouw J.M., Anson J., Dalhke R., Xu Z., Gomez C., Finch J.A. (1997) An automated data acquisition technique for settling tests. *Minerals Engineering*, 10: 1095-1110

Zhang Y., Gittins D. I., Skuse D., Cosgrove T., van Duijneveldt J. S. (2008) Composites of kaolin and polydimethylsiloxane. *Langmuir* 24: 12032-12039

Zentner G.M., Cardinal J. R., Kim S. W. (1981) Free fatty acid-induced platelet aggregation: studies with solubilized and nonsolubilized fatty acids. *Journal of Pharmaceutical Sciences* 70: 975-81

Point of zero charge and isoelectric point of phyllosilicate minerals

Abstract

The point of zero charge of electrokinetically anisotropic minerals (chlorite and serpentine) was determined using the Mular-Roberts (M-R) titration technique, and compared to the isoelectric point obtained from electrophoretic mobility measurements. To validate the M-R technique, the point of zero charge and isoelectric point of two isotropic minerals (alumina and silica) were shown to be comparable.

For serpentine and chlorite, respectively, the point of zero charge was found at pH 4.3 and 4.6, while the isoelectric point occurred at pH 3.2 and <3. Aggregation/dispersion tests using light scattering showed the highest dispersion index (DI) for chlorite over a

pH ranging from the i.e.p. to the p.z.c., suggesting that aggregation/dispersion is determined by the charge at both the edge and the face. Serpentine remained largely dispersed over the tested pH range.

4.1. Introduction

Magnesium silicates (MgO-minerals) are significant constituents of the gangue associated with nickel minerals (mainly pentlandite) in mafic and ultramafic ores (Edwards et al., 1980). A significant factor affecting flotation selectivity is considered to be through MgO-mineral slime coating on pentlandite particles. The extent of slime coating is principally controlled by the surface charge of the associated minerals. Isoelectric point (abbreviated to i.e.p. according to the convention adopted by IUPAC in 1972) estimated from zeta potential measurements is frequently used to predict the probability of slime coating occurring in a system. However, this may not be appropriate in the case of some MgO-minerals.

For the class of MgO-gangue classified as phyllosilicate mineral (e.g., serpentine, talc and chlorite depicted in Figure 4.1), the isoelectric point may differ depending whether measurement is on the edge or face (Nalaskowski et al., 2007; Fuerstenau and Pradip, 2005). This is because phyllosilicates are electrokinetically anisotropic due to their structure. These minerals are built of tetrahedral sheets bonded by octahedral sheets (Ciullo, 1996). The tetrahedral and octahedral sheets form stable structural units (layers), which are held together by van der Waals forces. During comminution, two kinds of surfaces are formed, one produced by cleavage along the layers (basal plane or face), and the other perpendicular to the face, created from breakage of chemical bonds (edge). The faces have a permanent charge, independent of pH, which may develop through lattice defects (e.g., vacancies and substitution) or incongruent dissolution (Fuerstenau and Pradip, 2005; Lyklema et al., 1991; Shaw, 1969). In contrast, the edge behaves as a mixed oxide (being acidic from the Si tetrahedral and basic from Mg octahedral) and its surface charge exhibits strong pH dependence (Fuerstenau and Pradip, 2005; Lyklema et

al., 1991; Leja, 1983). Consequently, these minerals do not have a single defined i.e.p. (Nalaskowski et al., 2007), making it impossible, for example, to infer the point of zero charge (p.z.c. in the same convention) from the i.e.p. Therefore, the use of other techniques to establish the p.z.c. is pertinent.

Potentiometric titration is a technique for measuring the point of zero charge (Ardizzone et al., 1981; Breeuwsma and Lyklema, 1971). This technique requires a precise measurement of the surface area of the particulate sample, which is frequently difficult to obtain (Hunter, 1981). Mular and Roberts (1966) proposed a simplified titration method. It exploits the effect on surface charge as the concentration of indifferent (background) electrolyte is changed. As with any titration method, it is only valid if there are no other processes competing for the potential determining ions.

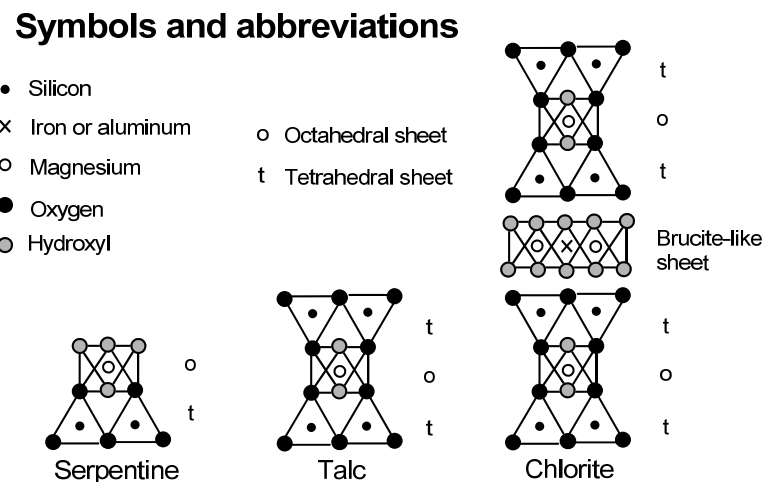


Figure 4.1 – Sketch diagrams of serpentine $[\text{Mg}_3\text{Si}_2\text{O}_5(\text{OH})_4]$, talc $[\text{Mg}_3\text{Si}_4\text{O}_{10}(\text{OH})_2]$ and chlorite $[(\text{Mg},\text{Fe}^{2+})_5(\text{Al},\text{Fe}^{3+})_2\text{Si}_3\text{O}_{10}(\text{OH})_8]$. Structures viewed parallel to the sheets

In the Mular and Roberts (M-R) technique the samples are prepared at different pH, but the same ionic strength (IS). The pH at IS_1 is recorded: pH_{IS_1} . By adding indifferent

electrolyte, the ionic strength is changed from IS_1 to IS_2 and when the new pH reading is stable, the value is noted: pH_{IS2} . From a plot of ΔpH ($= pH_{IS1} - pH_{IS2}$) as a function of pH_{IS2} , the pH at which ΔpH equals zero (i.e., where there is no effect on pH by changing ionic strength) corresponds to the point of zero charge.

The aim of the chapter is first to validate the M-R technique using electrokinetically isotropic minerals then to use the method to determine the p.z.c. of some phyllosilicate minerals encountered in processing ultramafic nickel ores and to compare the p.z.c. to the i.e.p. determined from zeta potential measurements. Dispersion index is subsequently used to determine which of the values, i.e.p. or p.z.c., controls state of aggregation/dispersion, a system property that may be relevant to flotation.

4.2. Experimental

4.2.1. Minerals

Two electrokinetically isotropic minerals, high purity alumina (Sigma-Aldrich) and silica (Fisher) were used in the validation tests. The anisotropic minerals were serpentine, chlorite and talc (Ward's Natural Science Establishment). These samples were crushed, pulverized and wet sieved to isolate the $-25 \mu m$ fraction.

Powder X-Ray Diffraction (XRD) was used for mineralogical examination (Philips P1770 with rotating Cu anode set at 40 kV and 20 mA; X'Pert Quantify and X'Pert High Score software were used for data acquisition and phase identification, respectively). The detection limit is about 5 %.

4.2.2. Determination of isoelectric point

An electrophoretic method (ZetaPlus Brookhaven Instruments) using the Smoluchowski approximation was used to measure zeta potential from electrokinetic mobility.

Suspensions were prepared using 0.1 g of solid in 500 mL distilled, deionized water (resistivity, 18.3 M Ω /cm). They were aged 24 hours (except when otherwise indicated) to reach chemical equilibrium before measurement. The experiments were performed using two KCl concentrations (viz., 10⁻² mol/L and 10⁻³ mol/L) as supporting electrolyte. The pH was adjusted using either KOH or HCl over the pH range 3-10 respecting the manufacturer's recommended limits. The pH was recorded 15 minutes after adjustment. The results reported are the average of at least two full repeat experiments. The error bar on the Figures represents the 95% confidence interval.

4.2.3. Dissolution

Suspensions were prepared at a mass fraction of 10 % and agitated overnight at ca. 21 ° C. Final pH values were noted. Samples were filtered to obtain the supernatant. Magnesium, iron and aluminum were measured using AAS.

4.2.4. Effect of Mg²⁺ concentration on zeta potential

The magnesium ions released into solution (see 'dissolution' above) are possible potential determining ions (p.d.i.) other than H⁺ and OH⁻; these experiments test, therefore, whether the M-R titration technique is applicable. Three concentrations of magnesium, added as MgCl₂·6H₂O (Anachemia, analytical grade) were used (typically 10⁻³, 5×10⁻⁴ and 10⁻⁴ mol/L). Suspensions were equilibrated for 24 hours, and the zeta potential measured at an acid, natural and alkaline pH.

4.2.5. Determination of point of zero charge

The mineral suspensions were prepared with 1 g of sample in 10⁻² mol/L KCl. The pH was adjusted to arbitrary values, using either KOH or HCl concentrated solution, and aged 24 hours before recording pH (i.e., pH_{IS1}). The required amount of solid KCl to increase the ionic strength ten-fold was added to each beaker. The suspension was

agitated using a magnetic stirrer to facilitate KCl dissolution. The final pH (i.e., pH_{IS2}) was recorded after it stabilized.

4.2.6. Aggregation/dispersion tests

Suspensions were prepared using 0.5 g of mineral in 100 mL of 10^{-2} mol/L of KCl solution and equilibrated for 24 hrs. Solids were maintained in suspension with a magnetic stirrer and the pH was adjusted using either KOH or HCl concentrated solution. The sample was transferred to a spectrographic cell to measure absorbance as a function of time using a UV/Visible spectrophotometer (Helios, Thermo) at a wavelength of 550 nm. The dispersion index reported is the slope of absorbance vs. time. The technique proved suited to the small quantity of sample available. The results are the average of at least two full repeats. Error bars on the Figures show the 95 % confidence interval.

4.3. Results

4.3.1. Mineralogical characterization

From XRD analysis, serpentine was identified as lizardite, chlorite as clinochlore with traces of serpentine-chlorite, and talc as steatite (Table 4.1).

Table 4.1 – Mineralogical characterization (XRD) of samples

Sample	General Formula	Specific gravity	Mineral Identified
Serpentine	$\text{Mg}_3\text{Si}_2\text{O}_5(\text{OH})_4$	2.3	Lizardite
Chlorite	$(\text{Mg},\text{Fe}^{2+})_5(\text{Al},\text{Fe}^{3+})_2\text{Si}_3\text{O}_{10}(\text{OH})_8$	2.6-3.3	Clinochlore minor serpentine-chlorite
Talc	$\text{Mg}_3\text{Si}_4\text{O}_{10}(\text{OH})_2$	2.7-2.8	Steatite

4.3.2. Validating M-R technique

The isoelectric point of alumina was found at pH 7.9 (Figure 4.2), a value similar to the point of zero charge measured by the M-R technique, pH 8.1 (Figure 4.3). Agreement between the two values was also found for silica: i.e.p. pH <3 (Figure 4.2) and p.z.c. pH ~2 (Figure 4.4). The values of i.e.p. in both cases are within the range reported in literature: for alumina pH 5 to 9.2, and for silica pH 1.6 to 3.5 (Kosmulski, 2002, 2004; Parks, 1965). For silica, it should be noted that to determine the point of zero charge, it was necessary to adjust the initial pH to <2. To mask the effect of the ionic strength contributed by this high acid condition, the initial indifferent electrolyte concentration was 0.1 mol/L and was increased to 1 mol/L.

In the case of alumina, the effect of the magnitude of the change in ionic strength on p.z.c. was explored (Figure 4.3). The p.z.c. was not affected, although as expected the larger change in ionic strength resulted in a greater change in pH (as a consequence of more potential determining ions being adsorbed).

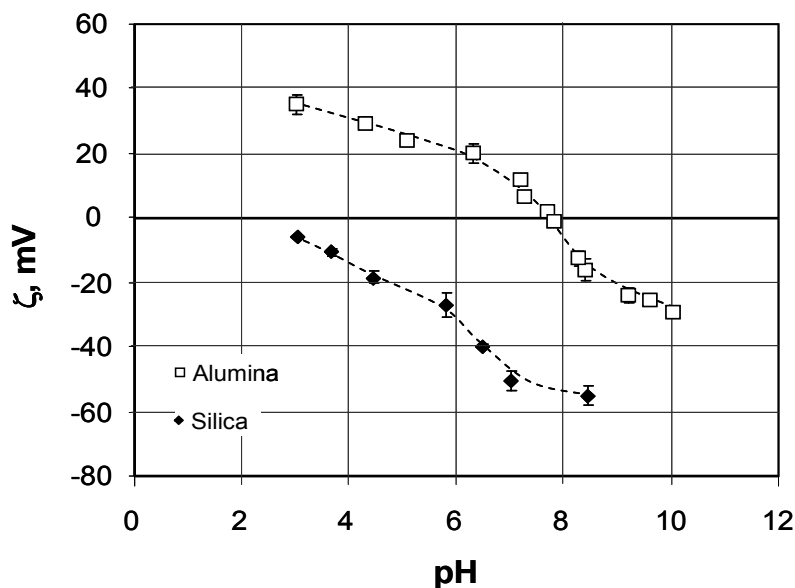


Figure 4.2 – Zeta potential of alumina (open squares) and silica (filled diamonds) as a function of pH. IS = 10^{-2} mol/L using KCl; i.e.p. occurs at ca. pH 7.9 and <3, respectively. The error bars represent the 95 % confidence interval from three observations

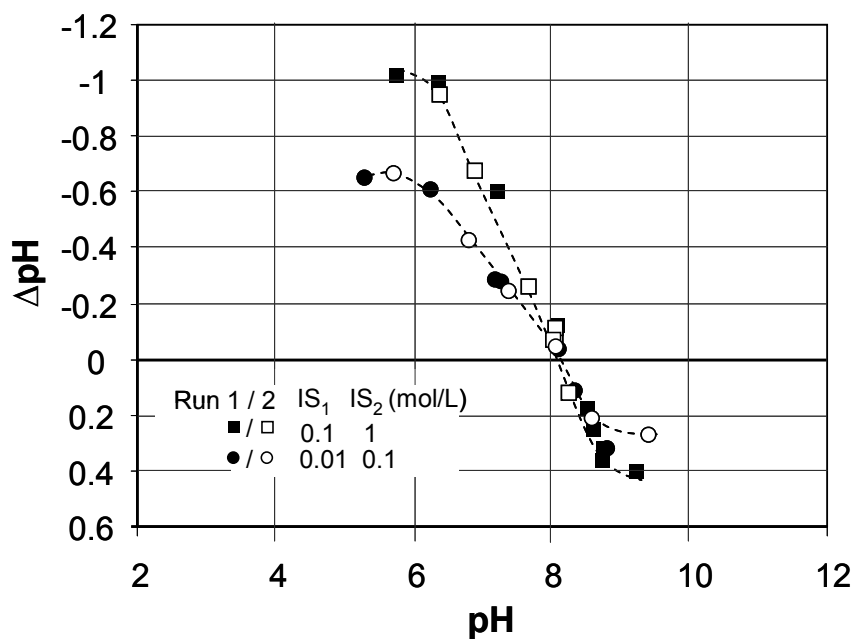


Figure 4.3 – ΔpH as a function of pH_{IS_2} for alumina. IS changed from 10^{-2} mol/L to 0.1 mol/L (circles), and from 0.1 mol/L to 1 mol/L (squares) using KCl; p.z.c. observed at ca. pH 8.1

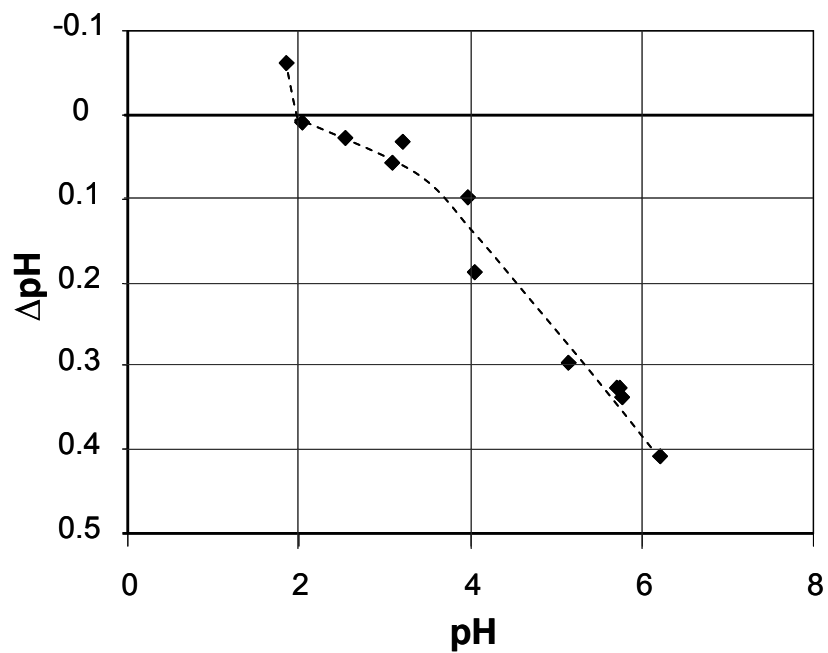


Figure 4.4 – ΔpH as a function of pH_{IS_2} for silica. IS changed from 0.1 mol/L to 1 mol/L; p.z.c. observed at ca. pH 2

4.4.3. Isoelectric point and effect of some experimental conditions

Effect of aging and solid/liquid ratio

The effect of aging is shown in Figures 4.5 to 4.7. Fresh and aged chlorite produced similar values, with i.e.p. at pH <3 (Figure 4.5). The same behaviour was observed with talc, where fresh and aged samples gave i.e.p. at pH <3 (Figure 4.7). In contrast, aging of serpentine resulted in a significant change in i.e.p. (Figure 4.6); the i.e.p. decreased from ca. pH 8 for the fresh sample to ca. pH 4 for the 24-hr aged sample which then remained constant. This aging effect on serpentine dictated the use of 24-hr aged samples for the comparison of i.e.p. and p.z.c.

The effect of solid/liquid ratio is shown for 'aged' chlorite in Figure 4.5. This variable did not change the zeta potential significantly. The value was fixed at the highest solid/liquid ratio, respecting equipment constraints (i.e., ~200 mg/L), to make the measurement less sensitive to possible contamination effects.

Figure 4.8 establishes that KCl is an indifferent electrolyte, as changing concentration did not affect the i.e.p. for either serpentine or chlorite (but the higher concentration did decrease zeta potential due to 'double layer compression').

Species dissolution

Species released from minerals and later chemisorbed may change their i.e.p. Magnesium, iron and aluminum ions were chosen as likely solution constituents of the phyllosilicate minerals examined. After aging for 24 hours in KCl solution at natural pH, the supernatant of serpentine and chlorite was tested by atomic absorption spectroscopy. Neither iron nor aluminum was detected; however, magnesium was released: for serpentine ca. 0.3 mg of Mg²⁺ per gram of sample, for chlorite 0.25 and talc 0.4.

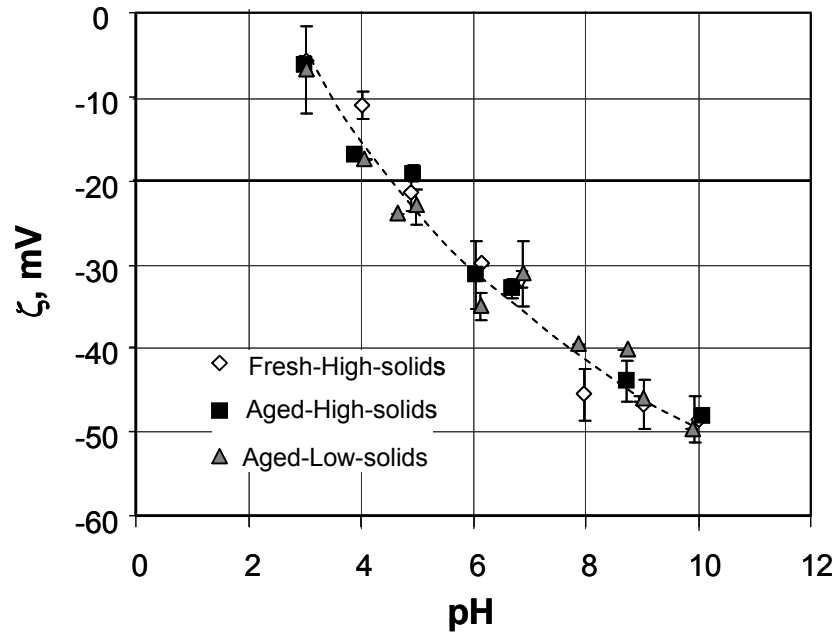


Figure 4.5 – Zeta potential of chlorite as a function of pH for aged (24-hr) and fresh samples. IS = 10^{-2} mol/L using KCl. Solid-liquid ratio was 200 mg/L (filled squares and open diamonds) and 100 mg/L (filled triangles)

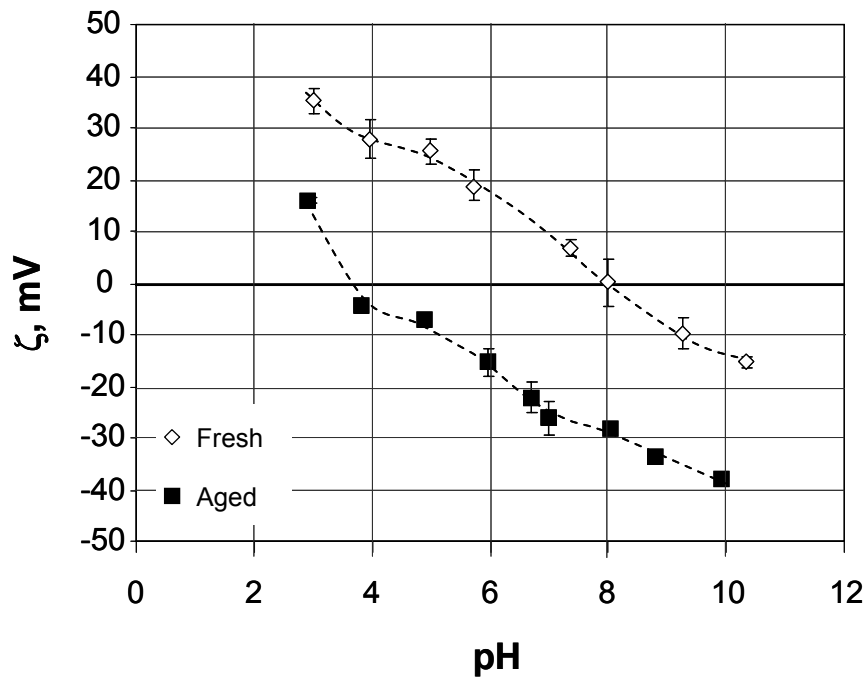


Figure 4.6 – Zeta potential of serpentine as a function of pH for aged (filled squares) and fresh (open diamonds) samples. IS = 10^{-2} mol/L using KCl

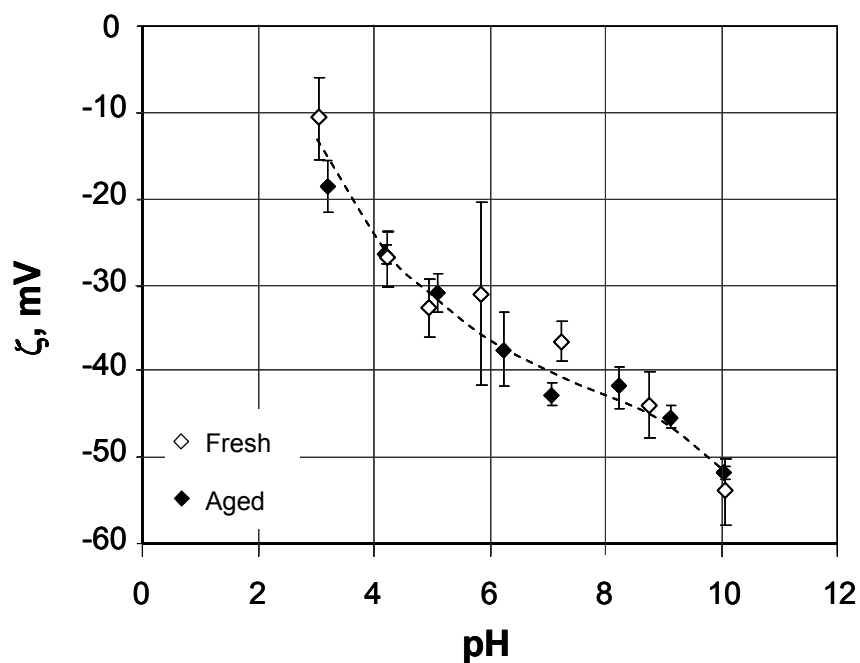


Figure 4.7 – Zeta potential of talc as a function of pH for 24-hr aged (filled diamonds) and fresh (open diamonds) samples. IS = 10^{-2} mol/L using KCl

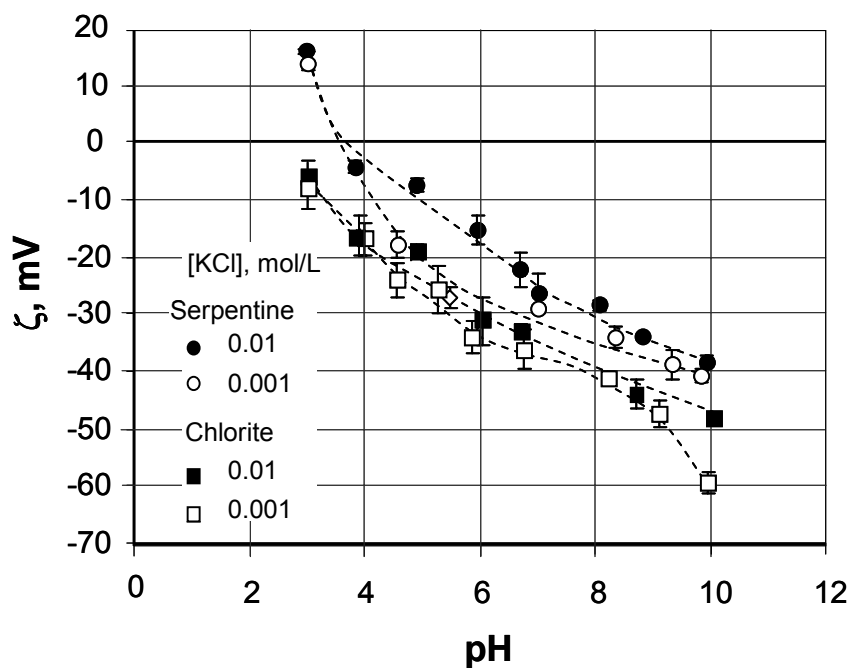


Figure 4.8 – Zeta potential of serpentine (circles) and chlorite (squares) as a function of pH for 24-hr aged samples. IS = 10^{-2} (filled symbols) and 10^{-3} mol/L (open symbols) using KCl

Effect of Mg^{2+}

It is understood that any titration technique for p.z.c. determination is only valid provided there are no p.d.i. other than H^+ and OH^- ions. Given its detected release, the effect of magnesium ions on zeta potential was tested.

For chlorite and serpentine (Figures 4.9, and 4.10, respectively), changes in zeta potential as a consequence of Mg^{2+} addition were negligible from acid to near neutral pH, although there was an effect at alkaline pH. In the case of talc (Figure 4.11), however, differences in zeta potential were observed over the full pH range tested, suggesting an exchange of Mg^{2+} between the mineral surface and the solution (i.e., Mg^{2+} is a p.d.i.). Subsequent titration test work proved unrepeatable and measurement of p.z.c. for talc was not pursued.

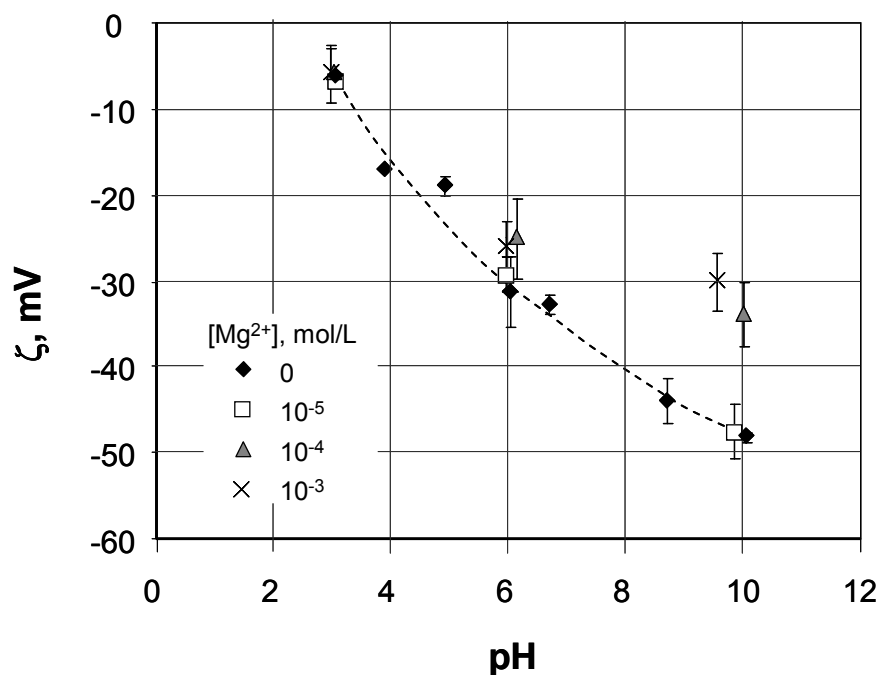


Figure 4.9 – Zeta potential of chlorite as a function of pH in 10^{-2} mol/L KCl for 0 mol/L (filled diamonds), 10^{-5} mol/L (open squares), 10^{-4} mol/L (filled triangles) and 10^{-3} mol/L (crosses) of magnesium

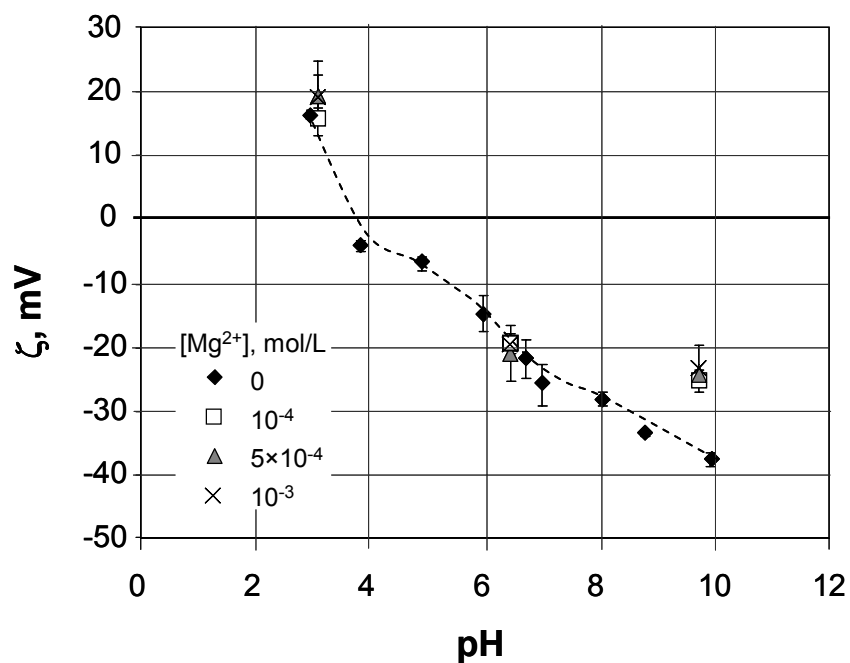


Figure 4.10 – Zeta potential of serpentine as a function of pH in 10^{-2} mol/L KCl for 0 mol/L (filled diamonds), 10^{-5} mol/L (open squares), 10^{-4} mol/L (filled triangles) and 10^{-3} mol/L (crosses) of magnesium

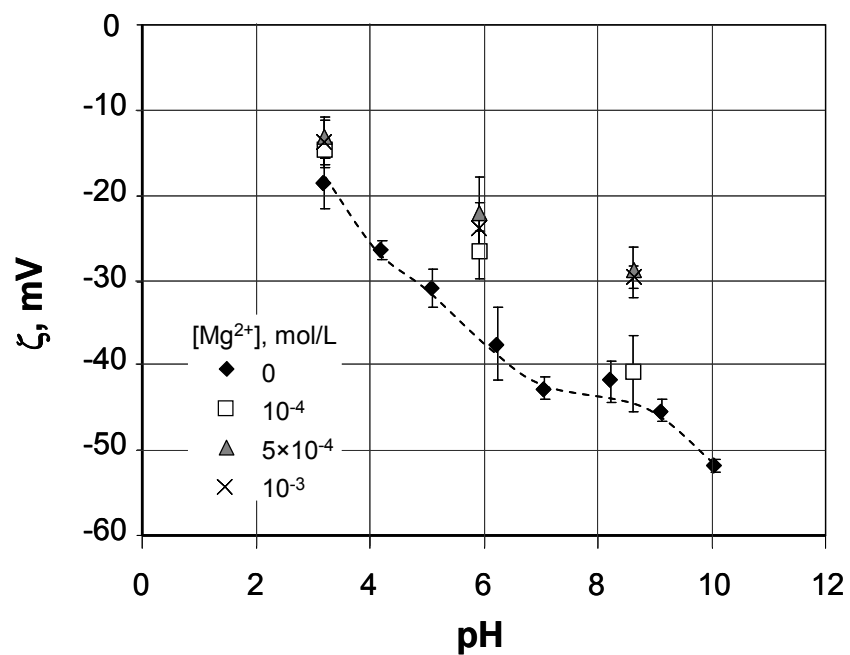


Figure 4.11 – Zeta potential of talc in 10^{-2} mol/L KCl for 0 mol/L (filled diamonds), 10^{-5} mol/L (open squares), 10^{-4} mol/L (filled triangles) and 10^{-3} mol/L (crosses) of magnesium

4.4.4. Point of zero charge

Figures 4.12 and 4.13 show ΔpH as a function of pH for chlorite and serpentine, respectively. The p.z.c. was found at pH 4.6 for chlorite and 4.3 for serpentine, regardless of the range of ionic strength used, as illustrated for chlorite (Figure 4.12). The p.z.c. values are significantly higher than the i.e.p. for these same 24-hr aged samples. Since the electrophoretic technique reflects the average zeta potential developed on both face and edge, the higher value of p.z.c. compared to i.e.p. may infer that the face is negatively charged. The same procedure failed to produce repeatable results for talc.

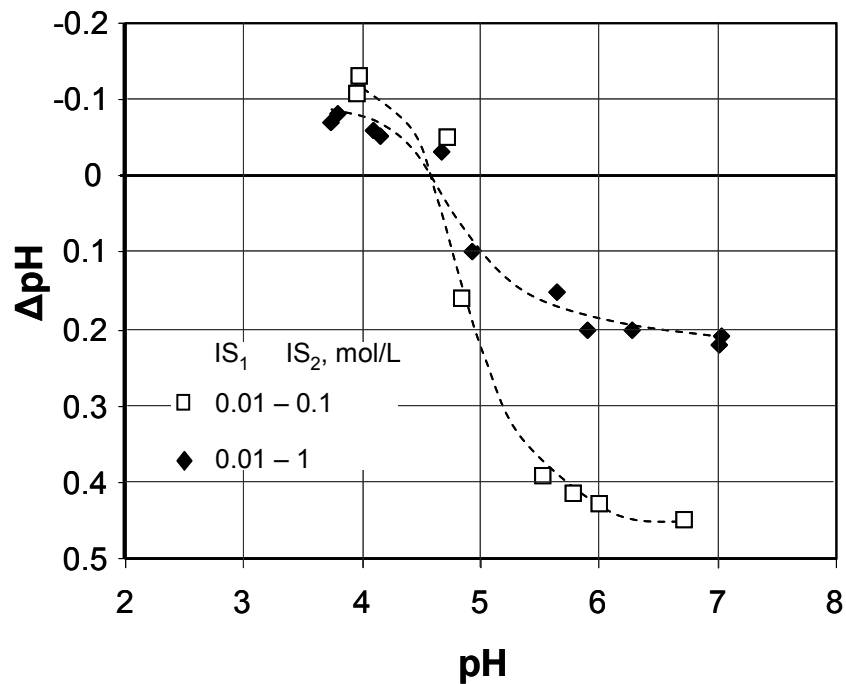


Figure 4.12 – ΔpH as a function of pH_{IS_2} for chlorite. IS changed from 10^{-2} mol/L to 0.1 mol/L (filled diamonds), and from 10^{-2} mol/L to 1 mol/L (open squares) using KCl. p.z.c. was observed at ca. pH 4.6

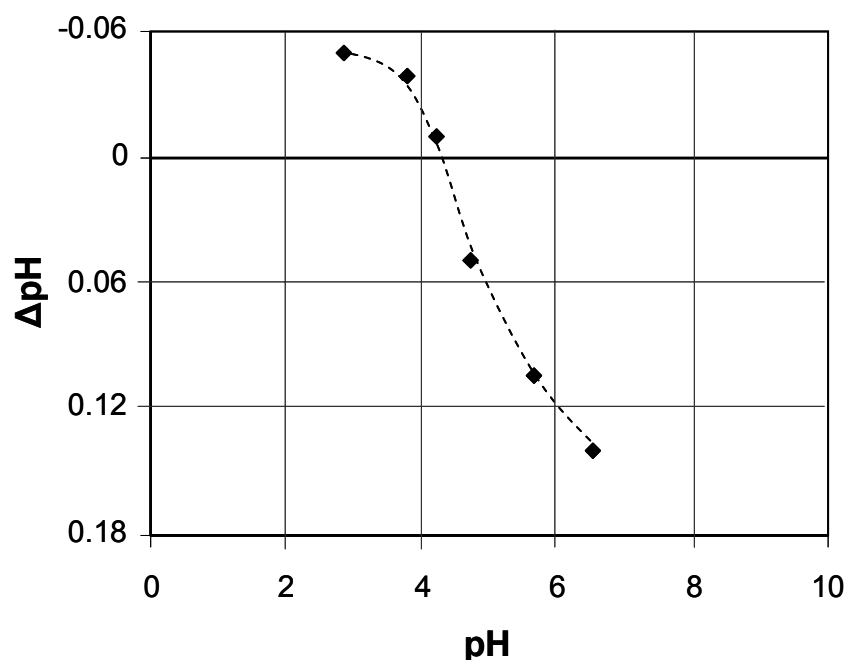


Figure 4.13 – ΔpH as a function of $\text{pH}_{\text{IS}2}$ for serpentine. IS change was from 10^{-2} mol/L to 0.1 mol/L using KCl. p.z.c. was observed at pH ca. 4.3

The i.e.p. and p.z.c. results for samples tested are summarized in Table 4.2.

Table 4.2 – Comparison between i.e.p. and p.z.c. for phyllosilicate minerals tested

Sample	i.e.p.	p.z.c.
Chlorite	<3	4.6
Serpentine	3.3	4.3
Talc	<3	ND

4.4.5. Aggregation/dispersion tests

Dispersion index calculated from turbidimetry was used to determine whether i.e.p. or p.z.c. controls aggregation/dispersion: high dispersion index is associated with aggregation, which is usually counter-productive for flotation (e.g. Silvestre et al., 2009). For chlorite, the maximum dispersion index was reached between pH 2.5 to 5.5; for serpentine, no definite maximum was observed (Figure 4.14).

The chlorite, therefore, showed aggregation over the range from the i.e.p. (less than pH 3) to the p.z.c. (4.6); i.e., both surface properties seem involved.

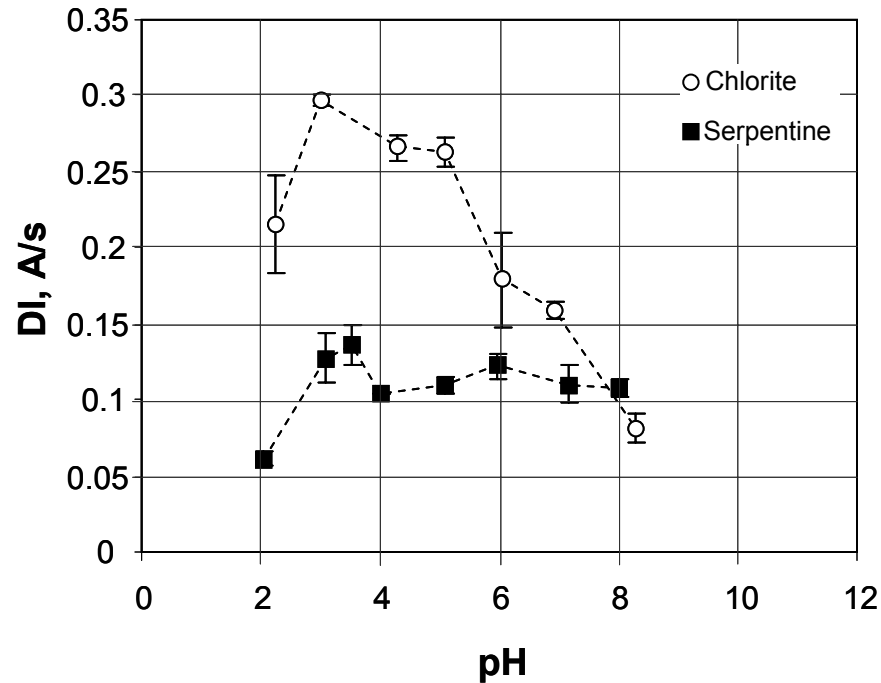


Figure 4.14 – Dispersion index in absorbance increment per second as a function of pH for chlorite (open circles) and serpentine (filled squares)

4.5. Discussion

The focus of this chapter was on determining the p.z.c. using the Mular-Roberts titration technique and comparing it to the i.e.p. determined by electrophoresis. A difference between p.z.c. and i.e.p. can be seen with electrokinetically anisotropic minerals such as the phyllosilicates examined here.

The M-R technique exploits the change in solution pH when ionic strength is adjusted; when the ΔpH is zero this gives the p.z.c. The technique was validated by testing two isotropic minerals, alumina and silica, and was shown to be robust in the face of changes in solid/liquid ratio and range in ionic strength. In the case of phyllosilicates where the charge on one crystal plane is pH dependent (i.e., the edge) while the other is not (basal plane) the M-R technique responds only to the former, whereas electrophoresis reflects an intermediate (average) behaviour resulting from both planes.

The i.e.p. values determined by electrophoresis in the case of phyllosilicates should be treated with some caution. The Smoluchowski equation used to convert electrophoretic mobility to zeta potential was developed for spherical particles and there is a lack of appropriate mathematical models for sheet minerals. The heterogeneous nature of the charge distribution discussed earlier also makes interpretation of results difficult (Burdukova et al, 2007; Lyklema et al., 1991). Nevertheless zeta potential determinations on such minerals are often reported (Kosmulski, 2002; Tartaj et al., 2000; Chowdhury and Kitchener, 1975; Parks, 1965) and the estimates of i.e.p. by electrophoresis do serve as a basis for comparison with p.z.c.

The measurement of zeta potential to estimate i.e.p. revealed an aging effect in the case of serpentine that determined the use of 24-hour aged samples for the comparison with p.z.c. Tartaj et al. (2000) also reported an i.e.p. shift on aging serpentine which they explained in terms of preferential dissolution of magnesium. However, as noted in the results, Mg^{2+} ions were released in quantities of the same order by all silicates. The change in i.e.p. may be produced by the hydration of serpentine: water molecules can change the adsorption of other ions.

The effect of ions released from the minerals was considered. Neither aluminum nor iron were released even though both are constituent elements of chlorite and commonly substitute magnesium and silicon in serpentine and talc (Tartaj et al., 2000); consequently, their effect on zeta potential was not examined. Magnesium was released

and on testing it was found did not change zeta potential of chlorite or serpentine until ca. pH 10; correspondingly there was no shift in i.e.p. The effect at alkaline pH is the common observation with polyvalent metallic ions (such as Mg^{2+}). This phenomenon is associated with cation hydrolysis and adsorption of hydroxy complexes (e.g., $MgOH^+$) and surface precipitation of metal hydroxide, which occurs at pH values just below those for bulk precipitation (Fuerstenau and Palmer, 1976; James and Healey, 1972 a, b). Since the i.e.p. did not change it is concluded that Mg^{2+} is not a p.d.i. in the case of chlorite and serpentine. However, magnesium did change the i.e.p. of talc, thus it seems to be a potential determining ion or at least a specifically adsorbing ion in the case of talc. The presence of released Mg ions is considered the reason the M-R technique did not give a result for this sample of talc. Others have succeeded in determining p.z.c. for talc using the M-R technique (Burdukova et al., 2007), suggesting the origin of the sample is a factor.

The results from the M-R technique are easy to interpret if there is only one plane exhibiting charge. In principle a face that is defect and contaminant free should have zero charge. There is no independent proof for this being the case here. Atomic force microscopy, by making measurements on individual planes, is one way to delve further into that aspect (Nalaskowski et al., 2007).

Rather, at this juncture a practical question is more pressing: which parameter, p.z.c. or i.e.p., is the factor controlling system properties that may influence flotation? Particle aggregation is one such property (Silvestre et al., 2009; El-Ammouri et al., 2002; Vergouw et al., 1998 a, b). To explore aggregation/dispersion turbidimetry measurements were employed. Given the small mass of sample available adapting a light scattering technique proved well suited to the task. Chlorite showed its highest aggregation over a pH ranging from the i.e.p. to the p.z.c., suggesting that aggregation/dispersion is determined by the charge at both the edge and the face. It has been reported that under certain conditions minerals with charges of different sign on the edge and face, can form

“house-of-cards” like aggregates (Lyklema et al., 1991). Serpentine, on the other hand, seems to remain largely dispersed over the tested pH range, possibly due to hydration effects maintaining a hydrophilic surface which promotes a dispersed condition. Chlorite consists of a positively charged brucite-like sheet and a negatively charged mica-like sheet, which make the interlayer bonding fairly strong (Hartman, 1983) and may restrict hydration. The interlayer bonding of serpentine, in contrast, is produced by the interaction between oxygen in the tetrahedral sheet and hydroxyl in the octahedral sheet of the next layer. This is a comparatively weak bonding, depending on isomorphous substitution (e.g., Al and Fe for Mg and Al for Si) to give it some amount of ionic character (Lyklema et al., 1991), making serpentine structure more likely to hydrate. Figure 4.15 shows a schematic of the interlayer conditions of serpentine (1:1 phyllosilicate) and chlorite (2:1 non-expanding phyllosilicate). The sketch of a 2:1 expanding phyllosilicate is also presented.

This chapter has presented results for specimen phyllosilicate minerals. The work established concepts and techniques that will be applied to the probing of mineral surface properties for a Ni-bearing ultramafic ore in subsequent chapters.

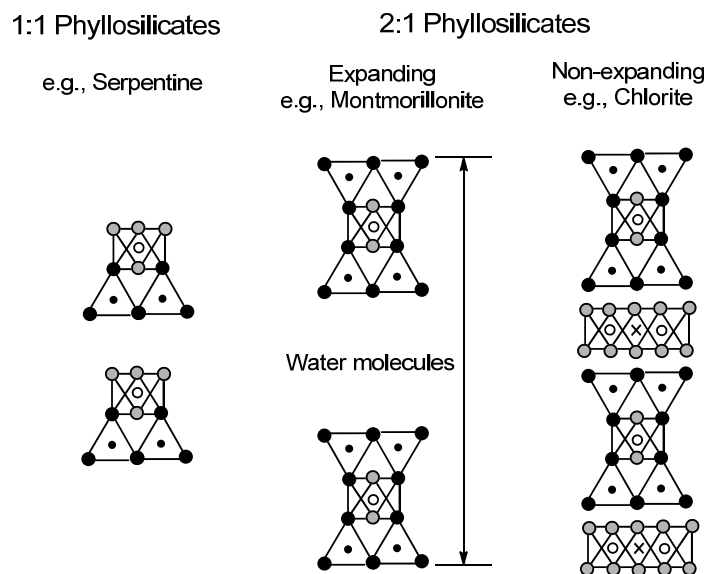


Figure 4.15 – Interlayer bonding for different types of phyllosilicates

4.6. Conclusions

The Mular-Robert titration technique (M-R), verified using electrokinetically isotropic minerals, was used to determine the point of zero charge (p.z.c.) for three anisotropic phyllosilicate minerals. The p.z.c. was compared to the isoelectric point (i.e.p.) determined by electrophoresis. For serpentine and chlorite, p.z.c. was greater than i.e.p. (pH 4.3 vs. pH 3.3, and pH 4.6 vs. pH <3, respectively). The M-R technique did not yield a p.z.c. for talc which is attributed to interference by released Mg ions. In the case of chlorite, aggregation occurred over the pH range from i.e.p. to p.z.c., suggesting both contribute to aggregation. The serpentine sample remained dispersed over the full pH range, tentatively attributed to hydration effects dominating dispersion.

References

- Ardizzone S., Siviglia P., Trasatti S. (1981) The point of Zero Charge of Ruthenium Dioxide. *Journal of Electroanalytical Chemistry* 122: 395-401
- Breeuwsma A., Lyklema J. (1971) Interfacial Electrochemistry of Haematite (α -Fe₂O₃). *Discussions of the Faraday Society* 52: 325-333
- Burdukova E., Bradshaw D.V., Laskowski J.S. (2007) Effect of CMC and pH on the rheology of suspensions of isotropic and anisotropic minerals. *Canadian Metallurgical Quarterly* 46: 273-278
- Chowdhury S, Kitchener JA (1975) The zeta potential of natural and synthetic chrysotiles. *International Journal of Mineral Processing* 2: 277-285

Ciullo, PA (1996). Silicate structure. In *Industrial Minerals and their uses – A Handbook and Formulary*. PA Ciullo (Ed). William Andrew Publishing

Edwards C.R., Kipkie W.B., Agar G.E. (1980) The effect of slime coatings of the serpentine minerals, chrysotile and lizardite, on pentlandite flotation. *International Journal of Mineral Processing* 7: 33-42

El-Ammouri E., Mirnezami M., Lascelles D., Finch J.A. (2002) Aggregation index and a methodology to study the role of magnesium in aggregation of sulphide slurries. *CIM Bulletin* 95: 67-72

Fuerstenau D.W., Pradip (2005) Zeta potentials in the flotation of oxide and silicate minerals. *Advances in Colloid and Interface Science* 114-115: 9-26

Fuerstenau M.C., Palmer B.R. (1976) Anionic flotation of oxides and silicates. M.C. Fuerstenau (Ed). *Flotation A.M. Gaudin Memorial Volume 1*, New York, 148-196

Hartman P. (1983) Calculation of electrostatic interlayer bonding energy and lattice energy of polar phyllosilicates: kaolinite and chlorite. *Clays and Clay Minerals* 31: 218-222

Hunter R.J. (1981) *Zeta Potential in Colloid Science—Principles and Applications*. Academic Press: New York, NY, USA

International Union of Pure and Applied Chemistry, Division of Physical Chemistry (1971) *Manual of symbols and terminology for physicochemical quantities and unites*. Appendix II: Definitions, terminology and symbols in colloid and surface chemistry. London Butter Worths

James R.O., Healey T.W. (1972 a) Adsorption of hydrolysable metal ions at the oxide-water interface. *Journal of Colloid and Interface Science* 40: 42-52

James R.O., Healey T.W. (1972 b), Adsorption of hydrolysable metal ions at the oxide-water interface. *Journal of Colloid and Interface Science* 40: 53-63

Kosmulski M. (2002) The pH-dependent surface charging and the points of zero charge. *Journal of Colloid and Interface Science* 253: 77-87

Kosmulski M. (2004) The pH-dependent surface charging and the points of zero charge. II Update. *Journal of Colloid and Interface Science* 275: 214-224

Leja J. (1983) *Surface Chemistry of Froth Flotation*, Plenum Press: New York, NY, USA

Lyklema J., van Leeuwen H.P., van Vliet M., Cazabat A.M. (1991) *Fundamentals of Interface and Colloid Science. Volume II: Solid-Liquid Interfaces*, Academic Press: London, UK

Mular A.L., Roberts R.B. (1966) A simplified method to determine isoelectric points of oxides. *Transactions of the Canadian Institute of Mining, Metallurgy and Petroleum* 69: 438-439

Nalaskowski J, Abdul B, Du H, Miller JD (2007) Anisotropic character of talc surfaces as revealed by streaming potential measurements, atomic force microscopy, molecular dynamics simulations and contact angle measurements. *Canadian Metallurgy Quarterly* 46: 227-235

Parks A. (1965) The isoelectric points of solid oxides, solid hydroxides, and aqueous hydroxo complex systems. *Chemistry Reviews* 65: 177-198

Shaw D. J. (1969) *Electrophoresis*, Academic Press: New York, NY, USA

Silvestre M.O., Pereira C.A., Galery R., Peres A.E.C. (2009) Dispersion effect on a lead-zinc sulphide ore flotation. *Minerals Engineering* 11: 752-758

Tartaj P., Cerpa A., Garcia-Gonzalez M.T., Serna C.J. (2000) Surface instability of serpentine in aqueous suspensions. *Journal of Colloid and Interface Science* 231: 176-181

Vergouw J.M., Difeo A., Xu Z., Finch, J.A. (1998 a) An agglomeration study of sulfide minerals using zeta-potential and settling rate. Part I: pyrite and galena. *Minerals Engineering* 11: 159-169

Vergouw J.M., Difeo A., Xu Z., Finch, J.A. (1998 b) An agglomeration study of sulfide minerals using zeta potential and settling rate. Part II: sphalerite/pyrite and sphalerite/galena. *Minerals Engineering* 11: 605-614

5

Effect of serpentine and dissolved mineral species on electrokinetic behaviour of pentlandite

Abstract

This chapter examines the mechanisms of depression of pentlandite in flotation of ultramafic ore through determination of the effect of dissolved metal ions and presence of serpentine fines on pentlandite electrophoretic mobility. Zeta potential was measured under three conditions designed to progressively approach the actual flotation environment: pentlandite and serpentine alone with indifferent background electrolyte; mixed mineral, with pentlandite in the presence of serpentine with indifferent background electrolyte; and mixed mineral with supernatant from an ore suspension as background

electrolyte. The “minerals alone” experiments showed that slime coating is expected as a consequence of electrostatic attraction, confirmed in the mixed mineral experiments with indifferent background electrolyte. In the presence of supernatant an additional effect on zeta potential due to adsorption of $\text{Mg}(\text{OH})_2$ precipitates was detected and confirmed with a scanning electron microscopy study.

5.1. Introduction

Pentlandite is the principal nickel sulphide and the source of the bulk of the world's current supply of nickel. The demand for nickel has increased significantly in recent years as a consequence of the rise in stainless steel production in China and India (Reck et al., 2010)

Some pentlandite deposits are associated with pyrrhotite and MgO-minerals (e.g., serpentine). These gangue minerals must be rejected in the flotation step to assist subsequent smelting: eliminating pyrrhotite reduces sulphur dioxide emission and eliminating MgO-minerals decreases the slag melting point. Flotation is usually with thiol collectors in an alkaline pulp.

MgO-mineral slimes formed during comminution are suspected of interfering with flotation by forming a coating on the pentlandite surface. Several studies have shown that a small amount of serpentine can depress pentlandite recovery (Bremmell et al., 2005, Mani et al., 1997, Edwards et al., 1980) and associated electrokinetic measurements suggested the cause is hetero-aggregation between positively charged serpentine and negatively charged pentlandite at the alkaline conditions of flotation (ca. pH 10).

Electrokinetic studies of minerals are frequently used to predict their behaviour in aqueous systems. Several researchers have shown that it is possible to establish a correlation between a desirable but difficult to measure parameter and the zeta potential, i.e., zeta potential is a surrogate (Adler et al., 2000, Chibowski, 1979). Regarding

flotation-related studies, some of the parameters that have been correlated to electrokinetic behaviour are adsorption of collectors (Fuerstenau, 2001, Fuerstenau and Shibata, 1999, Moudgil et al., 1988), oxidation of sulphide minerals (Fullston et al., 1999, Das et al., 1997, Prestidge and Rowlands, 1997), slime coating (Xu et al., 2003 b, Parsonage, 1985, Hunter and Neville, 1980), accidental activation of gangue (O'Connor et al., 2006, Malysiak et al., 2004, Malysiak et al., 2002, Fuerstenau and Palmer, 1976) and exchange of released ions among sulphide minerals (DiFeo et al., 1997; Zhang et al., 1992). Zeta potential is then considered to be an important tool for understanding and predicting the behaviour of flotation systems.

That being said, experiments are often performed under ideal conditions (e.g., pure minerals using an indifferent electrolyte as background), which are far from actual flotation conditions. Acar and Somasundaran (1992) showed that predictions based on single mineral tests often failed in mixed mineral systems mainly due to the interactions between the minerals and dissolved species. It is then necessary to mimic the pulp conditions as much as possible. One approach is to perform zeta potential on mixed minerals (at least pairs of minerals). In the present case the technique used by Zhang et al. (1997) was adopted whereby minerals of different size are conditioned together then separated to determine zeta potential.

The present work was conducted to determine the mechanism of depression of pentlandite in the presence of serpentine and dissolved species using electrokinetic measurements.

5.2. Experimental

5.2.1. Minerals

Pentlandite was isolated from a sample of concentrate obtained by processing a sample of an ultramafic ore from Thompson, Manitoba in the Vale mini-plant (Xu et al., 2003 a).

The concentrate contained mostly pentlandite, pyrrhotite and serpentine (clinochrysotile type) as determined by X-ray diffraction (XRD). The concentrate was screened and the fine material ($-75\ \mu\text{m}$) discarded. The pentlandite content was upgraded by gravity and magnetic separation. The $-106/+75\ \mu\text{m}$ fraction was cleaned with acetone to remove flotation reagents and kept in a freezer to limit surface oxidation. The elemental analysis of the sample determined by atomic absorption spectroscopy (model AA240FS, Varian) is shown in Table 5.1 along with electron microprobe (model JXA-8900, JEOL) analysis of 20 pentlandite grains. The slightly elevated Fe content of the sample (and depressed Ni assay) indicates some residual contamination primarily by pyrrhotite.

Serpentine was isolated from the same ultramafic ore sample by gravity and magnetic separation. Examination by XRD showed clinochrysotile as the main phase with minor pyrrhotite. The $-25\ \mu\text{m}$ fraction was used when the mineral was tested alone and the $+45/-75\ \mu\text{m}$ when it was mixed with pentlandite.

Table 5.1 – Measured elemental composition of the sample determined by AAS compared to ideal pentlandite composition and composition determined by microprobe analysis on identified pentlandite grains

Pentlandite	Element, %						
	Fe	Ni	Co	Pb	Zn	Cu	Insoluble
Ideal composition ^[1]	31.26	32.85	---	---	---	---	---
Electron microprobe ^[2]	30.70	35.00	1.20	---	---	0.07	---
Sample	40.35	30.99	0.88	0.00	0.15	0.04	8.56

^[1] Ideal is based on $(\text{Ni,Fe})_9\text{S}_8$

^[2] Electron microprobe analysis based in 20 pentlandite grains

5.2.2. Zeta potential

Serpentine

An electrophoretic method (ZetaPlus Brookhaven Instruments) which uses the Smoluchowski approximation was used to measure the zeta potential from electrokinetic mobility. Suspensions were prepared using 0.1 g of solid in 500 mL of distilled, deionized water (resistivity, 18.3 M Ω /cm). The suspensions were conditioned for 24 hours before measurement to reach chemical equilibrium based on prior experience (Chapter 4). The experiments were performed using two KNO₃ concentrations (viz., 10⁻² mol/L and 5 \times 10⁻³ mol/L) as supporting electrolyte and supernatant derived from an ore sample. The pH was adjusted using either KOH or HNO₃ over the pH range 3 to 10, respecting the manufacturer's recommended limits. The pH was recorded 15 minutes after adjustment. The results reported are the average of at least two full repeats with the 95% confidence interval indicated.

Pentlandite

Prior to measurement, about 0.2 g of pentlandite was ultrasonicated (model 275DA Crest) several times to eliminate slimes; the pentlandite was then placed in a flask with dilute HCl solution (ca. pH 2) and agitated on an orbital shaker model G-33 (New Brunswick Scientific) to dissolve oxidation products. The sample was then filtered and rinsed several times with distilled, deoxygenated water and placed in a desiccator. When dry, the pentlandite was ground in an agate mortar and placed in the test solution (N₂ purged for 20 minutes). The suspension was left to sit for 24 hours before measurement (to be consistent with the procedure used for serpentine). The pH was adjusted using either KOH or HNO₃ over the pH range of 3 to 10 and recorded 15 minutes after adjustment. The results (mean and 95% confidence interval) represent at least two full repeat experiments.

The tested background solutions were: KNO_3 (10^{-2} mol/L and 5×10^{-3} mol/L), supernatant, and Mg concentrations from 5 to 80 mg/L, added as $\text{MgCl}_2 \cdot 6\text{H}_2\text{O}$ (Anachemia, analytical grade). In order to fix the ionic strength (because variations could modify the zeta potential) 10^{-2} mol/L KNO_3 was added to the last two background solutions.

The supernatant was prepared from a ground ore (P80 ca. 100 μm) suspension (mass fraction of solids 10 %) agitated for 1 day. The solution was recovered by a combination of filter paper and membrane (pore size: 0.45 μm). The solution was analyzed by a combination of atomic absorption spectroscopy (metal ions), argentometric titration (chloride ion) and turbidimetry (sulphate ion).

Mixed mineral systems

The technique was based on Zhang et al., (1997). Different size fractions of pentlandite and serpentine (-25 μm and +150/-212 μm) were mixed to facilitate subsequent separation prior to zeta potential measurements. The coarse fraction (either pentlandite or serpentine) was allowed to settle and a sample of the remaining fine particle suspension was taken for zeta potential measurements. The background solutions for the mixed mineral case were as described above.

5.2.3. Scanning electron microscopy

For microscopic examination, pentlandite (-106/+75 μm) was conditioned in a similar way as for the zeta potential experiments. Samples were dried in a desiccator and placed in holders before they were gold/platinum-coated for examination. The Philips XL30 field emission gun system scanning electron microscope (FEM-SEM) was used for morphological characterization (secondary electrons) and elemental analysis (energy dispersive spectroscopy).

5.3. Results

5.3.1. Zeta potential

Individual minerals

In presence of indifferent electrolyte

For pentlandite (Figure 5.1) the isoelectric point (i.e.p.) was found at ca. pH 3. As with most sulphide minerals, the i.e.p. of pentlandite can vary, in this case from pH 2 (non-oxidized) to 10.5 (fully oxidized) (Bremmell et al., 2005, Fullston et al., 1999), the latter value approximating the i.e.p. of nickel hydroxide (Parks, 1965). Therefore, an i.e.p. of pH 3 approaches a largely oxide-free surface. The 95 % confidence interval indicates some uncertainty. Experimental error can be attributed to surface oxidation: sulphide minerals are relatively unstable and oxidize quickly in the presence of water containing oxygen (Kitchener, 1992). Although water was bubbled with N₂, it was not possible to eliminate dissolved oxygen completely. The error increased at alkaline pH, where hydroxide species form on the surface.

Figure 5.2 shows the zeta potential of serpentine as a function of pH. This serpentine sample shows a positive zeta potential over a wide pH range with an isoelectric point at about pH 10. Some caution regarding zeta potential measurements for minerals such as serpentine is required. There are two concerns: serpentine is a phyllosilicate mineral, and thus exhibits a heterogeneous surface charge (see Chapter 4); and the Smoluchowski approximation assumes a spherical particle and this clinochrysotile type serpentine is characterized by fibrous (acicular) morphology. However, the measurements can be used for comparative purposes.

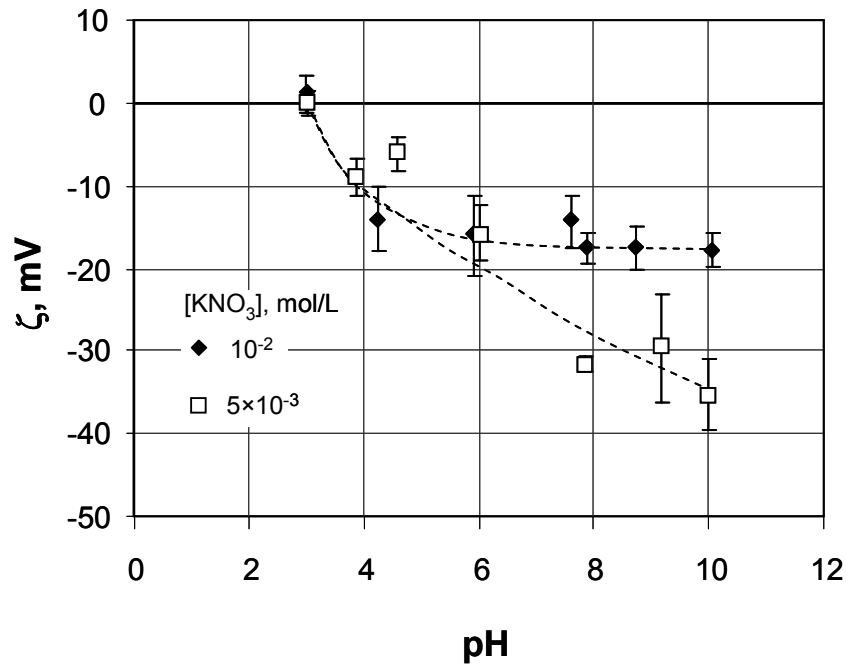


Figure 5.1 – Zeta potential of pentlandite as a function of pH at two values of ionic strength: 10^{-2} mol/L (filled diamonds) and 5×10^{-3} mol/L (open squares) KNO_3 . (Note, error bars are the 95 % confidence interval)

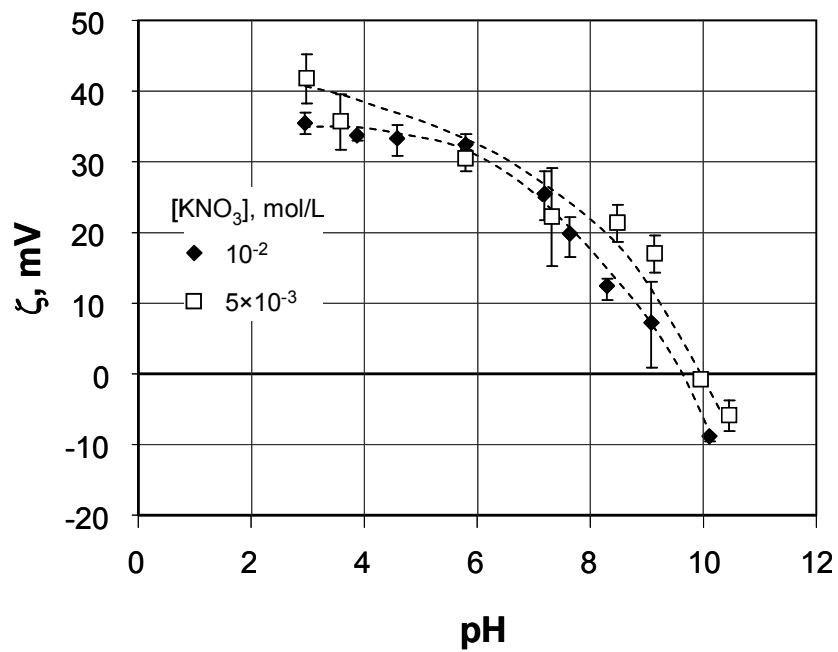


Figure 5.2 – Zeta potential of serpentine as a function of pH at two values of ionic strength: 10^{-2} mol/L (filled diamonds) and 5×10^{-3} mol/L (open squares) KNO_3

In presence of supernatant

Most minerals release some species to solution which may influence flotation. The released species can undergo further reactions such as hydrolysis, complexation, adsorption and precipitation. The nature of the complex equilibria involving such reactions will determine the interfacial properties of the particle, and consequently its floatability. In an attempt to take into consideration such effects, supernatant from an ore suspension was used as background for the zeta potential measurements.

The composition of the supernatant is presented in Table 5.2. Magnesium and chloride ions were the dominant species with Cu, Fe, Ni, Zn, Si and Al ions analyzed for but not detected.

Figure 5.3 shows the zeta potential of pentlandite in the presence of supernatant. The pentlandite became less negative over almost the whole range of pH tested and showed a point of charge reversal (p.c.r.) at ca. pH 9. For comparison, the trend for pentlandite with 10^{-2} mol/L KNO_3 as background is also presented.

For serpentine, the effect of supernatant became evident above pH 8: serpentine remained positive and did not exhibit i.e.p. over the pH range tested (Figure 5.4).

Table 5.2 – Chemical species in the supernatant

Chemical species	K⁺ [1]	Na⁺ [1]	Mg²⁺ [1]	Ca²⁺ [1]	Cl⁻ [2]	SO₄²⁻ [3]
Concentration mmol/L	0.27	0.26	3.64	0.94	9.38	0.14
mg/L	10.69	5.93	88.5	37.55	332.5	13.5

^[1] Determined by atomic absorption spectroscopy

^[2] Determined by argentometric titration

^[3] Determined by turbidimetry

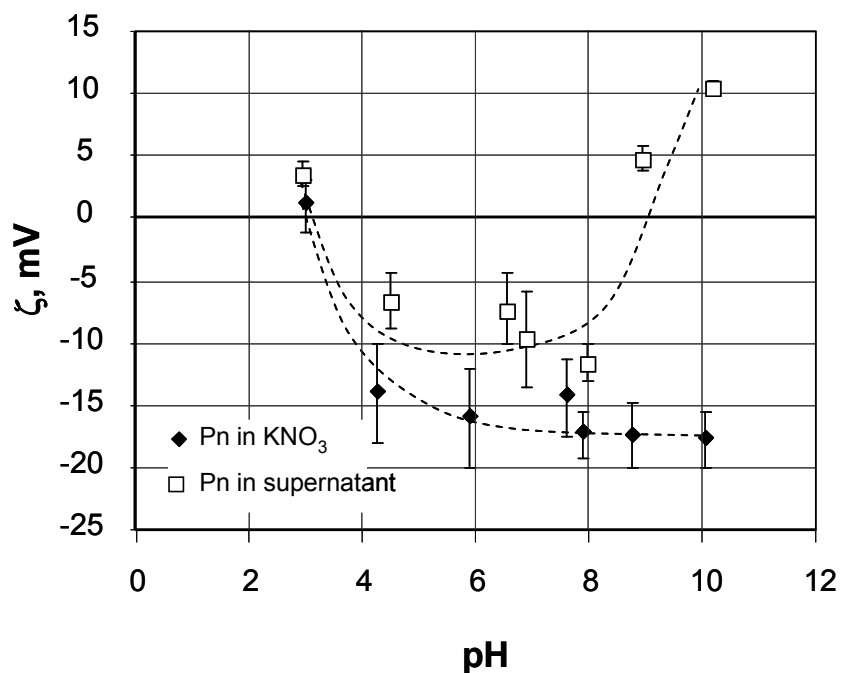


Figure 5.3 – Zeta potential of pentlandite as a function of pH with supernatant as background electrolyte compared to 10^{-2} mol/L KNO₃ as background electrolyte

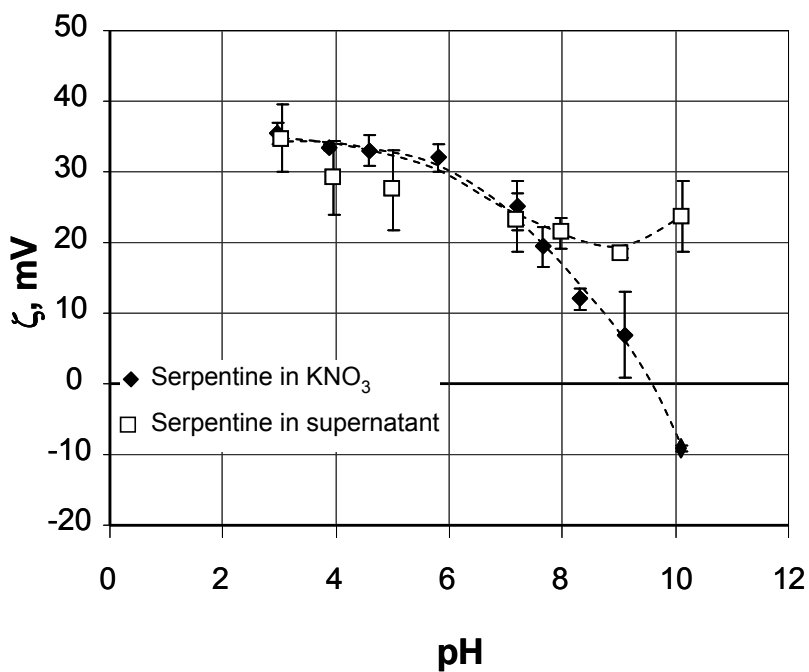


Figure 5.4 – Zeta potential of serpentine as a function of pH with supernatant as background electrolyte compared to 10^{-2} mol/L KNO₃ as background electrolyte

From the supernatant analysis and an understanding of metal ions effects, the impact of supernatant was considered to be due to the presence of Mg ions. Figure 5.5 shows zeta potential of pentlandite as a function of magnesium concentration at pH 10. The same increase in zeta potential observed with supernatant occurred with Mg concentrations above ca. 10 mg/L Mg^{2+} with charge reversal at ca. 40 mg/L. Magnesium at 50 mg/L (comparable to the concentration in the supernatant) produced a similar electrokinetic response to that with supernatant as background (Figure 5.6).

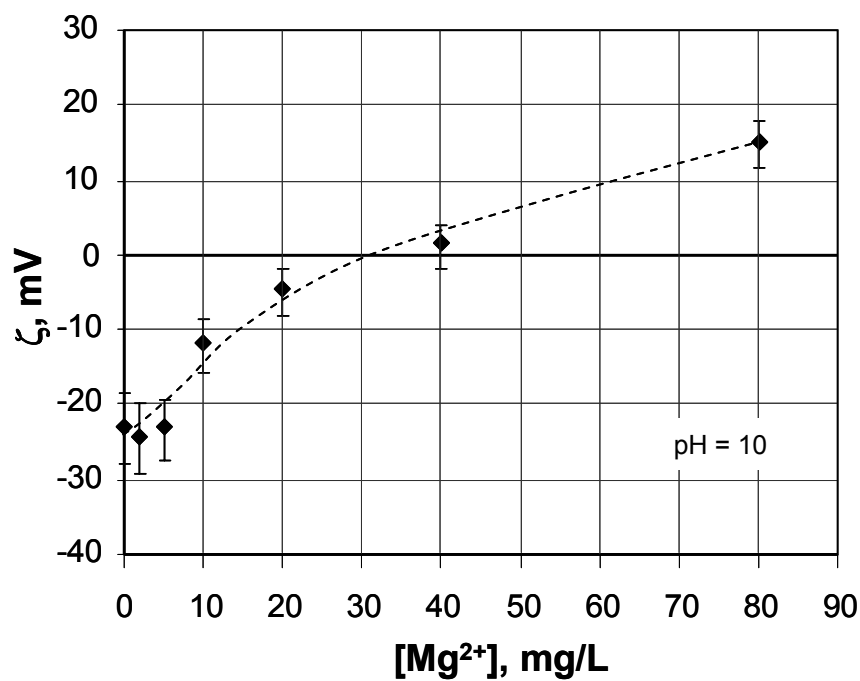


Figure 5.5 – Zeta potential of pentlandite as a function Mg^{2+} concentration at pH 10

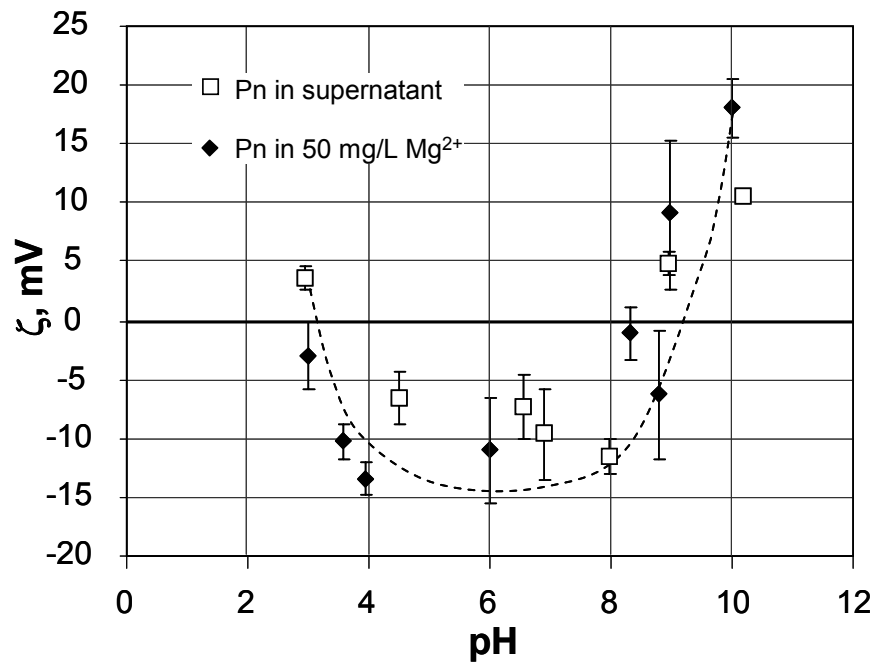


Figure 5.6 – Zeta potential of pentlandite as a function of pH in the presence of 50 mg/L Mg²⁺ compared to supernatant

Mixed mineral systems

In presence of indifferent electrolyte

Figure 5.7 shows the zeta potential of pentlandite after being conditioned in the presence of serpentine compared to pentlandite alone. Pentlandite was significantly affected by serpentine, now exhibiting positive zeta potential over the range of tested pH compared to the consistently negative charge in the absence of serpentine.

Figure 5.8 shows the zeta potential of serpentine after conditioning in the presence of pentlandite compared to serpentine alone. The curves almost superpose and the slight differences can be attributed to the experimental uncertainty; i.e., the presence of pentlandite fines has little impact on zeta potential of serpentine.

Pentlandite in presence of serpentine and supernatant

The above interpretation of Figure 5.7 implicates both adsorption of Mg species and hetero-aggregation with serpentine fines. To investigate which effect might dominate, the zeta potential of pentlandite conditioned with serpentine with supernatant as background was measured (Figure 5.9). The result for pentlandite conditioned with serpentine with KNO_3 as background electrolyte is included for comparison. The zeta potential of pentlandite under both these conditions is similar implying it is the presence of serpentine that dominates up to ca. pH 8 but above this even in the absence of supernatant there appears to remain a Mg species-like effect.

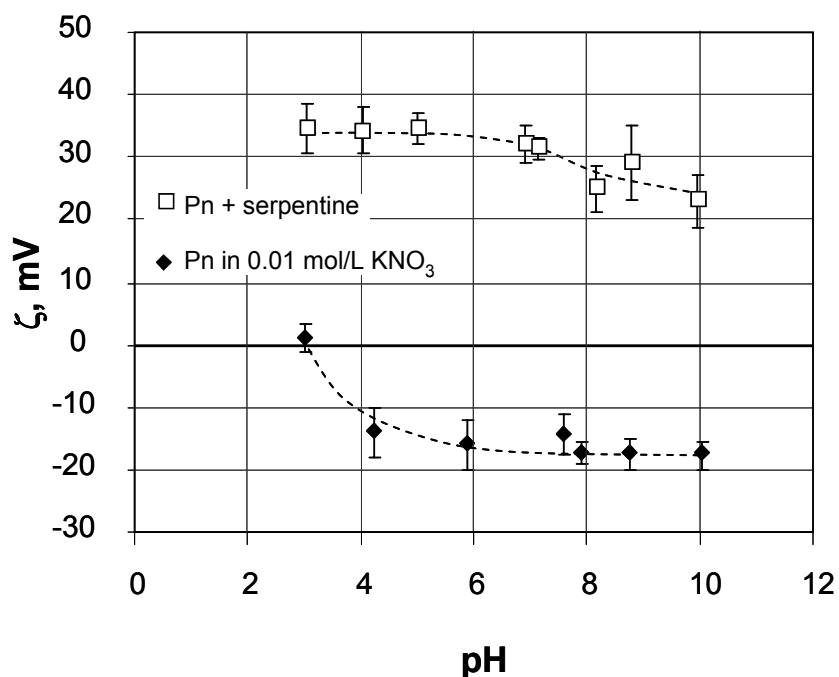


Figure 5.7 – Zeta potential of pentlandite conditioned with serpentine suspended in 10^{-2} mol/L KNO_3 (open squares) compared to result for pentlandite in 10^{-2} mol/L KNO_3 (filled diamonds)

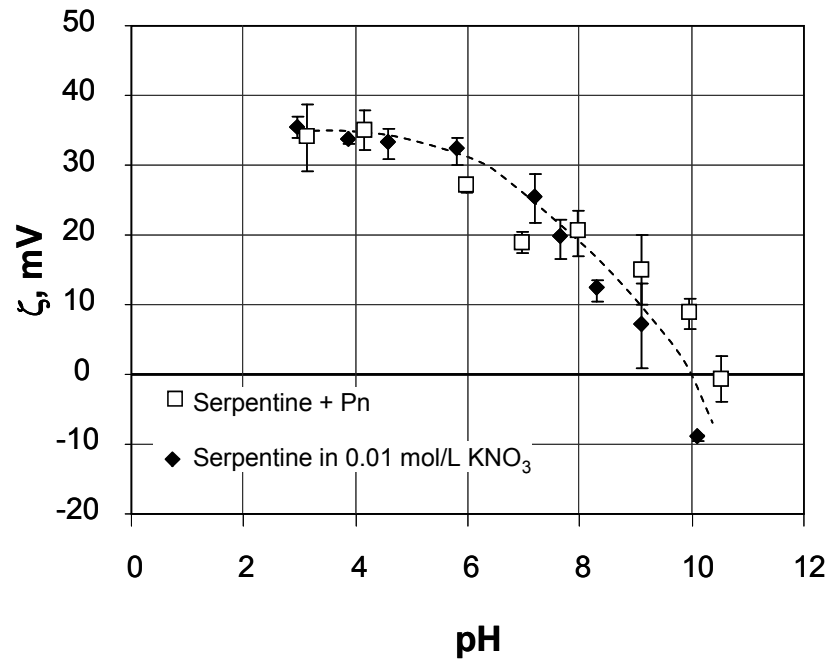


Figure 5.8 – Zeta potential of serpentine conditioned with pentlandite suspended in 10^{-2} mol/L KNO₃ (open squares) compared to the result for pentlandite in 10^{-2} mol/L KNO₃ (filled diamonds)

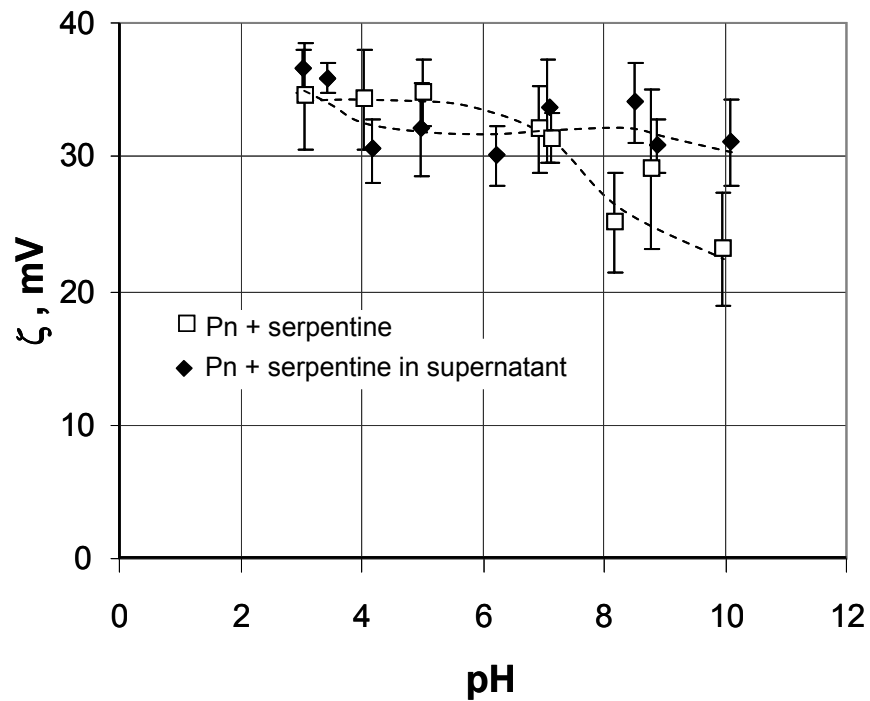


Figure 5.9 – Zeta potential of pentlandite conditioned with serpentine suspended in supernatant compared to result for pentlandite conditioned with serpentine suspended in 10^{-2} mol/L KNO₃ (open squares)

5.3.2. Scanning electron microscopy

Scanning electron microscopy was used for direct surface inspection of pentlandite particles (Figure 5.10). Micrographs of pentlandite conditioned in supernatant at pH 4 and 10 (i.e., a pH well below and at about the pH of magnesium hydroxide precipitation, respectively) showed clear differences: the surface at pH 4 (Figure 5.10 b) looked similar to that conditioned in KNO_3 (Figure 5.10 a) while pentlandite conditioned in supernatant at alkaline pH presented a rough surface, most likely due to $\text{Mg}(\text{OH})_2$ precipitation (Figure 5.10 c). Energy dispersive analysis showed that magnesium and silicon are present in the sample conditioned with supernatant. Micrographs of pentlandite conditioned with serpentine at pH 10 showed a surface extensively covered with fibrous particles (Figure 5.10 d) and EDS analysis revealed magnesium and silicon, presumably from adsorbed serpentine. Figure 5.10 e showed the fibril disaggregation of a particle, probably serpentine, which produced the slimes.

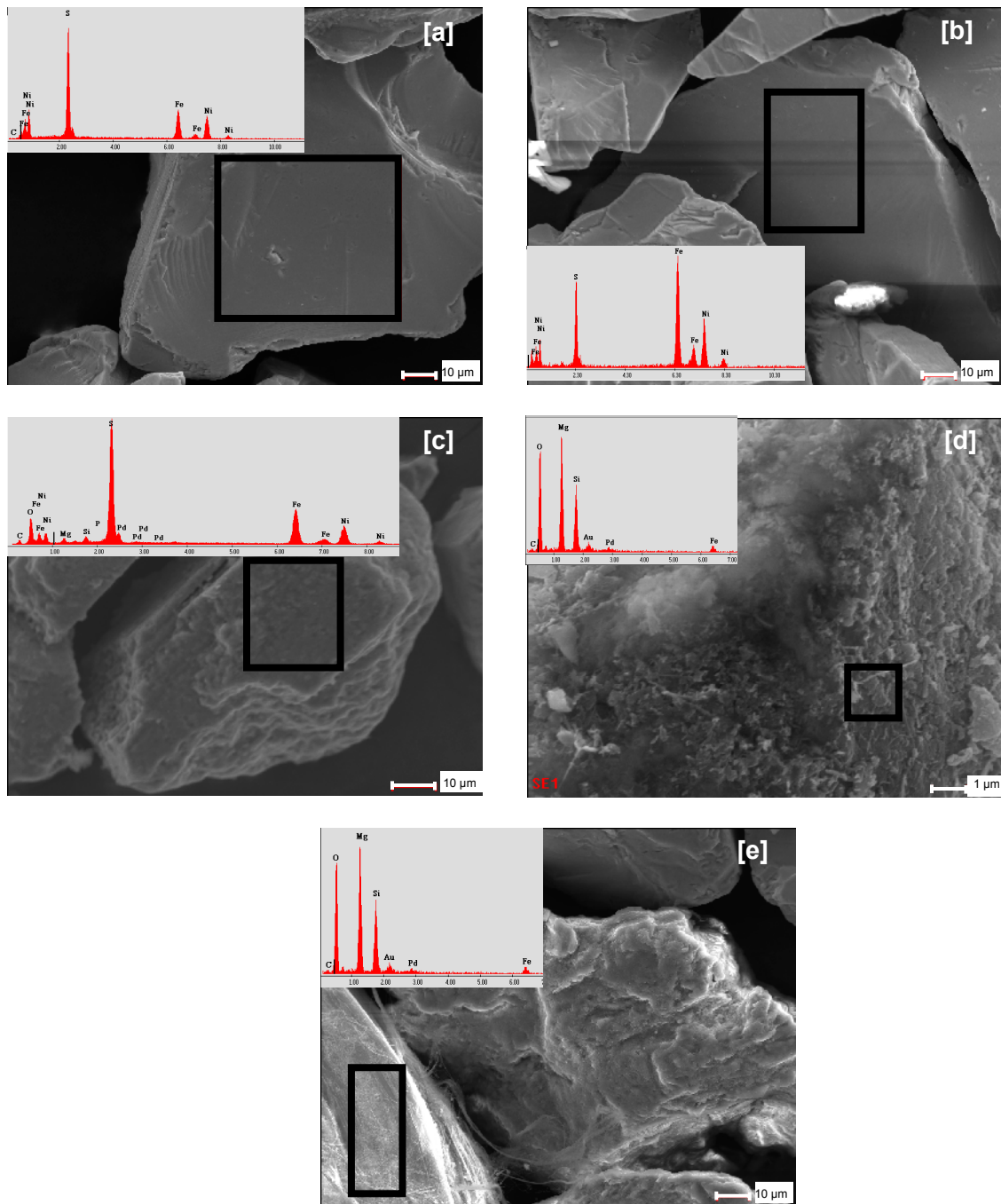


Figure 5.10 – Scanning electron micrographs of pentlandite conditioned alone in 10^{-2} mol/L KNO_3 solution at pH 10 [a]; conditioned alone in supernatant at pH 4 [b] and at pH 10 [c]; conditioned with serpentine at pH 10 [d] and a particle of fibrous serpentine [e]

5.4. Discussion

Though surface charge is not the primary cause of attachment of particles to bubbles, it plays other important roles in fine particle flotation systems notably controlling particle-particle interactions and adsorption of some chemical species. Zeta potential measurements are frequently used to predict aggregation/dispersion behaviour in aqueous systems, but in the case of flotation such predictions are usually made on the basis of experiments that differ from the operating conditions. The present work attempted to address this limitation by progressively establishing conditions closer to reality.

The possibility of pentlandite heterocoagulating with and becoming coated with serpentine slimes at the pH of flotation (ca. pH 9) is supported by the classical zeta potential measurements made on individual minerals in the presence of indifferent electrolyte: at pH 9, serpentine will be positively charged and pentlandite negatively charged and, consequently, electrostatic attraction between these two minerals is expected.

When the minerals were placed in supernatant derived from the ore, the results showed that the species released interacted with pentlandite, increasing the zeta potential, reversing the charge and making the surface positive at the flotation pH. Magnesium species were suspected to be the cause of the change in electrokinetic response based both on the concentration measured in the ore supernatant and previous experience with sulphide minerals (Mirnezami et al. 2003; El-Ammouri et al., 2002). Similar observations have been reported for other minerals in the presence of magnesium and other polyvalent cations, which adsorb when they hydrolyze to form hydroxyl complexes (Fuerstenau and Palmer, 1976). Charge reversal is associated with hetero-coagulation of $\text{Mg}(\text{OH})_2$ precipitates which form above ca. pH 10 and are positively charged (Mirnezami et al., 2003). Tests where Mg^{2+} was introduced (as MgCl_2) confirmed that Mg species could account for the effect of supernatant. Scanning electron microscopy images provided

evidence for their presence on the surface. The hetero-coagulation (or adsorption) of $\text{Mg}(\text{OH})_2$ precipitates can be counted as another example of slime coating. This impact of Mg ions makes predicting electrostatic interaction between pentlandite and serpentine at alkaline (i.e., flotation) pH less certain.

The mixed mineral systems, while not designed to this end initially, however confirm that slime coating of serpentine on pentlandite will occur. The evidence pointed to some disintegration of the coarse serpentine providing sufficient fines (slimes) to hetero-coagulate with pentlandite. The SEM micrographs confirmed that the surface carried fine serpentine fibres. Heterocoagulation being dominant holds true to about pH 9, i.e., approximately up to the i.e.p. of serpentine. Unlike serpentine alone, however, above this pH, the pentlandite (after contact with serpentine) remained positively charged. Consequently, slime coating of serpentine alone cannot account completely for the electrokinetic behaviour of pentlandite in contact with serpentine and seems to point to a combined effect with some released species from the serpentine. At these pHs (>9) this re-introduces a possible role of $\text{Mg}(\text{OH})_2$ precipitates, implying sufficient Mg being released by serpentine, or possibly directly transferred on particle contact to affect pentlandite zeta potential. It is evident that sufficient Mg release will also increase serpentine zeta potential at $\text{pH} > 9$ (Figure 5.4). The SEM micrographs provided ambiguous support for the combined adsorption of serpentine and $\text{Mg}(\text{OH})_2$ precipitates and since magnesium is present in both, EDS analysis did not resolve either. Thus while some uncertainty on the role of Mg species in the pentlandite-serpentine case with indifferent electrolyte remains it is evident that under flotation conditions a combined serpentine/ $\text{Mg}(\text{OH})_2$ slime coating effect will be at play. The wide use of soda ash (sodium carbonate) for pH adjustment in Ni-ore processing may have its origin in control of $\text{Mg}(\text{OH})_2$ sliming by sequestering magnesium as the carbonate.

5.5. Conclusions

An electrophoretic study was carried out to determine response of pentlandite and serpentine under conditions progressively approaching actual flotation. The principal outcomes are:

- Zeta potential measurements performed on pentlandite and serpentine individually in indifferent electrolyte showed the two minerals had opposite charge at flotation pH 10 and that slime coating could occur as a consequence of electrostatic attraction.
- When pentlandite was suspended in ore supernatant, the zeta potential reflected adsorption of magnesium species that reversed the charge at flotation pH.
- The mixed mineral case revealed an effect on pentlandite zeta potential at flotation pH attributed to a combined slime coating with serpentine and magnesium hydroxide precipitates.

References

- Acar S., Somasundaran P. (1992) Effect of dissolved mineral species on the electrokinetic behavior of sulfides. *Minerals Engineering* 5: 27-40
- Adler J.J., Singh P.K., Patist A., Rabinovich Y.I., Shah D.O., Moudgil B.M. (2000) Correlation of particulate dispersion stability with the strength of self-assembled surfactant films. *Langmuir* 16: 7255-7262
- Bremmell K.E., Fornasiero D., Ralston J. (2005) Pentlandite-lizardite interactions and implications for their separation by flotation. *Colloids and Surfaces A: Physicochemical and Engineering Aspects* 252: 207-212

- Chibowski E. (1979) Zeta potential and surface free energy changes: Quartz/n-heptane-water system. *Journal of Colloid and Interface Science*.69 (2): 326-329
- Das K.K., Pradip, Natarajan K.A. (1997) The effect of constituent metal ions on the electrokinetics of chalcopyrite. *Journal of Colloid and Interface Science* 196(1): 1-11
- DiFeo A., Xu Z., Finch J. A. Electrokinetic study of sulfide minerals in mixed systems J.A. Finch, S.R. Rao, I. Holubec (Eds.) *Processing of Complex Ores, Mineral Processing, and the Environment. International Symposium of the Metallurgical Society of CIM*, 257-271. 1997
- Edwards C.R., Kipkie W.B., Agar G.E. (1980) The effect of slime coatings of the serpentine minerals, chrysotile and lizardite, on pentlandite flotation. *International Journal of Mineral Processing* 7: 33-42
- El-Ammouri E., Mirnezami M., Lascelles D., Finch J. A. (2002) Aggregation index and a methodology to study the role of magnesium in aggregation of sulphide slurries. *CIM Bulletin* 95: 67-72
- Fuerstenau D.W. (2001) Excess nonequilibrium collector adsorption and flotation rates. *Minerals and Metallurgical Processing* 18(2): 83-86.
- Fuerstenau D.W., Shibata J. (1999) On using electrokinetics to interpret the flotation and interfacial behavior of manganese dioxide. *International Journal of Mineral Processing* 57(3): 205-217
- Fuerstenau M.C., Palmer B.R. Anionic flotation of oxides and silicates. M.C. Fuerstenau (Ed). In *Flotation A.M. Gaudin Memorial Volume 1*, 148-196. 1976. American Institute of Mining and Metallurgical Engineering, New York, U.S.A.

Fullston D., Fornasiero D., Ralston J. (1999) Zeta potential study of the oxidation of copper sulfide minerals. *Colloids and Surfaces, A: Physicochemical and Engineering Aspects* 146(1-3): 113-121

Hunter R.J., Neville P.C. (1980) Colloid chemical aspects of slime coating removal. *Colloids and Surfaces* 1(3-4): 257-68

Kitchener J.A. Minerals and Surfaces. J.S. Laskowski, J. Ralston (Eds) In *Developments in Mineral Processing Volume 12 (Colloid Chemistry in Mineral Processing)*, 1-35. 1992. Elsevier, Amsterdam, The Netherlands

Malysiak V., O'Connor C.T., Ralston J., Gerson A.R., Coetzer L.P., Bradshaw D.J. (2002) Pentlandite-feldspar interaction and its effect on separation by flotation. *International Journal of Mineral Processing* 66(1-4): 89-106

Malysiak V., Shackleton N.J., O'Connor C.T. (2004) An investigation into the floatability of a pentlandite-pyroxene system. *International Journal of Mineral Processing* 74(1-4): 251-262

Mani H., Xu M., Quinn P. The effect of ultramafic mineralogy on pentlandite flotation. J.A. Finch, S.R. Rao, I. Holubec (Eds). *Processing of Complex Ores, In Mineral Processing, and the Environment. International Symposium of the Metallurgical Society of CIM*, 63-76. 1997

Mirnezami M., Hashemi M.S., Finch J.A. Aggregation effect of Zn^{2+} and Mg^{2+} ions in sulphide mineral pulps. XXII International Mineral Processing Congress, Cape Town 2003

- Moudgil B.M., Soto H., Somasundaran P. (1988) Adsorption of surfactants on minerals, In Reagents in Mineral Technology, P. Somasundaran and B.M. Moudgil (Eds), Surfactants Science Series, Vol. 27, Marcel Dekker, New York, pp. 79-104
- O'Connor C.T., Malysiak V., Shackleton N.J. (2006) The interaction of xanthates and amines with pyroxene activated by copper and nickel. *Minerals Engineering* 19(6-8): 799-806
- Parsonage P.G. (1985) Effects of slime and colloidal particles on the flotation of galena. *Developments in Mineral Processing* 6: 111-139
- Parks G.A. (1965) The isoelectric points of solid oxides, solid hydroxides, and aqueous hydroxo complex systems. *Chemical Reviews* 65: 177-198
- Prestidge C.A., Rowlands W.N. (1997) Electroacoustic measurements of sulfide mineral particles. *Minerals Engineering* 10(10): 1107-1118
- Reck B.K., Chambon M., Hashimoto S., Graedel T.E. (2010) Global stainless steel cycle exemplifies China's rise to metal dominance. *Environmental Science and Technology* 44: 3940-3946
- Xu M., Quinn P., Wells P. (2003 a) A movable mineral processing miniplant. 35th Annual Meeting of the Canadian Mineral Processors Ottawa, ON, 317-329
- Xu Z., Liu J., Choung J.W., Zhou Z. (2003 b) Electrokinetic study of clay interactions with coal in flotation. *International Journal of Mineral Processing* 68(1-4): 183-196
- Zhang Q., Rao S.R., Finch J.A. (1992) Flotation of sphalerite in the presence of iron ions. *Colloids and Surfaces* 66: 81-89

Zhang Q., Xu Z., Bozkurt V., Finch J. (1997) Pyrite flotation in the presence of metal ions and sphalerite. *International Journal of Mineral Processing* 52: 187-201

6

Effect of flotation reagents on hetero-aggregation of pentlandite and serpentine

Abstract

This chapter investigates the effect of carboxymethyl cellulose (CMC), pH and xanthate on hetero-aggregation of pentlandite and serpentine as it relates to the processing of ultramafic Ni-ore. The state of aggregation/dispersion was determined using a light scattering technique. A 3-factor, 3-level central composite design with a replicated central point was used to determine the most important factors and their interactions. The levels of the variables were: CMC, 0 mg/L, 25 mg/L and 50 mg/L; pH, 6, 8 and 10; and

xanthate, 0 mg/L, 3 mg/L and 5 mg/L. The CMC concentration and the interaction between CMC and pH were the most important factors determining aggregation/dispersion. Optical microscopy validated the findings.

6.1. Introduction

Aggregation is usually counterproductive to physical separation processes unless selective aggregation can be achieved. A common form of aggregation is slime coating. Typically, this refers to fine particles ($< 20 \mu\text{m}$) of gangue that adhere to particles of valuable mineral and reduce flotation selectivity. The example of interest here is slime coating of serpentine minerals on pentlandite, which is a suspected hindrance to flotation selectivity in processing ultramafic Ni-ores (Bremmell et al., 2005; Edwards et al., 1980).

Inter-particle forces control slime coating. Two principal forces are electrostatic and van der Waals. Hydrophobic interaction, hydration and steric repulsion forces may also be involved. The magnitude of these forces is controlled in practice by the addition of reagents, including pH regulators.

Carboxymethyl cellulose (CMC) is a typical dispersant for gangue silicates like serpentine. CMC is an anionic linear polymer prepared by reacting cellulose in the presence of sodium hydroxide with chloro-acetic acid. CMC has proven to be effective at preventing silicate slime coating in flotation of nickel minerals (Pugh, 1989). CMC appears to adsorb onto silicates through hydrogen bonding between the hydroxyl groups of the CMC and the mineral surface oxygen sites such as those on the edge plane of serpentine (Shortridge et al., 2000). Adsorption of CMC on serpentine particles increases the negative surface charge (due to the carboxy, COO^- , group), which promotes electrostatic repulsion between serpentine and pentlandite at flotation pH (ca. pH 10). Additionally, the hydroxyl groups in the CMC structure render the serpentine hydrophilic, which also aids its dispersion (and depression) (Wellham et al., 1992; Pugh, 1989).

The purpose of this study is to determine the effect of amyl xanthate collector, CMC and pH on the hetero-aggregation of pentlandite and serpentine using a calculated dispersion index (DI) as the response.

6.2. Experimental

6.2.1. Minerals

Pentlandite concentrate was obtained from the Vale mini-plant processing an ultramafic ore from Thompson, Manitoba (Xu et al., 2003). . The concentrate was sieved and the fine material (-75 μm) discarded. The pentlandite content of the -106/+75 μm fraction was further upgraded by gravity and magnetic separation. This purified pentlandite was ground and sieved and the -25 μm fraction reserved for testing. Using this procedure, creating fine material from coarse gives fresh surface and mitigates the effect of residual reagents (Mirnezami and Finch, 2003).

Serpentine from a ground sample of the ultramafic ore was isolated by gravity and magnetic separation. The final product was examined by X-ray diffraction, which showed clinochrysotile as the main silicate phase with minor pyrrhotite. The upgraded sample was sieved and the -25 μm fraction was used for testing.

6.2.2. Reagents

The following reagents were used:

- Sodium carboxymethyl cellulose (Sigma) with a molecular weight of 700 000 g/mol and a degree of substitution of 0.65-0.85 (i.e., the amount of hydroxyl groups substituted by carboxymethyl groups for each monomer of glucopyranose). As a note, carboxymethyl cellulose for industrial flotation has a wide range of molecular weight and degree of substitution. For example, CMC

Depramin 347 (Akzo Nobel Functional Chemicals) has a molecular weight of 510 600 g/mol and a degree of substitution of 0.47, as reported by Bicak et al. (2007).

Carboxymethyl cellulose was added from a stock solution with a concentration of 5000 mg/L agitated overnight to ensure its complete dissolution.

- Potassium amyl xanthate (PAX Prospec Chemicals) industrial grade, purified by dissolution-recrystallization, according to the procedure described by Rao (1971).
- Potassium nitrate (Fisher) 99.6 % purity, as background electrolyte.
- KOH and HCl (Fisher) as pH modifiers.

6.2.3. Aggregation/dispersion tests

Suspensions were prepared with 4 and 2 g/L of pentlandite and serpentine, respectively (equivalent to a volumetric fraction of 0.08 % of each mineral); minerals were separately placed in 10^{-2} mol/L KNO_3 and PAX solution. The pH was then adjusted and allowed to stabilize. Suspensions were mixed with a magnetic stirrer and CMC added as required. An aliquot was transferred to a quartz cell (cell constant = 2) and placed in a UV/Visible spectrophotometer (Helios, model etc). Absorbance as a function of time was monitored to indicate dispersion index. This scale of test setup suited the limited amount of sample available.

A 3-factor, 3-level central composite design ($\alpha = 1$) with a replicated central point was chosen, shown in Figure 6.1. This design allows major factors and interactions to be identified. An estimation of experimental precision is calculated from the centre point repeats. The levels were estimated from typical Vale mini-plant operation, the xanthate and CMC dosage being converted from the original g/t basis to g/L based on typical pulp % solids.

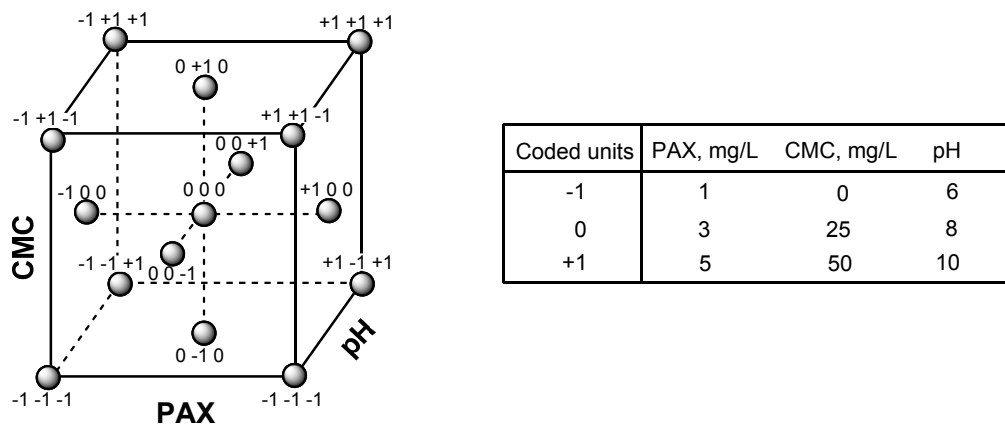


Figure 6.1 – Representation of the experimental design in coded units; original units are displayed in the table on the right side

6.2.5. Optical microscopy

Optical microscopy was used to evaluate the state of aggregation/dispersion and augment the dispersion index data. The sample conditioning procedure was the same as for the aggregation/dispersion tests. After conditioning, a pipette was used to transfer an aliquot of the suspension to a beaker and the sample was diluted ten times with supernatant. A sub-sample was taken and placed in a Petri dish and examined under a microscope (Leitz Laborluz 11POL) equipped with a video camera (Sony CCD Iris). The procedure is based on that described by Kissa (1999). Single-mineral systems were also examined at the same solids volumetric concentration as used in the mixed-mineral case.

6.3. Results

6.3.1. Dispersion index

Table 6.1 shows the dispersion index in absorbance units per second (A/s). Runs 9 and 10 correspond to the central points, which have a standard deviation of 0.0105 A/s and relative standard deviation of 3.09 %.

Table 6.2 displays the coefficient for the factors or interactions on the first regression model. An F-test was used to verify the significance of individual coefficients; a P value gives the probability of being wrong if it is assumed that the factor or interaction is significant. The rule adopted was to drop all factors with $P > 0.1$ (10 % of probability of being wrong). This retained the CMC factor, its quadratic term and the pH-CMC interaction term. Also, a common rule is to retain a factor in the model if one of its interaction terms is significant. Thus, pH was also retained, even though its P value was high (0.5660).

To check the validity of the regression model an F-test was again used. If $P < 0.05$ the model is considered significant at better than the 95 % confidence level. The model had a

P value = 0.0066 thus was significant at greater than the 99 % confidence level. A high correlation coefficient (R^2) is also an indication of the model fit. Both R^2 and adjusted R^2 were acceptable in the first regression.

Table 6.1 – Dispersion index for the experimental design

Run	Random order	Factors			Dispersion index, A/s
		PAX, mg/L	CMC, mg/L	pH	
1	10	1	0	6	0.4372
2	9	1	0	10	0.5520
3	4	1	50	6	0.3232
4	7	1	50	10	0.3160
5	15	5	0	6	0.4972
6	16	5	0	10	0.5120
7	2	5	50	6	0.3312
8	3	5	50	10	0.3012
9	8	3	25	8	0.3460
10	5	3	25	8	0.3312
11	13	1	25	8	0.3792
12	1	5	25	8	0.3032
13	14	3	0	8	0.4892
14	11	3	50	8	0.3200
15	12	3	25	6	0.3800
16	6	3	25	10	0.3440

Table 6.2 – Coefficient and P values of the factors and interactions on the first regression model

Factor or interaction	Coefficient	P (two-tail)	Considered for next regression
Mean	0.34463	0.0000	---
PAX	-0.00628	0.5244	No
CMC	-0.08960	0.0002	Yes
pH	0.00564	0.5660	Yes
PAX-CMC	-0.00335	0.7574	No
PAX-pH	-0.01535	0.1951	No
CMC-pH	-0.02085	0.0980	Yes
PAX-CMC-pH	0.00965	0.3904	No
PAX ²	-0.00644	0.7334	No
CMC ²	0.05696	0.0244	Yes
pH ²	0.01436	0.4585	No
		R ²	0.9601
		Adjusted R ²	0.8804
		P	0.0066

Table 6.3 shows the coefficients and P values for the factors and interactions in the final regression model. Since coefficients are coded their magnitude indicates their relative importance in the model. The most important factor was CMC concentration followed by CMC² indicating that the relationship between CMC concentration and dispersion index is non-linear. Noting the linear term is negative while the squared CMC coefficient is positive this means that initially as CMC is increased there is a negative effect on dispersion index (i.e. the system is more dispersed); however, as CMC is increased above the mid-point value, the positive non-linear term negates this trend and dispersion index becomes nearly constant over the upper concentration range. While the pH coefficient alone is small, negative and within the error of the system (high P value), the CMC-pH interaction is significant at better than the 95 % confidence level and of some importance in the model. The final regression model is presented below in both coded (Equation 6.1) and uncoded (Equation 6.2) forms. The goodness-of-fit parameters R² (0.93) and adjusted R² (0.90) attest to the appropriateness of the final model which is significant at greater than the 99.99 % confidence level. Figure 6.2 shows the Pareto chart for the coefficients in the final regression. The chart displays the coefficients as bars in descending order of significance and the cumulative percentage total as a line. Figure 6.3 compares predicted versus actual dispersion index.

Table 6.3 – Coefficient and P values of the factors and interactions on the final regression model

Factor or interaction	Coefficient	P (two-tail)
Mean	0.34727	0.0000
CMC	-0.08960	0.0000
pH	0.00564	0.5190
CMC-pH	-0.02085	0.0498
CMC ²	0.06065	0.0011
	R ²	0.9255
	Adjusted R ²	0.8983
	P	0.0000

$$\hat{y} = 0.34727 - 0.08960x_1 + 0.00564x_2 - 0.02085x_1x_2 + 0.06065x_1^2 \quad 6.1$$

$$\hat{y} = 0.39156 - 0.0051x_1 + 0.01325x_2 - 0.000417x_1x_2 + 0.000097x_1^2 \quad 6.2$$

where \hat{y} is dispersion index (A/s); x_1 is CMC concentration (in mg/L for the uncoded form); and x_2 is pH.

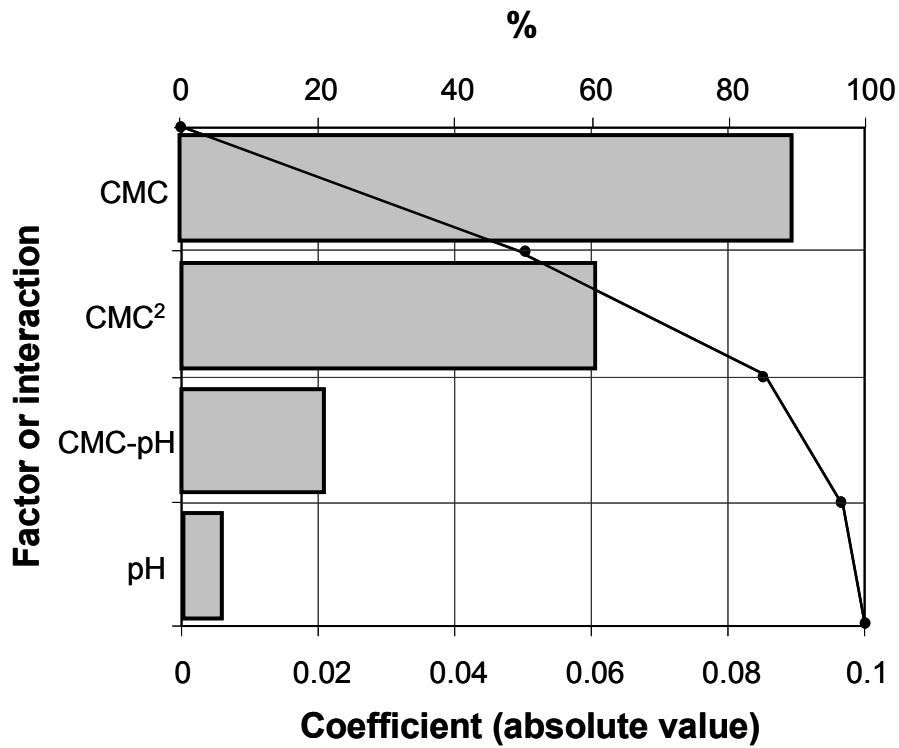


Figure 6.2 – Pareto chart of regression coefficients

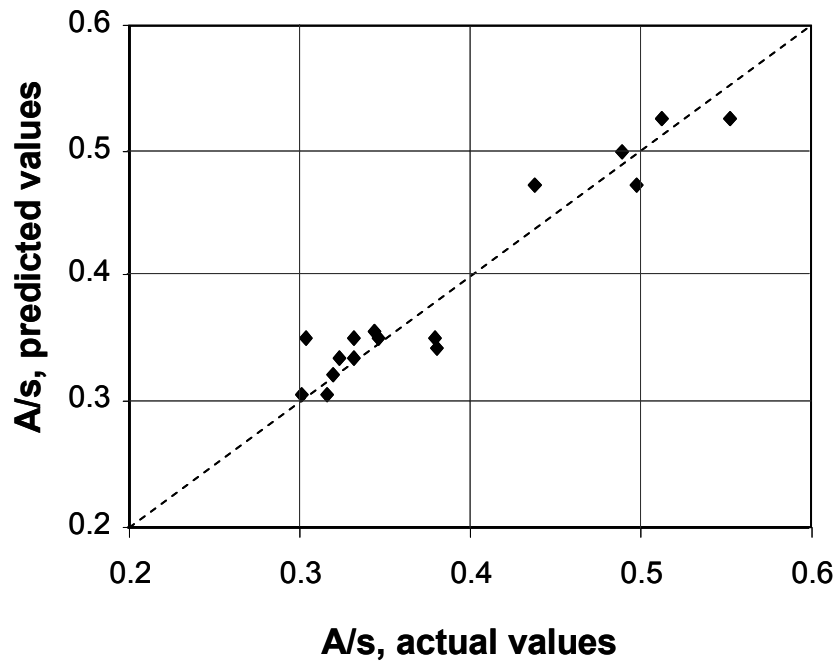


Figure 6.3 – Comparison of modeled versus actual dispersion indexes

The contour plot of dispersion index as a function of pH and CMC concentration is shown in Figure 6.4. This type of plot is selected to represent the three-dimensional surface in a two-dimensional format. The lines show the equal values of the response. Figure 6.4 shows that as CMC concentration increases dispersion index decreases (i.e., system is more dispersed) and dispersion index increases (i.e., system is less dispersed) when pH increases.

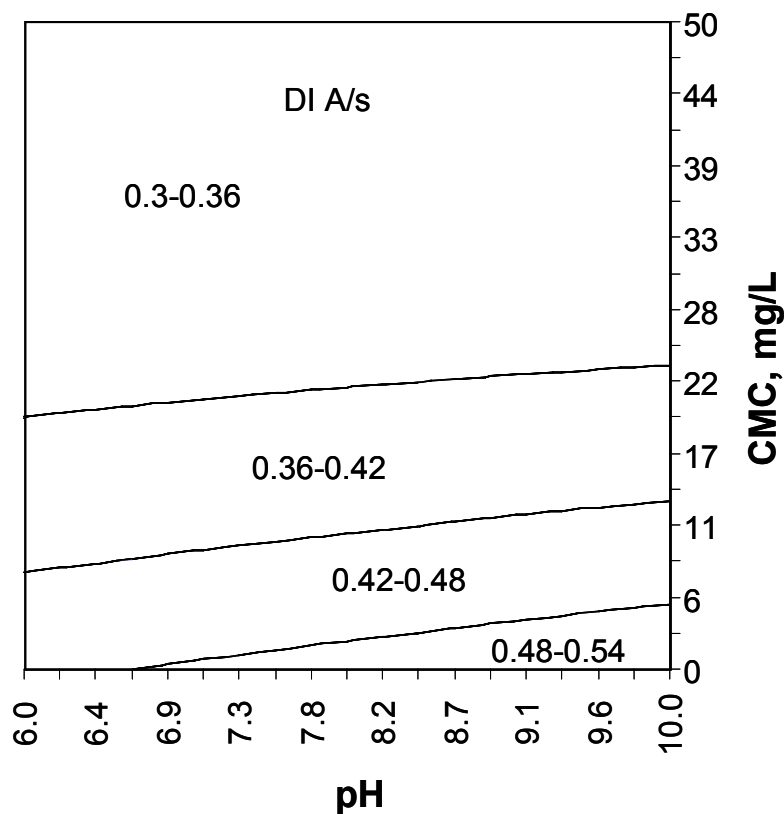


Figure 6.4 – Contour plot of dispersion index (A/s) as a function of pH and CMC concentration (mg/L). PAX content was fixed at its centre level (3 mg/L)

Dispersion index as a function of CMC concentration for pH 6, 8 and 10 is plotted in Figure 6.5. This Figure demonstrates the interaction between CMC and pH. It is observed that CMC is effective up to about 30 mg/L for pH 6 and 8. At pH 10 the dispersion index

continues to decrease by increasing CMC concentration up to 40 mg/L. However the advantage is small at the cost of consuming significantly more CMC and pH modifier. In the range 25 mg/L to 35 mg/L the effect of pH is minimal. The slope of the trend increases when pH increases, which implies that the same amount of CMC will produce a larger change in dispersion index at higher pH (i.e., CMC is slightly more effective at higher pH). This becomes more evident with the following example: at pH 6 if CMC is increased from 0 to 10 mg/L, dispersion index decreases from 0.471 A/s to 0.407 A/s (net variation: ca. 14 %) while at pH 10 the same increase in CMC decreases dispersion index from 0.524 A/s to 0.441 A/s (net variation: ca. 16 %).

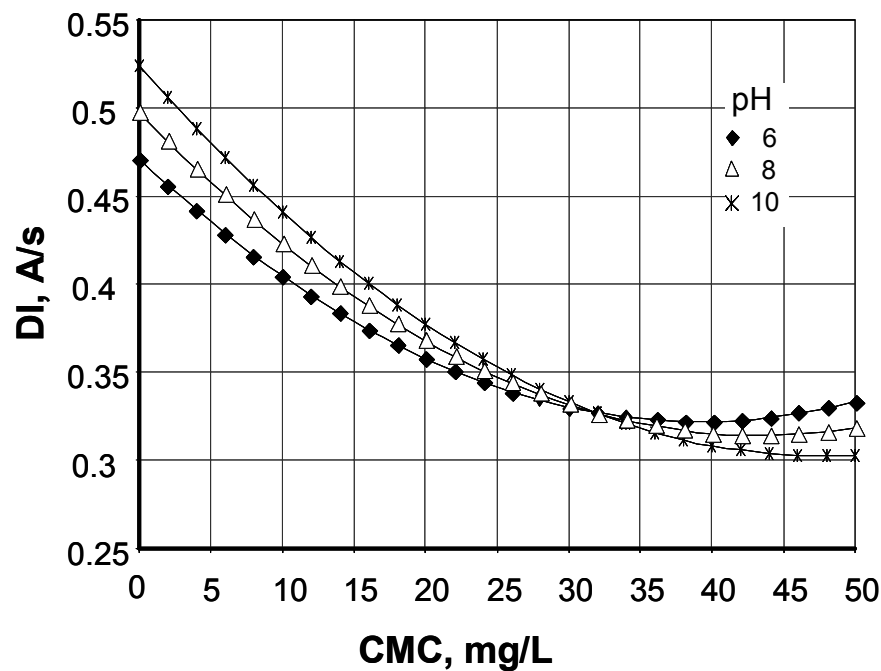


Figure 6.5 – Dispersion index as a function of CMC concentration for pH 6, 8 and 10. (Note, symbols are to identify the trends)

6.3.2. Optical microscopy

The tests were conducted at pH 10, which is a common condition for flotation of ultramafic ores (Dai et al., 2009). Homo-aggregation was not observed with either pentlandite or serpentine (Figure 6.6 a, b). In mixed mineral systems with no CMC added (conditions giving maximum dispersion index), aggregates of ca. 1 mm were observed (Figure 6.6 c). In the presence of 50 mg/L CMC, dispersion was evident (Figure 6.6 d). The variation in dispersion index therefore is related to the visual state of aggregation/dispersion of the suspensions.

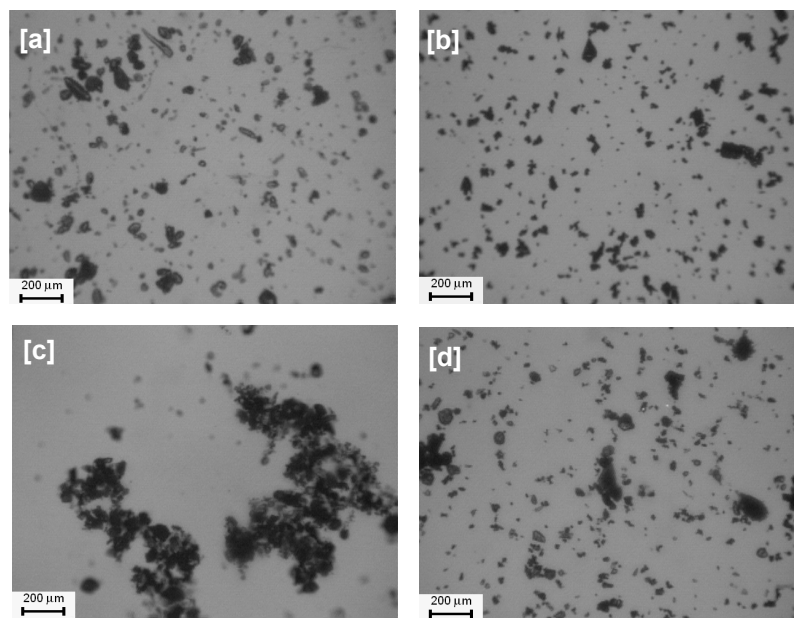


Figure 6.6 – Optical micrographs of pentlandite-serpentine systems (pH 10, 3 mg/L PAX, 10^{-2} mol/L KNO_3): (a) serpentine alone; (b) pentlandite alone; (c) serpentine and pentlandite; (d) serpentine and pentlandite with 50 mg/L CMC

6.4. Discussion

An experimental design methodology was employed to determine the effect of three variables (amyl xanthate concentration, CMC concentration, and pH) on the aggregation/dispersion of -25 μm pentlandite-serpentine particle mixtures using dispersion index as the response. To accommodate the small mass of sample available a light scattering technique using a standard UV/Visible spectrophotometer was employed. The dispersion index measured by rate of change in absorbance (A/s) proved reliable and the inferred aggregation/dispersion state correlated with the visual information.

The aim is to identify conditions for processing ultramafic ores with high serpentine content: those giving dispersion are considered a good starting point. The three variables tested reflect common practice for processing Ni-sulphide ores with silicate gangue. The concentrations of xanthate and CMC were selected based on conditions in the Vale mini-plant processing ultramafic ore from the Thompson (Manitoba) area. A common pH for Ni-sulphide flotation is ca. pH 10 but lower pH (i.e., requiring less pH modifier) is generally desirable.

Initial tests employed dosages based on a g/t basis equivalent to that used in the mini-plant. Using the same experimental design the variables showed no effect on dispersion index. The decision was taken to re-test based on the equivalent solution concentration (i.e. mg/L) knowing the slurry density (% solids). This approach yielded a response. This observation points to a difficulty in scaling down to laboratory conditions. Fundamentally, it may mean that reagent concentration in solution is the main driver and not the more common mass per tonne basis used in concentrator practice.

The results showed the significance of CMC in promoting dispersion. Edwards et al. (1980) found that hetero-aggregation between serpentine and pentlandite is controlled by their surface charge, as demonstrated in Chapter 5: at alkaline pH the minerals are oppositely charged and electrostatic attraction occurs. Aggregation is also promoted by

compression of the double layer under the action of electrolytes (Klassen and Mokrousov, 1963). In the present work, double-layer compression may be at play causing the aggregation observed at pH 6, which is close to the isoelectric point of mildly oxidized pentlandite (Bremmell et al., 2005, Fullston et al., 1999).

Another mechanism of hetero-aggregation is attributed to hydrophobic interaction resulting from adsorbed collector (Johnson et al, 2000; Klassen and Mokrousov, 1963). The concentration of PAX used (up to 5 mg/L, ca. 2.5×10^{-5} mol/L) does not seem sufficient to produce this type of aggregation. It has been reported that the small amounts of collector sufficient to make minerals hydrophobic are insufficient to produce aggregation (Klassen and Mokrousov, 1963).

In some cases pH not only affects adsorption of chemical species by controlling mineral surface charge but also by changing the degree of solution species dissociation. The latter does not seem to be a factor here for either CMC or xanthate. In other cases, OH^- and H^+ may compete for the adsorption sites on the mineral surfaces. The final regression model derived here indicates that pH alone is not as significant as the pH-CMC interaction term in promoting dispersion in the pentlandite-serpentine system. In effecting dispersion, it is evident that pH affects mineral-CMC interaction and not mineral-mineral interactions, as supported by direct visual observation.

6.5. Conclusions

A UV/Visible spectrophotometer was utilized to estimate the dispersion index by monitoring the light absorption of a suspension as a function of time. Optical microscopy provided visual evidence of correlation between the dispersion index and the state of aggregation/dispersion.

The technique was applied to investigate dispersion in the pentlandite-serpentine system using an experimental design with carboxymethyl cellulose (CMC) concentration, amyl

xanthate concentration and pH as factors. CMC and the interaction between pH and CMC were the most important factors controlling dispersion. The effect of CMC is non linear and works to reduce the effect on dispersion as concentration is increased. Interaction between CMC and pH indicated that CMC is more effective in dispersion at high pH.

References

- Bicak O., Ekmekci Z., Bradshaw D.J., Harris P.J. (2007) Adsorption of guar gum and CMC on pyrite. *Minerals Engineering* 20: 996-1002
- Bremmell K.E., Fornasiero D., Ralston J. (2005) Pentlandite-lizardite interactions and implications for their separation by flotation. *Colloids and Surfaces A: Physicochemical and Engineering Aspects* 252: 207-212
- Dai Z., Bos J.A., Quinn P., Lee A., Xu M. Flowsheet development for Thompson ultramafic low-grade nickel ores. C.O. Gomez; J.E. Nasset, S.R. Rao (Eds.)
- Advances in Mineral Processing Science and Technology. International Symposium of the Metallurgical Society of CIM, 217-228.2009*
- Edwards C.R., Kipkie W.B., Agar G.E. (1980) The effect of slime coatings of the serpentine minerals, chrysotile and lizardite, on pentlandite flotation. *International Journal of Mineral Processing* 7: 33-42
- Johnson S.B., Franks G.V., Scales P.J., Boger D.V., Healy T.W. (2000) Surface chemistry-rheology relationship in concentrated mineral suspension. *International Journal of Mineral Processing* 58:267-304
- Kissa E (1999) *Dispersions. Characterization, Testing, and Measurements.* A.T. Hubbart (Ed). Surfactant Science Series. Marcel Dekker: New York, USA

Klassen V.I., Mokrousov V.A. (1963) *An Introduction to the Theory of Flotation*, Butterworths: London, UK

Mirnezami, M., Restrepo, L., Finch, J. A. (2003) Aggregation of sphalerite: role of zinc ions. *Journal of Colloid and Interface Science* 259: 36-42

Pugh R.J. (1989) Macromolecular organic depressants in sulphide flotation-A review, 1. Principles, types and applications. *International Journal of Mineral Processing* 25: 101-130

Rao S.R. (1971) *Xanthates and Related Compounds*, Marcel Dekker, Inc., New York

Shortridge PG, Harris PJ, Bradshaw DJ, Koopal LK (2000) The effect of chemical composition and molecular weight of polysaccharide depressants on the flotation of talc. *International Journal of Mineral Processing* 59: 215-224

Wellham E.J., Elber L., Yan D.S. (1992) The role of carboxy methyl cellulose in the flotation of a nickel sulphide transition ore. *Minerals Engineering* 5: 381-395

Xu Z., Liu J., Choung J.W., Zhou Z. (2003) Electrokinetic study of clay interactions with coal in flotation. *International Journal of Mineral Processing* 68(1-4): 183-196

Contact angle measurements and flotation study in the pentlandite-serpentine system

Abstract

This chapter investigates the effect of carboxymethyl cellulose (CMC), pH, magnesium ions, copper activation and presence of serpentine particles on hydrophobicity of pentlandite as measured by captive bubble contact angle. The results are compared to floatability determined by recovery in a Partridge/Smith cell through a 2^{5-1} fractional factorial experimental design. The pH was the most important factor, acidic pH favoring both hydrophobicity and floatability. Copper activation enhanced both properties as well; magnesium ions reduced hydrophobicity at alkaline pH, but it did not show a clear effect on floatability; serpentine was detrimental over the range of pH tested; and CMC was

capable of partially restoring both hydrophobicity and floatability in the presence of serpentine.

7.1. Introduction

Among the suspected mechanisms that cause serpentine minerals to reduce selective flotation of pentlandite is slime coating (Edwards et al., 1980). Slime coating can affect performance through lowered grade by contamination of concentrate when ‘lightly’ coated pentlandite particles are floated, and through reduced recovery of ‘heavily’ coated pentlandite.

The formation of slime coating is attributed to electrostatic attraction between the positively charged serpentine and the negatively charged pentlandite at the typical flotation pH (i.e., ca. pH 10) (Bremmell et al., 2005; Edwards et al., 1980). The presence of MgO-minerals can release Mg ions which at alkaline pH form Mg(OH)_2 precipitates that can also produce slime coatings. Dispersants such as carboxymethyl cellulose (CMC) are used to combat slime coating (Wellham et al., 1992).

The purpose of this study is to determine the effect of solution species, xanthate collector, carboxymethyl cellulose dispersant and Mg ions, and the presence of serpentine particles on the hydrophobicity and floatability of pentlandite. Copper ions as pentlandite activator are considered as well. To accomplish the aim, contact angle (hydrophobicity) and small-scale flotation (floatability) experiments were performed.

7.2. Experimental techniques

7.2.1. Minerals

Contact angle experiments

Pentlandite crystals were obtained from Vale's Voisey's Bay operation. These were analyzed by ICP-OES (inductively coupled plasma-optical emission spectroscopy) to determine the elemental composition (Table 7.1).

Flotation experiments

Pentlandite was isolated from concentrate obtained in the Vale mini-plant processing ultramafic ore from Thompson, Manitoba. The concentrate was sieved and the fine material (-75 μm) discarded. The sample was further upgraded by gravity and magnetic separation. The -106/+75 μm fraction was cleaned with acetone to remove flotation reagents and kept in a freezer to limit surface oxidation. Particle size analysis (LS100 Coulter) showed a P80 ca. 120 μm . The elemental analysis is in Table 7.1.

Serpentine was isolated from the same ore by gravity and magnetic separation. The final product was examined by XRD, showing clinochrysotile as the main phase with minor pyrrhotite. Particle size distribution showed that the P80 is ca. 25 μm .

Table 7.1 – Elemental composition of pentlandite samples for contact angle and small-scale flotation tests. Theoretical composition of is also shown

Pentlandite sample	Element, %						
	Fe	Ni	Co	Pb	Zn	Cu	Insoluble
Theoretical composition	39.04	41.03	---	---	---	---	---
Used in contact angle	31.81	37.45	0.22	0.00	0.18	0.06	7.33
Used in small-scale flotation	40.35	30.99	0.88	0.00	0.15	0.04	8.56

Note: theoretical is based on $(\text{Ni,Fe})_9\text{S}_8$

7.2.2. Reagents

The reagents, supplier and purity are listed below:

- Sodium carboxymethyl cellulose (Sigma) with a molecular weight of 700 000 g/mol and a degree of substitution of 0.65-0.85 (i.e., the amount of hydroxyl groups substituted by carboxymethyl groups for each monomer of glucopyranose). Carboxymethyl cellulose was added from a stock solution with a concentration of 5000 mg/L agitated overnight to ensure its complete dissolution.
- Potassium amyl xanthate (Química Michoacana) industrial grade, purified by dissolution-recrystallization, according to the procedure described by Rao (1971).
- Sodium nitrate (Sigma-Aldrich) 99.9 % purity, as background electrolyte.
- Copper sulphate (Jalmek) >98 % purity, as pentlandite activator.
- Magnesium nitrate (Fermont) >98 % purity, as source of Mg ions.
- NaOH and HCl (Fisher) as pH modifiers.

7.2.3. Contact angle measurement

The crystals of pentlandite mounted in metallographic epoxy were polished and kept in an oxygen-free environment. After conditioning, the sample was transferred to the experimental set-up (Figure 3.6). A bubble of about 1 mm in diameter produced by a digital syringe was placed in contact with the sample. A picture was then taken and processed with an image analyzer to determine the advancing contact angle. Experiments were done in duplicate, with three to five bubbles tested each time. The error bar on the Figures represents the 95% confidence interval. Table 7.2 presents the conditioning strategy.

Table 7.2 – Conditioning of pentlandite for contact angle measurements

Exp.	Stage I ^[1]			Stage II					
	Cu ²⁺ , 50 mg/L	pH	t, min	PAX, 10 ⁻⁴ mol/L	Mg ²⁺ , 50 mg/L	Serpentine, 1 g/L ^[1]	CMC, 50 mg/L	pH	t, min
1	No	4, 7, 10	15	Yes	No	No	No	4, 7, 10	5
2	Yes	10	30	Yes	No	No	No	10	5
3	Yes	5.4 ^[3]	30	Yes	No	No	No	4, 7, 10	5
4	Yes	5.4	30	Yes	Yes	No	No	4, 7, 10	5
5	Yes	5.4	30	Yes	No	Yes	No	4, 7, 10	5
6	Yes	5.4	30	Yes	No	No	Yes	4, 7, 10	5
7	Yes	5.4	30	Yes	No	Yes	Yes	4, 7, 10	5

^[1] The background electrolyte in conditioning solutions of both stage I and II was NaNO₃ 0.001 mol/L.

^[2] To remove the serpentine settled on pentlandite and not attached, sample was washed and transferred to a solution of NaNO₃ 10⁻³ mol/L at the pH of the experiment prior to image being taken.

^[3] Natural pH (ca. pH 5.4).

7.2.4. Flotation experiments

The tests were carried out in a flotation cell based on the design of Partridge and Smith (1971) (Figure 3.7). One-gram samples of pentlandite (-106/+75 µm) were used for the tests. Using this relatively coarse size restricts recovery by hydraulic entrainment, estimated experimentally at <10 %. Flotation was for 5 minutes with nitrogen at 23 mL/min, equivalent to a superficial velocity of 0.072 cm/s. The conditioning prior to flotation was comparable to that used for the contact angle measurements.

Concentrate and tails were filtered and dried at 50 °C and weighed to determine recovery (the dependent variable or “response”) as a function of the pH, serpentine concentration, CMC dosage, Mg²⁺ and Cu²⁺ concentration (the independent variables or “factors”). A previous experiment showed that a mass fraction of 5 % serpentine was enough to completely depress pentlandite under the current experimental conditions. In order to detect an effect of the other factors, therefore, the high level of serpentine content was set at 1 %.

A 2^{5-1} experimental design with three centre-point repeats was used. This is a resolution V design in which no main effects or two-factor interactions are aliased with any other main effect or two-factor interaction. The levels of the design are displayed in Table 7.3.

Table 7.3 – Levels of the factors considered in the experimental design

Factors	Level		
	Low	High	Middle
pH	4	10	7
Serpentine (%)	0	1	0.5
CMC (mg/L)	0	50	25
Mg (mg/L)	0	50	25
Cu (mg/L)	0	50	25

7.3. Results

7.3.1. Contact angle measurements

Effect of xanthate

Figure 7.1 shows the contact angle obtained in the presence of xanthate collector (PAX) as a function of pH. It is observed that the contact angle decreases as the pH increases; at pH 10 the pentlandite showed no interaction with the bubble. Contact angle in absence of collector is also shown. It is observed that pentlandite alone was hydrophilic at neutral and alkaline conditions and at $\text{pH} < 4$ became slightly hydrophobic with a contact angle ca. 25° .

Cu-activation

It was initially surprising that pentlandite did not exhibit hydrophobic properties with xanthate at alkaline pH, since the typical pH in operations is 9 or higher (Dai et al., 2009). Xanthate concentration was increased two-fold and the pentlandite remained hydrophilic at alkaline pH. This behaviour has been reported elsewhere (Malysiak et al., 2004). Copper ions have been shown to activate various sulphides including pentlandite (Kelebek et al., 2005; Malysiak et al., 2004).

Accordingly, the specimen was conditioned in the presence of Cu^{2+} (from CuSO_4) for 30 minutes at natural pH (ca. pH 5), then conditioned with PAX (10^{-4} mol/L) as a function of pH for 5 minutes. Figure 7.2 shows that the hydrophobicity of pentlandite is increased for all tested pH and Cu-activation was more effective as the pH increased. Copper-activated pentlandite was used for most subsequent studies into the effect of the other variables on hydrophobicity.

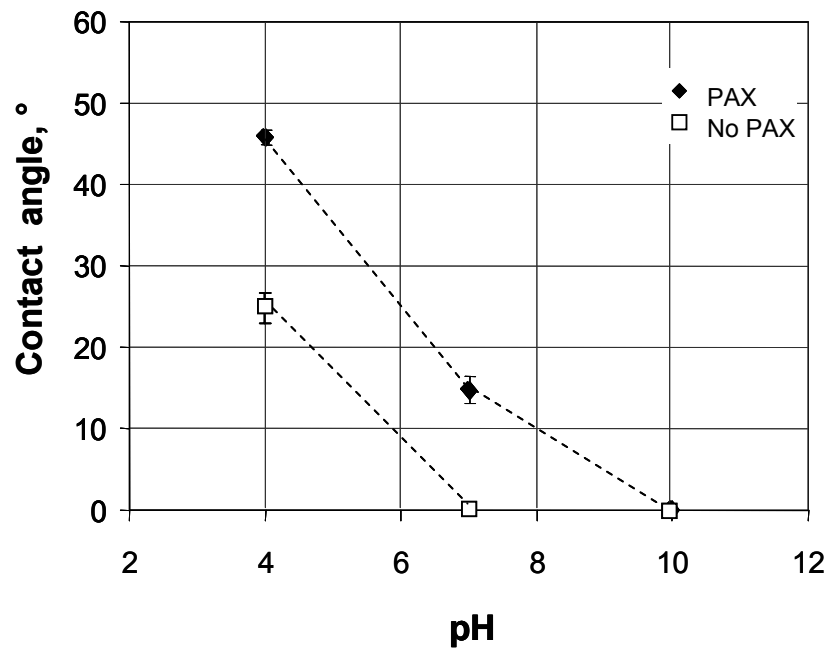


Figure 7.1 – Contact angle of pentlandite as a function of pH; PAX = 10^{-4} mol/L (filled diamonds) and no PAX (open squares), $\text{NaNO}_3 = 10^{-3}$ mol/L. Error bars indicate 95 % confidence interval

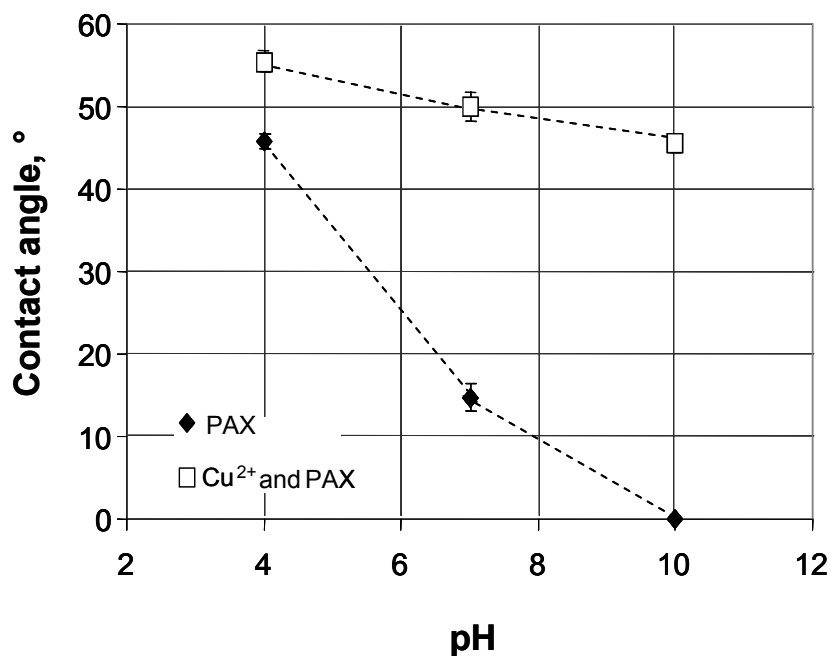


Figure 7.2 – Contact angle of Cu-activated pentlandite as a function of pH (open squares). PAX = 10^{-4} mol/L, $\text{NaNO}_3 = 10^{-3}$ mol/L. For comparison the result for non-activated pentlandite is included (filled diamonds)

Effect of magnesium ions

The effect of magnesium ions on the hydrophobicity of Cu-activated pentlandite was a visible reduction of contact angle at pH 10 but no effect at pH 4 and 7 (Figure 7.3). Figure 7.4 shows that when soda ash is used to reach pH 10, the effect of magnesium is less.

Effect of serpentine

The presence of serpentine particles had a notable impact on the hydrophobicity of the (Cu-activated) pentlandite as reflected by the large reduction of contact angle at all tested pH (Figure 7.6). The greatest effect was at pH 10 when the contact angle decreased to zero. These findings are in accord with the zeta potential measurements on pentlandite

where the charge reversed from negative to positive at alkaline pH in the presence of serpentine (see Chapter 5).

Effect of CMC

Carboxymethyl cellulose (CMC) was tested as a serpentine dispersant. To allow for any impact on hydrophobicity by itself CMC was tested first in the absence of serpentine. Figure 7.5 shows that the dispersant lowered the hydrophobicity of pentlandite at pH 4 and 7, while it remained practically unchanged at pH 10.

Figure 7.6 shows that CMC largely restored hydrophobicity to pentlandite and the effectiveness improved as pH increased.

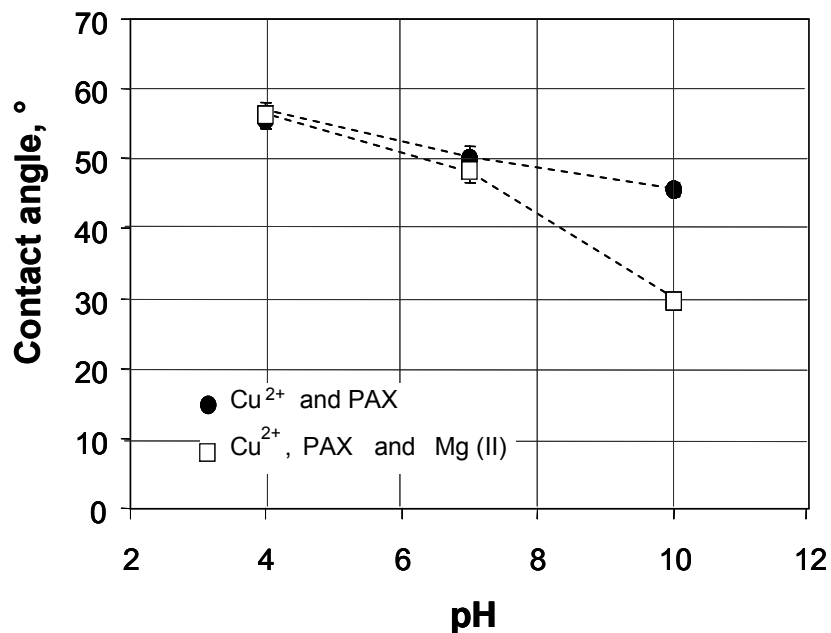


Figure 7.3 – Contact angle on Cu-activated pentlandite as a function of the pH in the presence of magnesium ions (50 mg/L) (open squares). PAX = 10^{-4} mol/L, NaNO₃ = 10^{-3} mol/L. For comparison the curve for the Cu-activated pentlandite in absence of magnesium is included (filled circles)

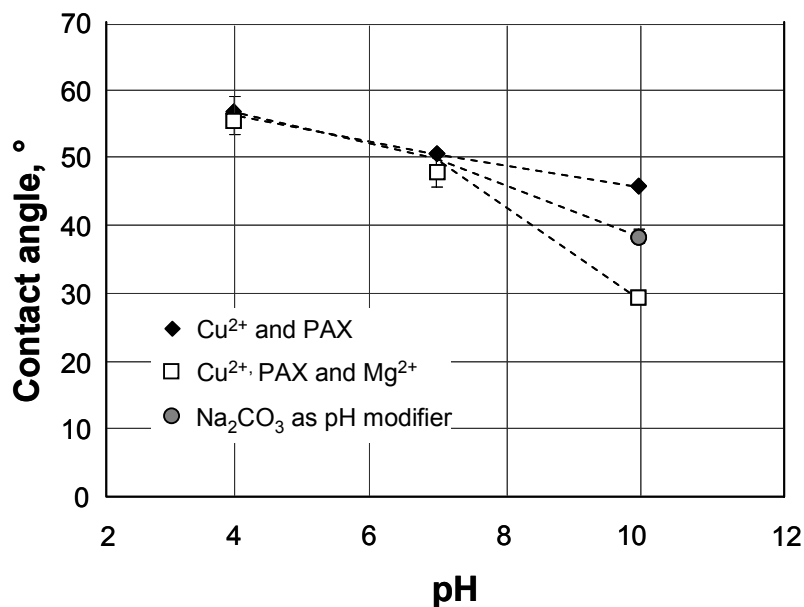


Figure 7.4 – Contact angle on Cu-activated pentlandite as a function of the pH in the presence of magnesium (50 mg/L) (filled circles) when Na₂CO₃ pH is used as pH modifier. PAX = 10⁻⁴ mol/L, NaNO₃ = 10⁻³ mol/L. For comparison the curves for the Cu-activated pentlandite in the presence of PAX (filled diamonds), and in the presence of PAX and magnesium (50 mg/L) (open squares) when NaOH is used as pH modifier are included

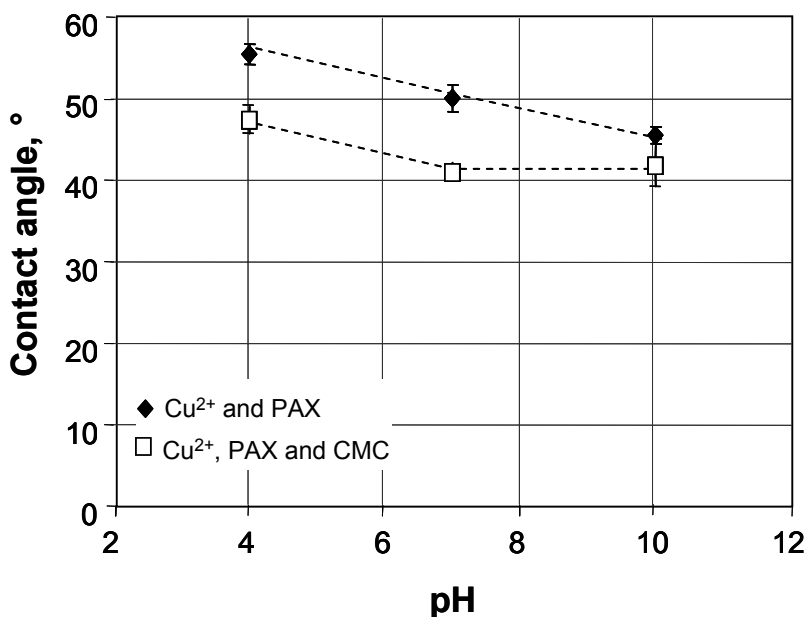


Figure 7.5 – Contact angle on Cu-activated pentlandite as a function of the pH in the presence of CMC (50 mg/L) (open squares). PAX = 10⁻⁴ mol/L, NaNO₃ = 10⁻³ mol/L. For comparison the curve for the Cu-activated pentlandite is included (filled diamonds)

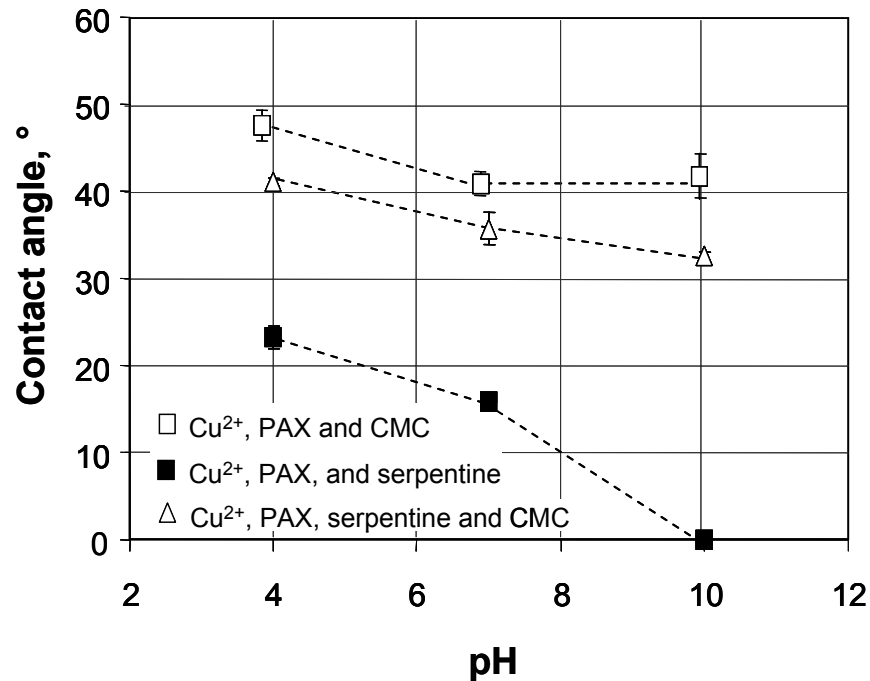


Figure 7.6 – Contact angle on Cu-activated pentlandite as a function of the pH in the presence of serpentine (0.1 g/L) and CMC (50 mg/L) (open triangles). PAX = 10^{-4} mol/L, $\text{NaNO}_3 = 10^{-3}$ mol/L. For comparison, curves for Cu-activated pentlandite with PAX and CMC (open squares), and with PAX and serpentine (filled squares) are included

7.3.2. Flotation tests

The flotation experiments tested the impact of the variables under conditions closer to practice. Table 7.4 summarizes the recovery of pentlandite for the experimental design. The random order in which the tests were performed is also shown.

The effect of a factor is defined as the change in response produced by a change in the level of the factor. This is normally called “main effect”. An interaction between two factors occurs when the difference in response between the levels of one factor is different at all levels from the other factor. The effect of a factor or interaction is given by the coefficient of the regression model in coded units. The coefficients of the first polynomial regression model are shown in Table 7.5. The most significant factor is pH

(low pH favored recovery) followed by activation with copper (more pentlandite floated) and serpentine content (an adverse effect on flotation). Serpentine-CMC was the most significant interaction: CMC improved flotation when serpentine was present, and had an adverse effect when it was not. The pH-Mg²⁺ and pH-CMC interactions were not significant.

An F-test was used to verify the significance of individual coefficients; $P < 0.05$ suggests the effect or interaction is significant at greater than 95 % confidence level. High factor/interaction coefficients also indicate significance. These two significance criteria were used to choose the factors and interactions considered for the next regression. The correlation coefficient (R^2) is indication of the model fit. Both R^2 and adjusted R^2 were acceptable in the first regression.

Table 7.6 presents the final regression, the P values and the coefficients of correlation. Equations 1 and 2 show the polynomial regression in coded and uncoded units, respectively. The goodness-of-fit parameters R^2 (0.98) and adjusted R^2 (0.96) attest to the appropriateness of the final model. Figure 7.7 shows a comparison of predicted and actual pentlandite recoveries. A plot of studentized residuals (calculated by dividing residuals by the estimated standard deviation) as a function of the predicted values is shown in Figure 7.8. A random (even) distribution of the residuals about zero is evident; if they were not evenly distributed, it would suggest there is a missing factor or interaction in the model. Studentized residuals are preferred over simple residuals, because they can be compared (Montgomery, 2005).

Table 7.4 – Recovery of pentlandite according to experimental design

Run	Random order	Pentlandite recovery, %
1	1	96.3
2	9	91.6
3	5	64.0
4	13	64.3
5	18	25.1
6	11	19.9
7	7	88.9
8	15	61.1
9	17	7.2
10	10	62.5
11	6	65.7
12	14	8.6
13	19	26.3
14	12	12.3
15	8	44.6
16	16	39.3
17	2	42.3
18	3	43.7
19	4	48.5

Table 7.5 – Coefficient of the first regression model

Factor or interaction	Coefficient	P (two-tail)	Considered for next regression
Mean	47.987	0.0000	---
pH	-15.298	0.0008	Yes
Serpentine	-8.925	0.0038	Yes
CMC	5.955	0.0121	Yes
Mg	-3.661	0.0439	Yes
Cu	9.306	0.0034	Yes
pH-serpentine	6.233	0.0106	Yes
pH-CMC	0.293	0.8060	No
pH-Mg	1.019	0.4194	No
pH-Cu	5.856	0.0127	Yes
Serpentine-CMC	12.825	0.0013	Yes
Serpentine-Mg	-2.884	0.0775	No
Serpentine-Cu	-5.386	0.0159	Yes
CMC-Mg	-7.579	0.0061	Yes
CMC-Cu	0.694	0.5701	No
Mg-Cu	-7.740	0.0058	Yes
	R ²	0.9958	
	Adjusted R ²	0.9747	

Table 7.6 – Coefficients of the final regression model

Factor or interaction	Coefficient	P (two-tailed)
Mean	47.987	0.0000
pH	-15.298	0.0000
Serpentine	-8.925	0.0004
CMC	5.955	0.0036
Mg	-3.661	0.0336
Cu	9.306	0.0003
pH-serpentine	6.233	0.0028
pH-Cu	5.856	0.0039
Serpentine-CMC	12.825	0.0000
Serpentine-Cu	-5.386	0.0061
CMC-Mg	-7.579	0.0009
Mg-Cu	-7.740	0.0008
R ²	0.9841	
Adjusted R ²	0.9590	

$$y = 47.7 - 15.3x_1 - 8.9x_2 + 5.9x_3 - 3.7x_4 + 9.3x_5 + 6.2x_1x_2 + 5.8x_1x_5 + 12.8x_2x_3 - 5.4x_2x_5 - 7.6x_3x_4 - 7.7x_4x_5 \quad 7.1$$

$$y = 101.33 - 9.13x_1 - 61.81x_2 + 0.03x_3 + 0.47x_4 + 0.35x_5 + 4.16x_1x_2 + 0.01x_1x_5 + 1.02x_2x_3 - 0.43x_2x_5 - 0.01x_3x_4 - 0.01x_4x_5 \quad 7.2$$

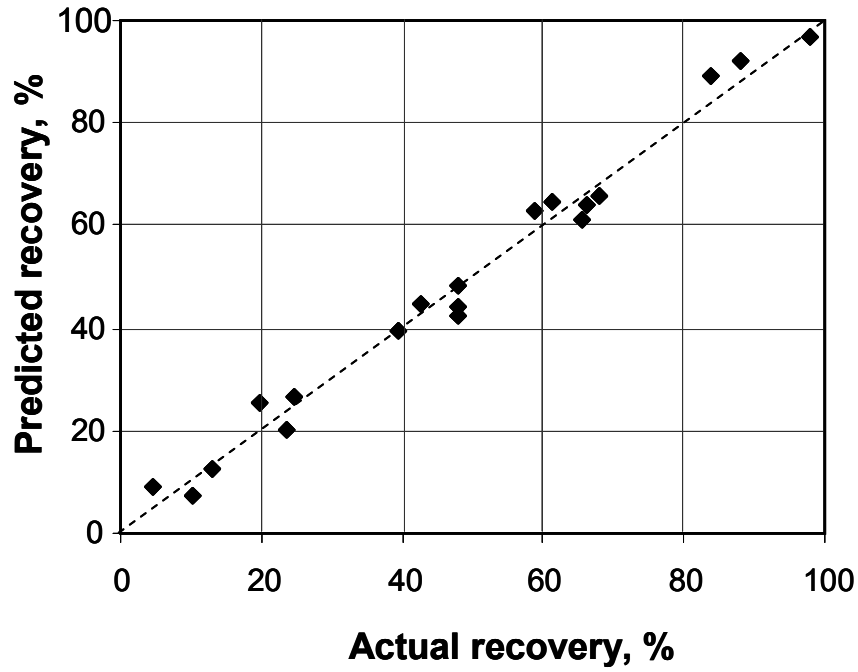


Figure 7.7 – Comparison of modeled versus actual recoveries

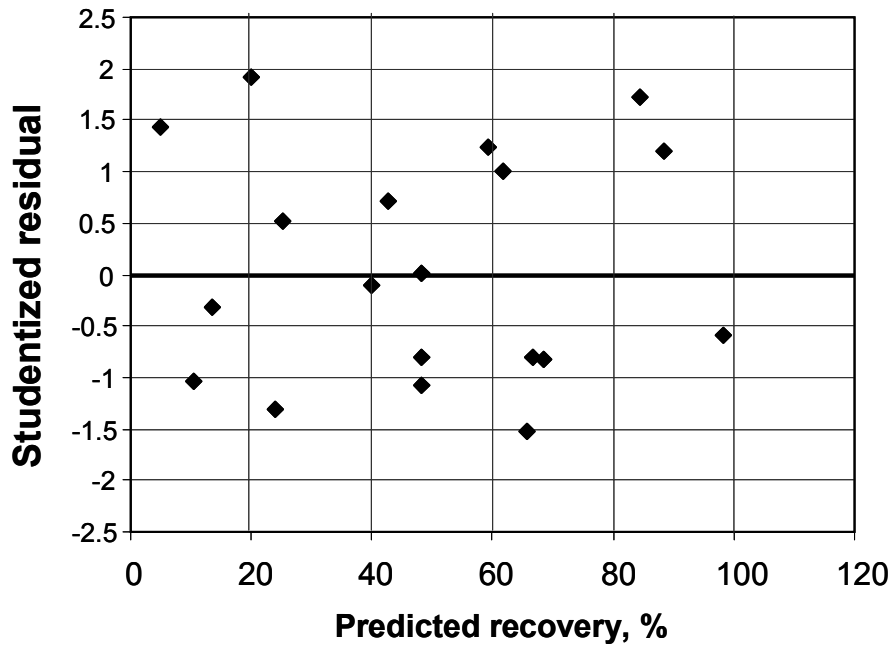


Figure 7.8 – Studentized residuals as a function of the predicted recovery

The Pareto chart of the coefficients in the final regression is displayed in Figure 7.9. Bars give the absolute value of these coefficients in descending order of significance and the curve shows the cumulative fit. This Figure reveals that pH, activation with copper and serpentine content remain the most important factors. Serpentine-CMC continues to be the main interaction. Magnesium content has the least effect (but is negative).

The contour plots of recovery as a function of serpentine and CMC and as a function of pH and serpentine are shown in Figures 7.10 and 7.11, respectively. The other factors were set constant at their centre point. This type of plot is useful to represent a three-dimensional surface in a two-dimensional format. The contours display constant values of the response. As seen in Figure 7.10, recovery of pentlandite decreases rapidly as the content of serpentine increases. Carboxymethyl cellulose at 50 mg/L restores the floatability of pentlandite completely when serpentine content is high. However, CMC seems to decrease recovery slightly in the absence of serpentine. Similar observations were also evident in the contact angle data.

Figure 7.11 shows that flotation is strongly impacted by pH, recovery being higher as pH decreases. Recovery remains moderately high in the presence of serpentine at acidic pH. Pentlandite depression is more severe when the serpentine and pH are at the highest levels.

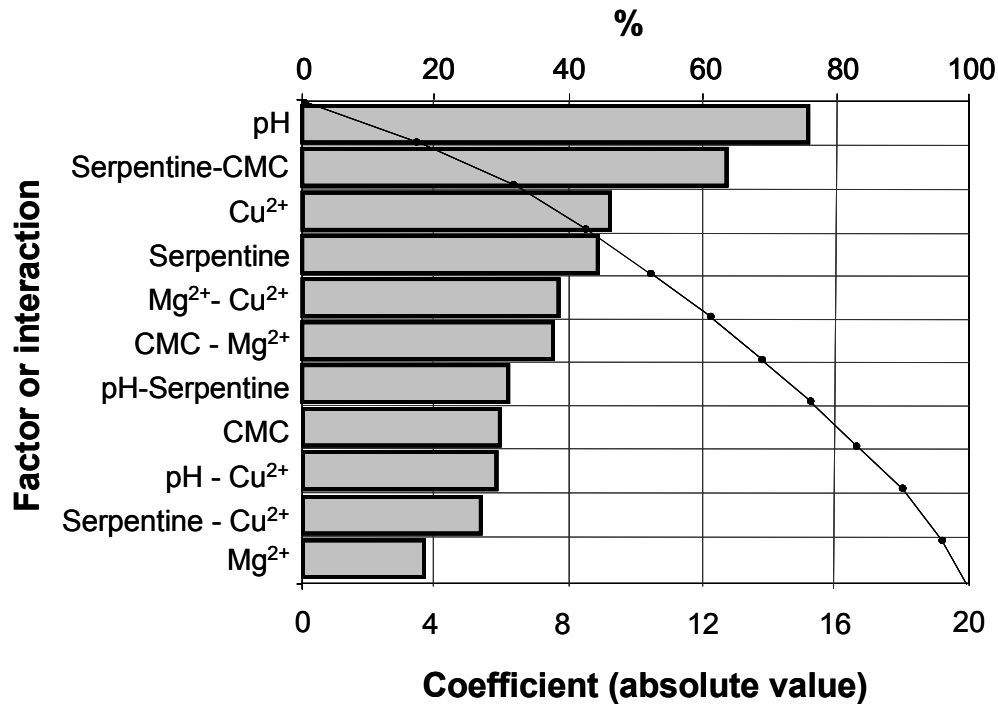


Figure 7.9 – Pareto chart of regression coefficients

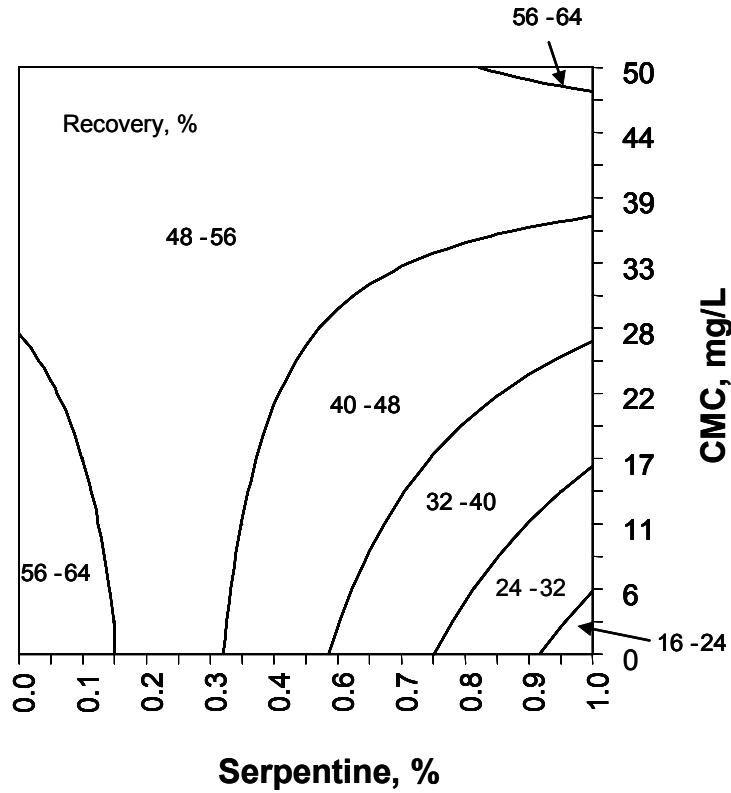


Figure 7.10 – Contour plot of pentlandite recovery as a function of serpentine content and CMC concentration. pH, magnesium and copper concentrations were fixed at their centre level

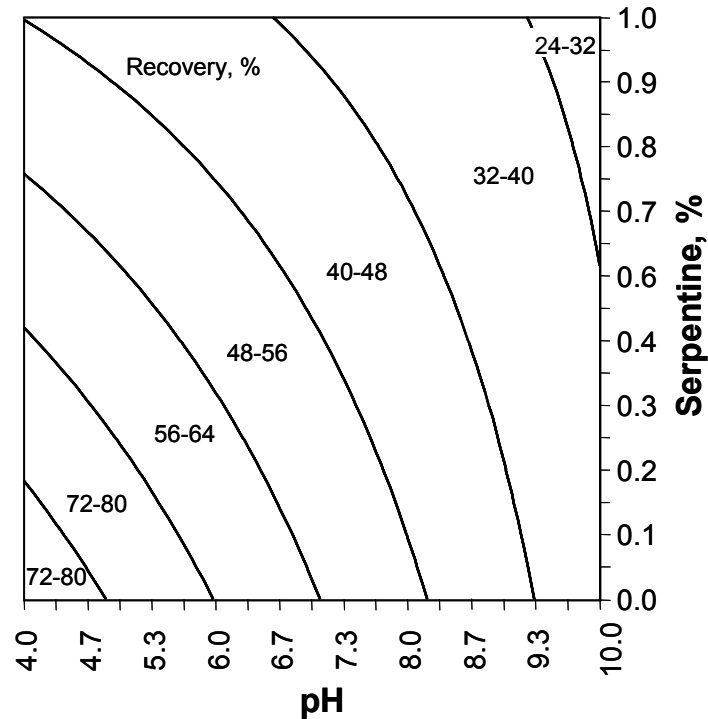


Figure 7.11 – Contour plot of pentlandite recovery as a function of pH and serpentine content. CMC, magnesium and copper concentrations were fixed at their centre level

7.4. Discussion

The hydrophobicity developed by the pentlandite in the absence of xanthate at acidic pH has been documented for pentlandite and other sulphide minerals and is known as self-induced or collectorless flotation (Ralston et al., 2007; Rao and Leja, 2004; Kelebek and Yoruk, 2002). The phenomenon is attributed to superficial oxidation releasing some metal ions to solution and leaving metal deficient or polysulphide species on the surface which present hydrophobic sites. With sufficient oxidation elemental sulphur may form. The process is favored at low pH as metal ions readily solubilize while at alkaline pH some competition with hydrophilic metal hydroxy species occurs. The system electrochemical potential is another factor. For example, the oxidation of sulphide to

elemental sulphur occurs above ca. 0 mV (vs. SHE) and typical open systems such as those here exhibit potentials around 350 mV (Rao and Leja, 2004).

The hydrophobicity is enhanced by chemisorption of xanthate. Collector uptake on pentlandite seems less at alkaline pH as revealed by the contact angle and flotation tests. This observation is supported by the work of Malysiak et al. (2004) who found from zeta potential measurements and surface analysis that only a small amount of xanthate was adsorbed at alkaline pH.

The hydrophobicity and flotation response of pentlandite with xanthate at pH 10 was increased by addition of copper ions. Shackleton et al. (2003) indicated that above pH 9 in the presence of copper ions pentlandite held some hetero-coagulated $\text{Cu}(\text{OH})_2$ precipitates which were reduced to their Cu^+ equivalent. When xanthate is added the hydrophobic cuprous-xanthate species forms, which renders the pentlandite hydrophobic.

Depression due to magnesium ions occurs at ca. pH 10 coinciding with hydroxide precipitation (Figure 7.12). The results demonstrate that depression is not caused by hindrance of collector uptake due to the precipitation of $\text{Mg}(\text{OH})_2$, but rather is attributable to the hydrophilic character of the hydroxide itself. Lascelles et al. (2002) observed similar behaviour in the case of Cu-activated sphalerite in the presence of Mg ions. The effect of magnesium was diminished by using soda ash for pH regulation due to precipitation and dispersion of magnesium carbonate. Soda ash is frequently used as dispersant when magnesium ions are present (Sadler and Sim, 1991).

The flotation results were not as clear as the contact angle measurements in showing the effect of pH-Mg interaction. This difference may be linked to experimental resolution: the higher surface area available in the flotation system means the magnesium concentration per unit of surface area is lower and the extent of precipitate coverage is correspondingly less than in the contact angle case.

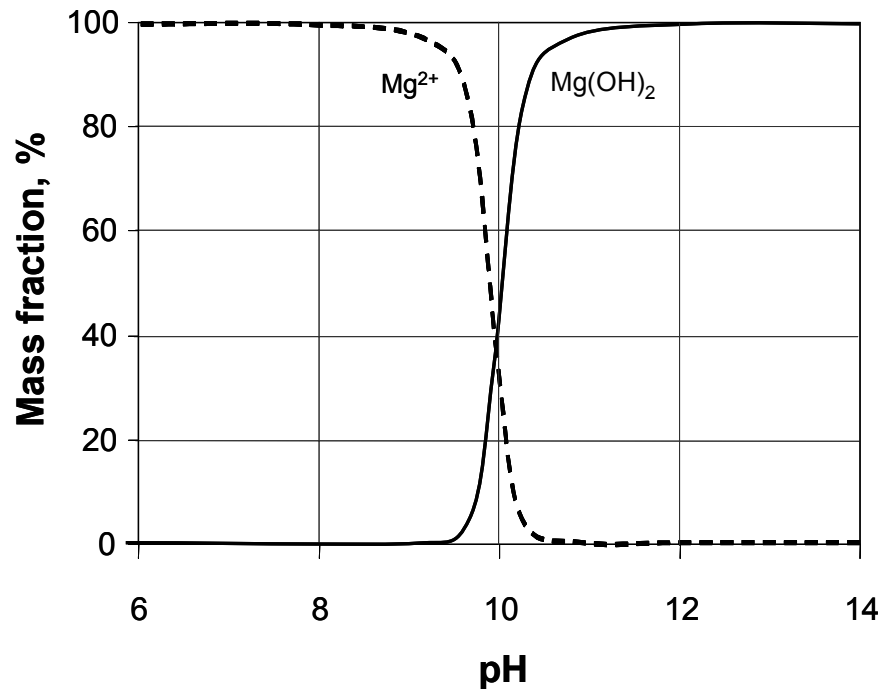


Figure 7.12 – Species distribution diagram of magnesium in concentration percentage as a function of pH. Mg species concentration equal to 50 mg/L (modified from Sui and Huang, 1998)

Experiments showed that a small amount of serpentine is enough to depress Cu-activated pentlandite. The implication is that slime coating is responsible. Similar findings were reported by Edwards et al. (1980), who observed almost total depression of pentlandite flotation at chrysotile content of only 0.5 %. At much higher serpentine content the fibrous nature of these minerals may create physical entrapment of pentlandite, which can severely limit flotation (Uddin et al., 2010) but is not the focus here.

Carboxymethyl cellulose was effective in restoring pentlandite hydrophobicity as shown by both contact angle and flotation experiments. It is believed that CMC adsorbs on serpentine through hydrogen bonding (Shortridge et al., 2000). The contact angle measurements showed CMC was more effective at alkaline pH but flotation did not reveal any strong pH-CMC interaction. Again, the difference in pentlandite surface area between the two test approaches may be the reason.

7.5. Conclusions

Contact angle and flotation recovery measurements were performed to determine the impact of process variables on, respectively, hydrophobicity and floatability of pentlandite. The main findings are:

- pH was the most important factor under the selected experimental conditions, acidic pH enhancing hydrophobicity and floatability
- Hydrophobicity was enhanced when pentlandite was activated with copper. Cu-activation seems more efficient at alkaline than at acidic pH.
- Serpentine depressed hydrophobicity and floatability markedly at all tested pH but the effect was greatest at pH 10 which correlates with a hetero-coagulation mechanism (serpentine being positively charged, pentlandite negatively charged at alkaline pH).
- Magnesium ions were detrimental to pentlandite hydrophobicity at pH 10, suggesting interaction with $Mg(OH)_2$ precipitates. When soda ash was used for pH adjustment, the negative effect of magnesium on hydrophobicity was reduced. Floatability did not show significant impact of Mg.
- CMC restored hydrophobicity to pentlandite conditioned with serpentine but floatability did not show a strong CMC/pH interaction effect.
- The difference in available surface area between the two tests systems, much higher in testing floatability than hydrophobicity, is considered to contribute to differences in the two responses.

References

- Bremmell K.E., Fornasiero D., Ralston J. (2005) Pentlandite-lizardite interactions and implications for their separation by flotation. *Colloids and Surfaces A: Physicochemical and Engineering Aspects* 252: 207-212
- Dai Z., Bos J.A., Quinn P., Lee A., Xu M. Flowsheet development for Thompson ultramafic low-grade nickel ores. C.O. Gomez; J.E. Nasset, S.R. Rao (Eds.) *Advances in Mineral Processing Science and Technology. International Symposium of the Metallurgical Society of CIM*, 217-228.2009
- Edwards C. R., Kipkie W. B. and Agar G. E. (1980). The effect of slime coatings of the serpentine minerals, chrysotile and lizardite, on pentlandite flotation. *International Journal of Mineral Processing* 7(1): 33-42
- Kelebek S., Thompson J.M., Tukul C. (2005) The impact of copper activation on the scavenging of Ni-Cu sulphide ores, in *Proceedings Centenary of Flotation Symposium*, pp 869-873 (AusIMM: Brisbane) 6-9 June 2005
- Kelebek S., Yoruk S. (2002) Bubble contact angle variation of sulfide minerals in relation to their self-induced flotation. *Colloids and Surfaces, A: Physicochemical and Engineering Aspects* 196: 111-119
- Lascelles D., Finch J.A., Sui C. (2002) Depressant action of Ca and Mg on flotation of Cu activated sphalerite. *Canadian Metallurgical Quarterly* 40(2): 133-140
- Malysiak V., Shackleton N.J., O'Connor C.T. (2004) An investigation into the floatability of a pentlandite-pyroxene system. *International Journal of Mineral Processing* 74: 251-262

Montgomery D.C. Design and Analysis of Experiments, John Wiley & Sons, Phoenix, Arizona, USA, 2005

Partridge A.C., Smith G.W. (1971) Small-sample flotation testing: a new cell. Transaction of the Institution of Mining and Metallurgy Section C: Mineral Processing and Extractive Metallurgy 80: 199-200

Ralston J., Fornasiero D., Grano S., (2007) Pulp and Solution Chemistry. In Froth Flotation: A Century of Innovation, M. Fuerstenau, G. Jameson R.H. Yoon Eds. Society for Mining, Metallurgy and Exploration Inc., USA, 227-258

Rao S.R. Leja J. (2004) Surface Chemistry of Froth Flotation, Kluwer Academic Publishers, New York

Rao S.R. (1971) Xanthates and Related Compounds, Marcel Dekker, Inc., New York

Sadler L.Y., Sim K.G. (1991) Reduction of coal-water mixture consistency with soda ash and lime. Canadian Journal of Chemical Engineering 69: 1224-1228

Shackleton N. J., Malysiak V., O'Connor C.T. (2003) The use of amine complexes in managing inadvertent activation of pyroxene in pentlandite-pyroxene flotation system. Minerals Engineering 16: 849-856J

Shortridge P.G., Harris P. J., Bradshaw D.J., Koopal L.K. (2000) The effect of chemical composition and molecular weight of polysaccharide depressants on the flotation of talc. International Journal of Mineral Processing , 59: 215-224

Sui C., Wang J. (1998) EQUILCOM A software for chemical thermodynamics analysis, McGill University

Uddin S. (2010) Acidic fiber disintegration in the grinding of ultramafic ore. Department of Mining and Materials. McGill University. Work in progress

Wellham E.J., Elber L., Yan D.S. (1992) The role of carboxy methyl cellulose in the flotation of a nickel sulphide transition ore. *Minerals Engineering* 5: 381-395

8

Conclusions, contributions and future work

8.1. Conclusions

This thesis comprises the results of a surface chemistry study initiated to determine phenomena restricting selective flotation of pentlandite from ultramafic ore. The work is divided in two parts. The first compared isoelectric point (obtained by zeta potential calculated from electrophoretic mobility) and point of zero charge (calculated using the Mular-Roberts titration technique) of some specimen MgO-minerals belonging to the electrophoretically anisotropic phyllosilicate mineral class. The main findings are listed below.

- For the serpentine and chlorite, p.z.c. was greater than i.e.p. (pH 4.3 vs. pH 3.3, and pH 4.6 vs. pH <3, respectively) while the M-R technique did not yield a p.z.c. for talc.
- In the case of chlorite, aggregation occurred over the pH range from i.e.p. to p.z.c., suggesting both contribute to aggregation, while for serpentine the sample remained dispersed over the pH range, attributed to hydration effects.

The second part comprised an examination of the effect of selected variables on the two main components isolated from an ore sample (Thompson, Manitoba): the valuable mineral pentlandite and the main identified MgO-gangue, serpentine. This part includes an electrokinetic study (zeta potential), aggregation/dispersion, hydrophobicity (contact angle) and small-scale flotation.

Zeta potential measurements of pentlandite alone and mixed with serpentine using different background solutions were carried out in an attempt to synthesize actual flotation processing conditions. Scanning electron microscopy analysis helped validate the findings. The main results are:

- Zeta potential measurements on pentlandite and serpentine individually in indifferent electrolyte showed that slime coating is predicted as a consequence of electrostatic attraction at flotation pH 9-10.
- The mixed mineral case revealed significant effect on pentlandite interpreted as the result of slime coating by serpentine and magnesium hydroxide precipitates at alkaline pH.

Dispersion was measured by turbidimetry using a UV/visible spectrophotometer. The variables considered in an experimental design were carboxymethyl cellulose (CMC) concentration, amyl xanthate concentration and pH. Optical microscopy helped confirm the findings. The main results are:

- CMC and the interaction between pH and CMC were the most important factors controlling dispersion.
- The effect of CMC was non linear and worked to reduce the effect on dispersion as concentration was increased.
- Interaction between CMC and pH indicated that CMC has more influence on dispersion at high pH.

Hydrophobicity was measured by captive bubble contact angle and floatability by recovery in a small-scale Partridge/Smith flotation cell. The main results are:

- The pH was the most important factor, acidic pH enhancing hydrophobicity.
- Copper ions in presence of xanthate enhanced hydrophobicity being particularly effective at alkaline pH.
- Serpentine depressed pentlandite markedly at all tested pH but its effect was greatest at pH 10.
- Magnesium ions were detrimental to pentlandite hydrophobicity at pH 10, suggesting interaction with $Mg(OH)_2$. When soda ash was used, the negative effect of magnesium was reduced. Floatability did not show significant response to Mg/pH interaction.
- Carboxy-methyl cellulose (CMC) restored hydrophobicity to pentlandite conditioned with serpentine. Floatability did not show significant response to CMC/pH interaction.

8.2. Contribution to knowledge

- Comparison of isoelectric point and point of zero charge of some phyllosilicates relevant to processing ultramafic ores.
- Study of mechanisms of depression of pentlandite through determination of the effect of dissolved metal ions and serpentine fines on pentlandite electrophoretic mobility under conditions approaching the flotation environment.
- Validation of a technique for aggregation/dispersion studies suitable for small samples.
- Determination of effects and interactions of process variables (e.g., collector, carboxymethyl cellulose dosage, pH) on hydrophobicity (contact angle) and floatability (flotation recovery) of pentlandite.

8.3. Future work

- The effect of aging on zeta potential of serpentine was attributed to the release of magnesium ions. Although releasing magnesium to a similar extent, neither talc nor chlorite showed an aging effect. Surface analysis (e.g., XPS) is suggested to determine differences due to aging.
- Testing the effect of dispersants and other flotation reagents on zeta potential might be revealing.
- In the same tenor, investigating the role of magnesium release by serpentine in mixed mineral tests may help explain the persistent positive charge on pentlandite at alkaline pH.

- Expand the dispersion and flotation studies to include the effect of selected reagents and other species (e.g., the use of supernatant as background to simulate actual flotation conditions).

Appendix 1: Characterization of phyllosilicates

High purity samples of chlorite, serpentine and talc from Ward's Natural Science Establishment were prepared by crushing, hand sorting, pulverizing, wet sieving and gravity separation, (if necessary), to obtain purity $-25\ \mu\text{m}$ fraction.

To determine the mineral type and its structure X-Ray Diffraction (XRD) was used. Serpentine as lizardite, chlorite was identified as clinochlore with traces of serpentine-chlorite, and talc as steatite (Figures A-1.1-A-1.3).

Particle size distribution was determined by a laser scattering technique (Horiba LA 920), gave a P80 of ca. $40\ \mu\text{m}$ for serpentine and 30 for chlorite and talc (Figure A-1.4).

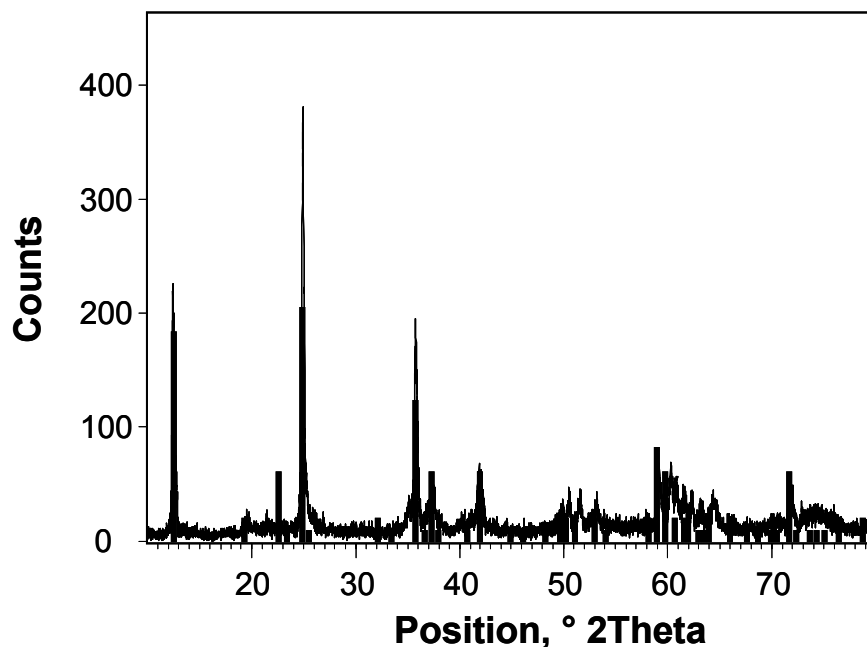


Figure A-1.1 – X-ray diffraction of serpentine identified as lizardite. The diffraction peaks for lizardite is shown

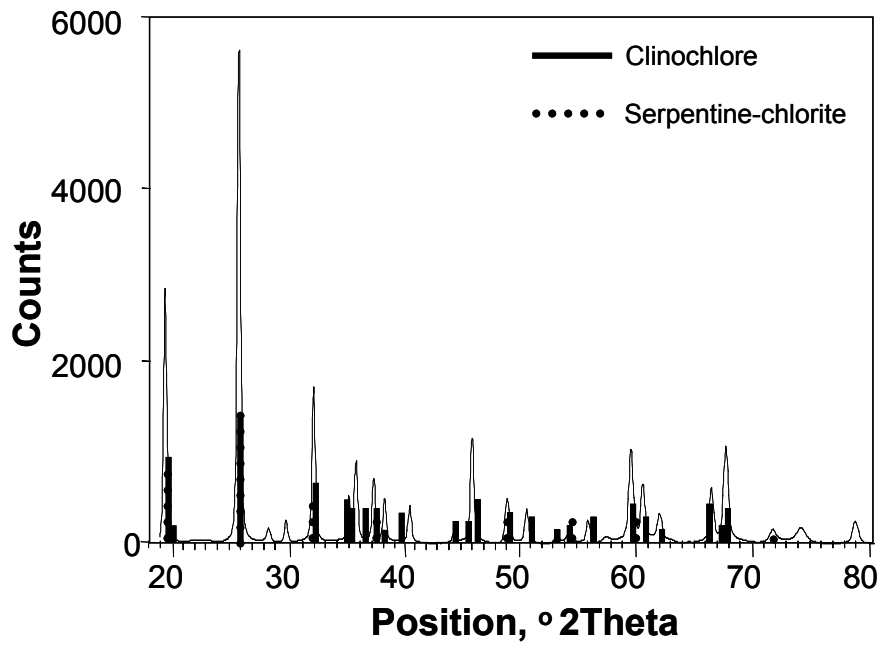


Figure A-1.2 – X-ray diffraction of chlorite identified as clinochlore with minor serpentine-chlorite. The diffraction peaks for clinochlore (continuous line) and chlorite-serpentine (dashed line) are shown

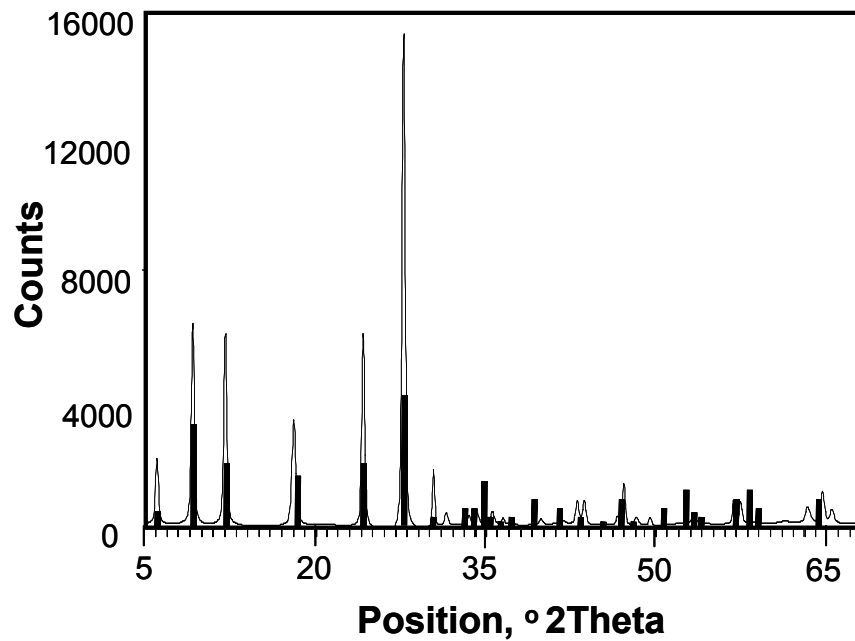


Figure A-1.3 – X-ray diffraction of talc identified as steatite. The diffraction peaks for steatite is shown

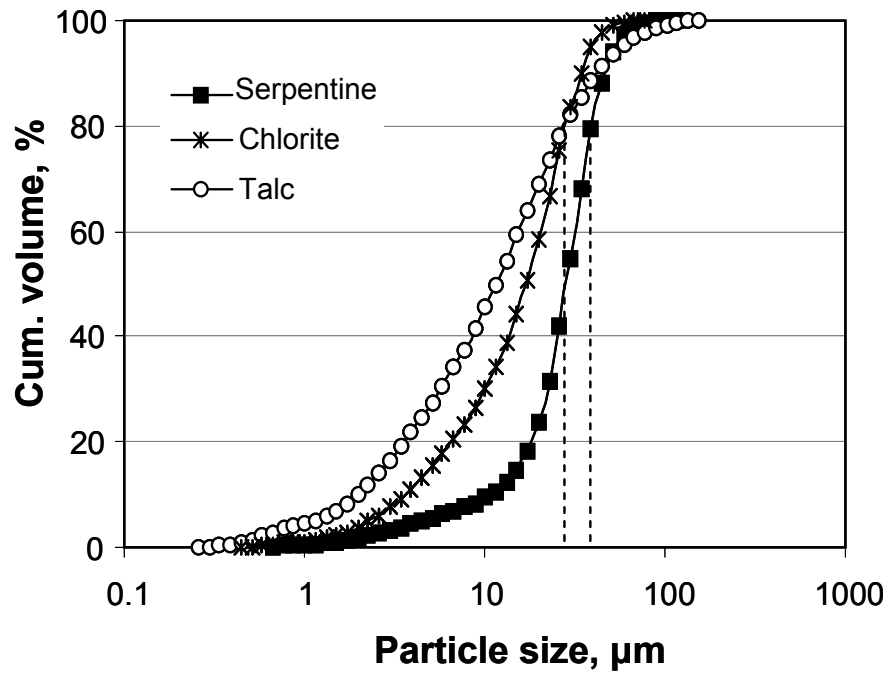


Figure A-1.4 – Particle size distribution for serpentine, chlorite and talc. P80 ca. 40 μm for serpentine and 30 μm for chlorite and talc

Appendix 2: Isolation of mineral phases and characterization of samples

For part of the study pentlandite and serpentine samples were isolated from Thompson area ultramafic ore.

Pentlandite is the ore's principal nickel mineralization, distantly followed by violarite, a mineral associated with weathering and oxidation of pentlandite. More than 90 % of the nickel in the ore is present in these two phases, the rest being split between minor nickel sulphides and serpentine. Serpentine is the major MgO-gangue (it contributes more than 80 % of the magnesium present in the ore), followed by olivine and chlorite. The other important minerals are pyrrhotite and magnetite. Table A-2.1 summarizes the main mineral phases present in the ore, as identified by Vale. The specific gravity and magnetic properties information was used to design the mineral isolation procedure.

A-2.1 – Main mineral phases in the Thompson ultramafic ore

Mineral phase	Chemical formula	Specific gravity	Magnetic properties	Volumetric fraction, %
Pentlandite	(Fe,Ni) ₉ S ₈	4.6-5	No	1.01
Violarite	(Ni,Fe) ₃ S ₄	4.79	No	0.15
Chalcopyrite	CuFeS ₂	4.1-4.3	No	0.06
Pyrite	FeS ₂	4.9	No	0.46
Magnetite	Fe ₃ O ₄	5.2	Strong	6.34
Pyrrhotite ^[1]	Fe _{1-x} S	4.6-4.7	Moderate	5.07
Olivine	(Mg,Fe) ₂ SiO ₄	3.3-4.3	No	11.99
Chlorites	(Mg,Fe ²⁺) ₅ (Al,Fe ³⁺) ₂ Si ₃ O ₁₀ (OH) ₈	2.6-3.3	No	3.45
Mica (biotite)	K(Fe,Mg) ₃ AlSi ₃ O ₁₀ (OH) ₂	2.8-3.2	No	0.59
Serpentine	Mg ₃ Si ₅ O ₁₀ (OH) ₂	2.3	Weak	63.29
Talc	Mg ₃ Si ₄ O ₁₀ (OH) ₂	2.7-2.8	No	0.08
Dolomite	CaMg(CO ₃) ₂	2.9	No	3.13

^[1] Pyrrhotite predominantly monoclinic

To obtain serpentine, an ore sample provide by Vale was used. It was split into sub-samples of ca. 400 g using a rotary riffler. The samples were wet ground in a tumbling mill (steel rod grinding media). The resulting slurry was processed over a magnetic drum. The nonmagnetic product was processed in a Knelson (gravity) concentrator; a concentrate (i.e., dense material) and tailings (i.e., light material) were obtained. The tailings were treated with hand magnets to remove the remaining magnetic material. The dense product was processed on a Mozley table (gravity separation) into three products; the densest fraction was treated with a hand magnet. Figure A-2.1 shows a schematic of the procedure.

To retrieve pentlandite, flotation concentrate samples from the Vale mini-plant were used. The concentrate was sieved and the finest material ($-75\ \mu\text{m}$) discarded. The coarsest material was separated with a Mozley table and the heaviest fraction reprocessed on the table. Finally, the magnetic material was removed by hand magnet (Figure A-2.2).

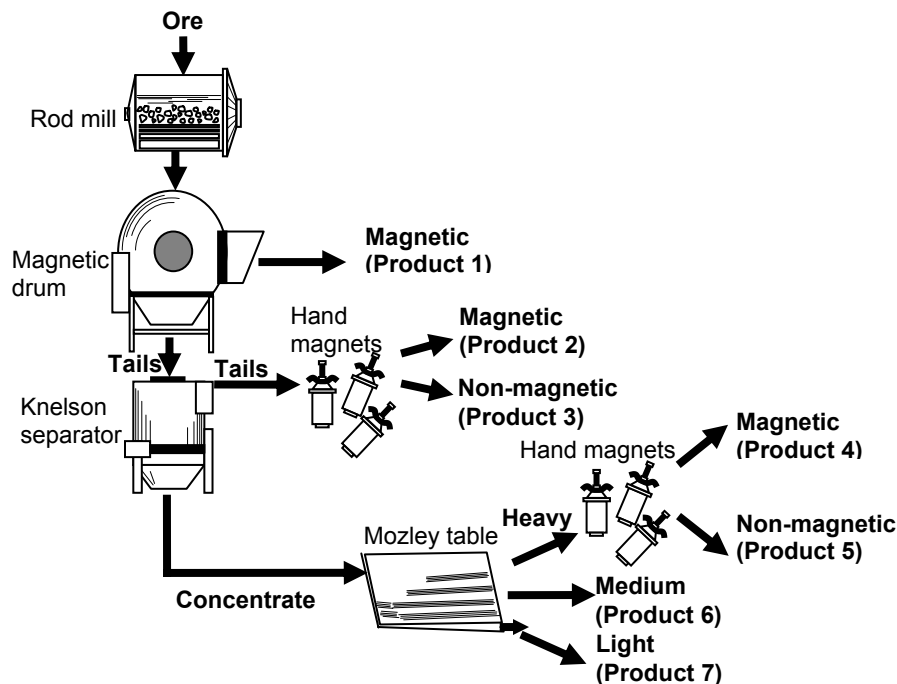


Figure A-2.1 – Schematic diagram of the ore processing

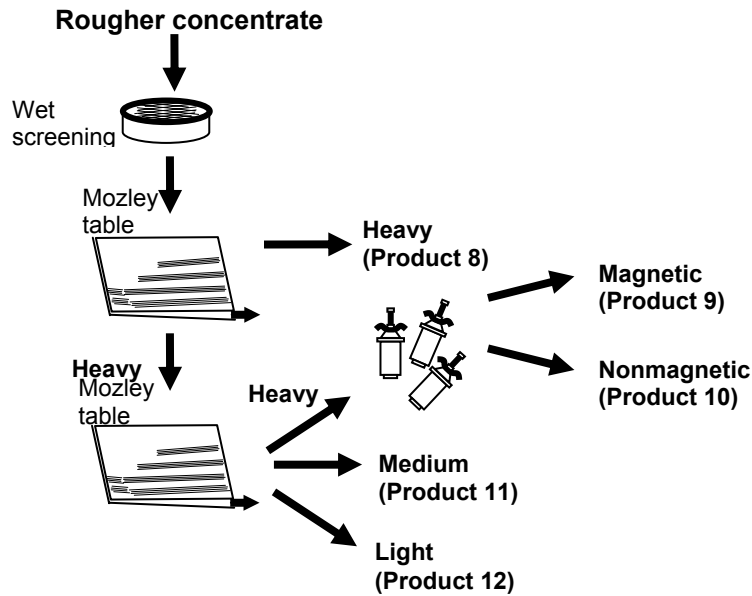


Figure A-2.2 – Schematic diagram of the flotation concentrate processing

A-2.1. Product identification

The serpentine and pentlandite samples obtained were characterized by X-ray diffraction (Figures A-2.3 and A-2.4). Product 3 (see Figure A-2.1) was identified as predominantly clinochrysotile with other minor MgO-minerals (Figure A-2.4); products 5 and 10 were mainly pentlandite with some hexagonal pyrrhotite (Figure A-2.3).

Particle size distribution was determined by a laser scattering technique (Coulter LS100), gave a P80 of ca. 120 μm (Figure A-1.5) and 25 μm (Figure A-2.6), respectively. Figure A-2.7 shows optical micrographs of these products.

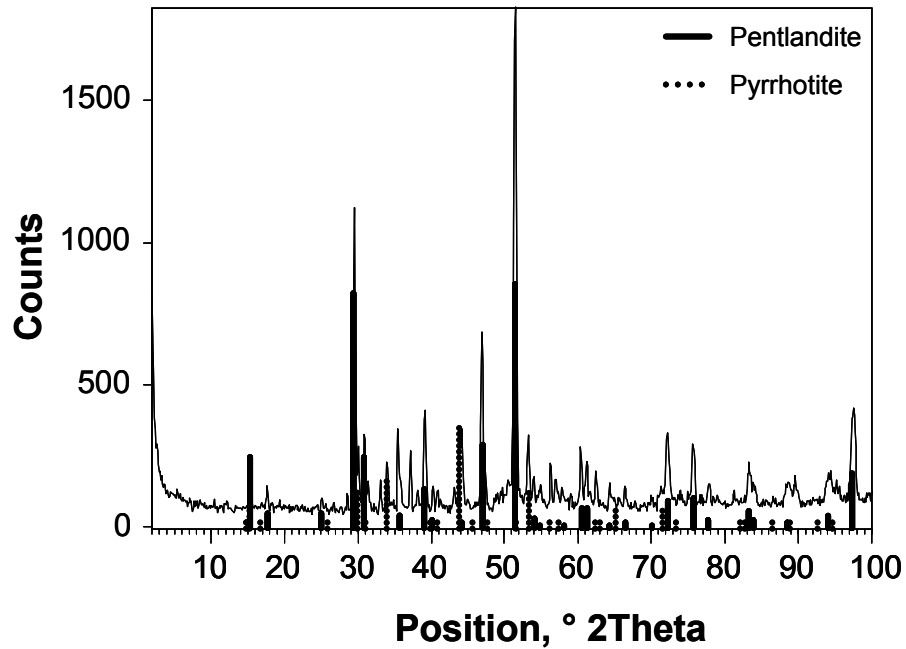


Figure A-2.3 – X-ray diffraction of pentlandite used for small-scale flotation. The diffraction peaks for pentlandite (continuous line) and pyrrhotite (dashed line) are shown

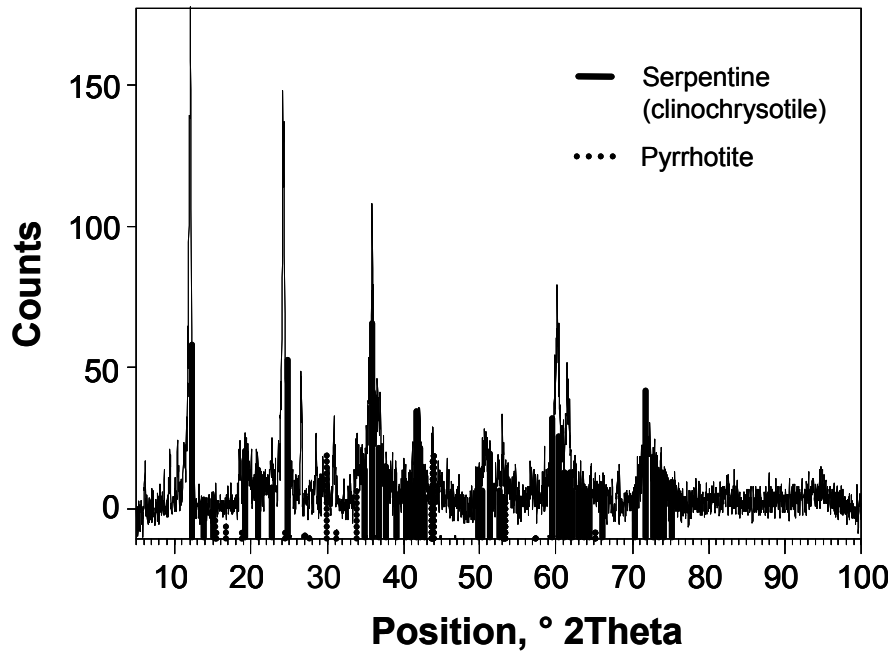


Figure A-2.4 – X-ray diffraction of serpentine used for small-scale flotation. The diffraction peaks for clinochrysotile (continuous line) and pyrrhotite (dashed line) are shown

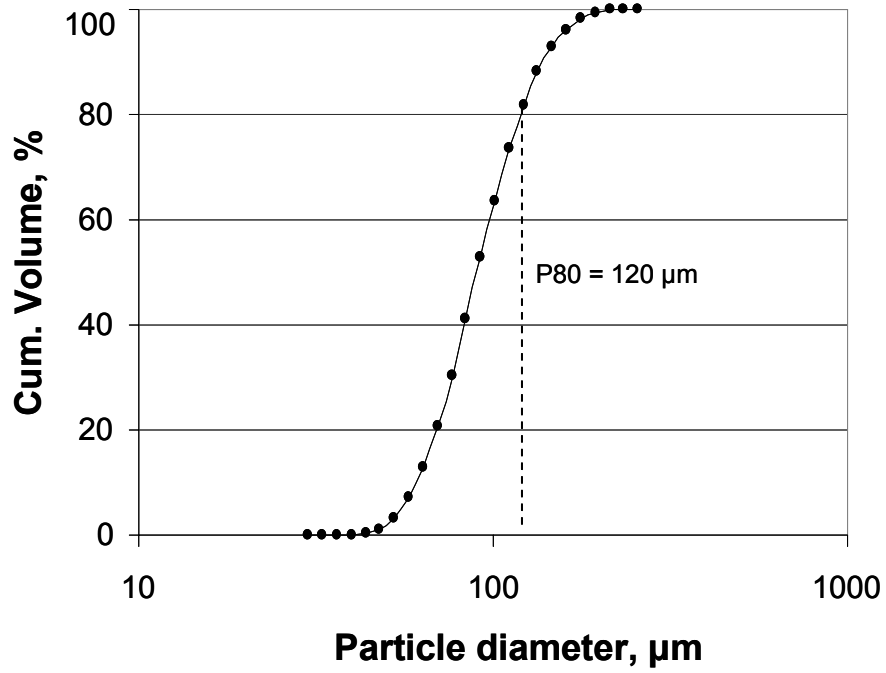


Figure A-2.5 – Particle size distribution for pentlandite used in the flotation tests. P80 ca. 120 μm

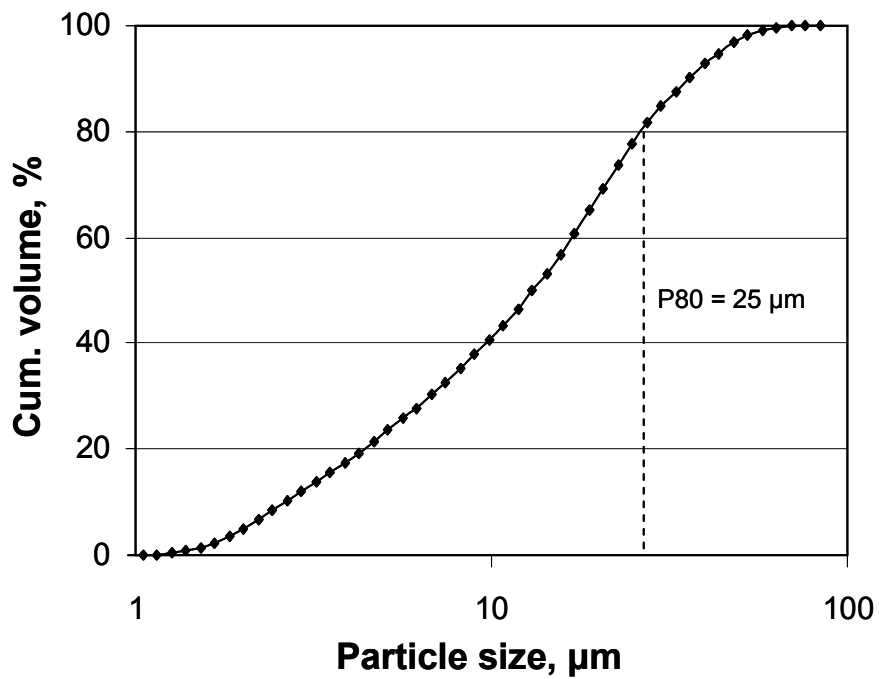


Figure A-2.6 – Particle size distribution for serpentine used in the flotation and contact angle tests. P80 ca. 25 μm

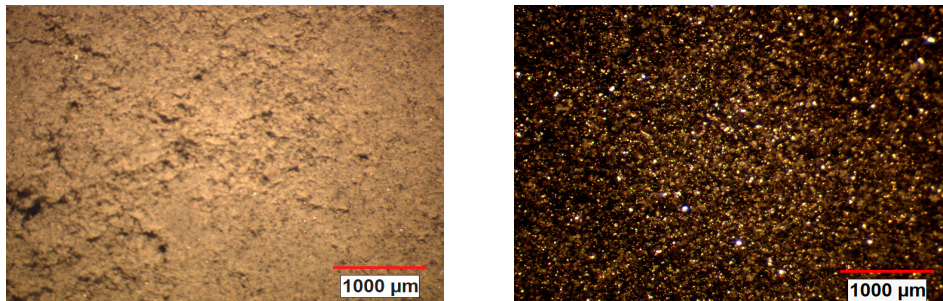


Figure A-2.7 – Optical micrographs of serpentine (left) and pentlandite (right)

A-2.2. Pentlandite for contact angle measurements

For the contact angle experiments, pentlandite crystals were obtained from Vale's Voisey's Bay operation. Figure A-2.8 shows the X-ray diffraction pattern of the sample. No other mineral phases other than pentlandite were identified.

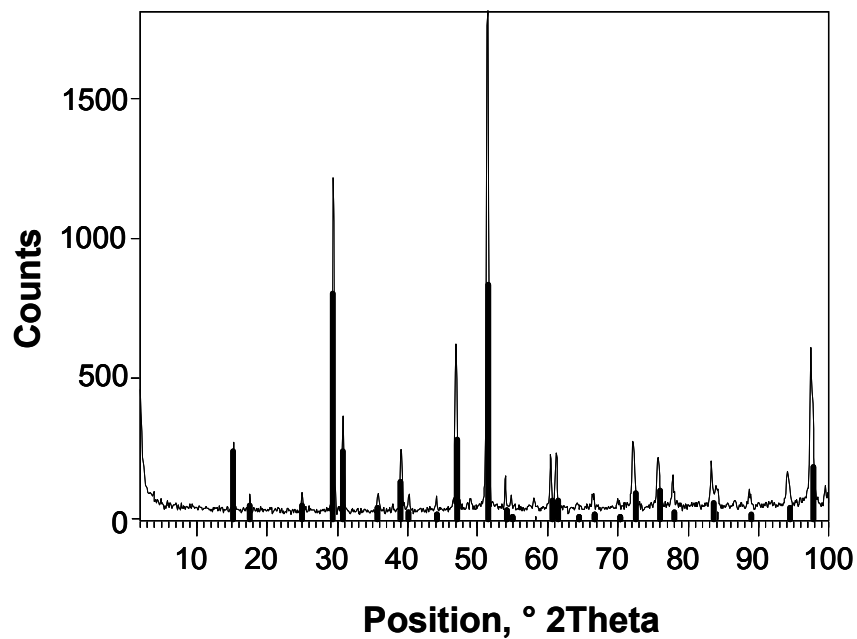


Figure A-2.8 – X-ray diffraction pattern of Voisey's Bay pentlandite used for contact angle measurements compared to the standard diffraction pattern for pentlandite (thick lines)

Appendix 3: Supernatant analysis

Supernatant was prepared using a mass fraction of 10 % solids of Thompson ultramafic ore (40 g of ore + 360 g of water) agitated using a magnetic stirrer. To determine the preparation time, samples of supernatant were taken at 1, 15, 24 and 48 hours and magnesium concentration was determined (Figure A-3.1). Equilibrium was reached after about 15 hours. The preparation time was then set to 24 hours.

Metals in the supernatant were analyzed by atomic absorption spectrometry in at least two different batches of supernatant (Table A-3.1). Sulphates were analyzed by precipitation with barium and turbidity measurements (Table A-3.2). Chlorides were analyzed by using the argentometric titration method (Table A-3.3).

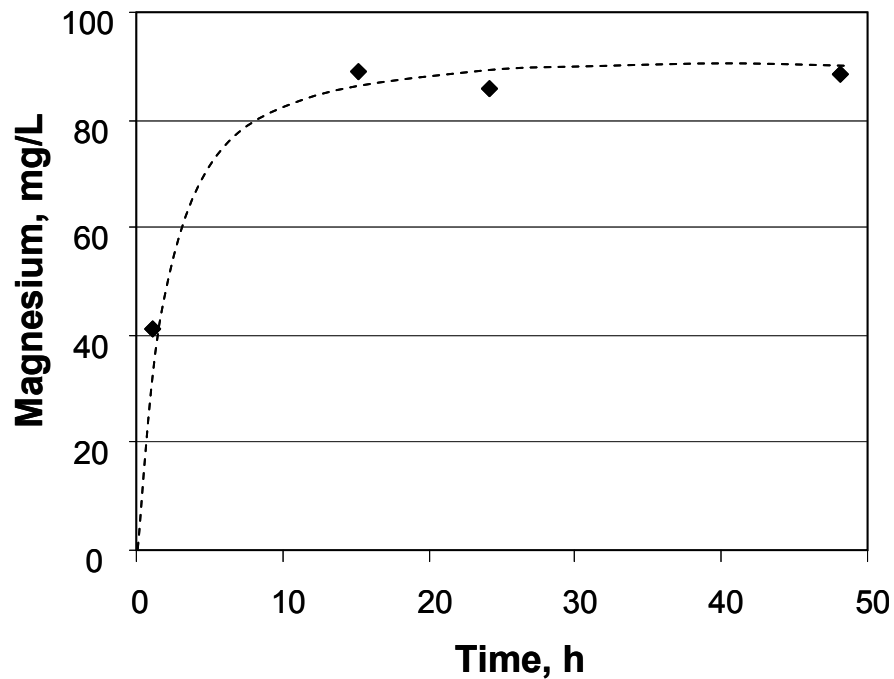


Figure A-3.1 – Magnesium in solution as a function of time in supernatant

Table A-3.1 – Metals in solution in supernatant

Element	Supernatant concentration, mg/L				
	1	2	3	Average	95 % CI
K	10.2	11.17	Missing	10.69	±0.97
Mg	88.3	81.86	95.34	88.5	±7.79
Na	8.09	4.76	4.94	5.93	±2.16
Cu	--	--	--	---	
Fe	--	--	--	---	
Ni	--	--	--	---	
Zn	--	--	--	---	
Ca	33.76	41.31	Missing	37.535	±7.55
Si	--	--	--	---	
Al	--	--	--	---	

Table A-3.2 – Sulphate concentration in supernatant calculated by turbidimetry

Supernatant	SO ₄ ²⁻ , mg/L	Average	95 % CI
1	12.72		
2	11.00	13.89	±3.21
3	16.92		

Table A-3.3 – Chloride concentration in supernatant calculated by argentometric titration

Supernatant	Cl ⁻ , mg/L	Average	95 % CI
1	343.87		
2	353.87	332.48	±33.28
3	299.70		

Appendix 4: Analysis of sulphate and chloride

A-4.1. Analysis of sulphate: turbidimetric method

Apparatus

- (a) Spectrophotometer at 420 nm, providing a light path of 4-5 cm
- (b) Magnetic stirrer (important to keep the speed of stirring constant for each batch of samples and standards; adjust to the maximum at which no splash occurs)
- (c) Stopwatch

Reagents

- (a) Conditioning reagent: Mix 50 mL glycerol (Anachemia) with a solution containing 30 mL conc HCl, 300 mL distilled water, 100 mL 95 % ethyl or isopropyl alcohol, and 75 g of NaCl.
- (b) Barium chloride, BaCl₂ (Anachemia), crystals sized for turbidimetric work. To ensure uniformity of results, construct a standard curve for each batch of BaCl₂ crystals.
- (c) Standard sulphate solution. Dissolve 147.9 mg anhydrous Na₂SO₄ (Fisher Scientific) in distilled water and dilute to 1000 mL.

Procedure

- Measure 100 mL of sample or a suitable portion made up to 100 mL into a 250 mL Erlenmeyer flask. Add 5 mL conditioning reagent and mix in stirring apparatus. While stirring, add a spoonful of BaCl₂ crystals (about 1 g) and begin timing immediately. Stir for 1 min at constant speed.
- Immediately after the stirring period has ended, pour solution into adsorption cell of photometer and measure turbidity at 30-s interval for 4 minutes. Consider turbidity to be the maximum reading obtained in the 4 minutes interval.

- Prepare calibration curve (Figure A-4.1). Estimate sulphate concentration by comparing turbidity with a calibration curve. Set photometer to zero using distilled water treated for sulphate analysis. Space standards at 5 mg/L in 5 mg/L increments over the 0 – 40 mg/L sulphate range.

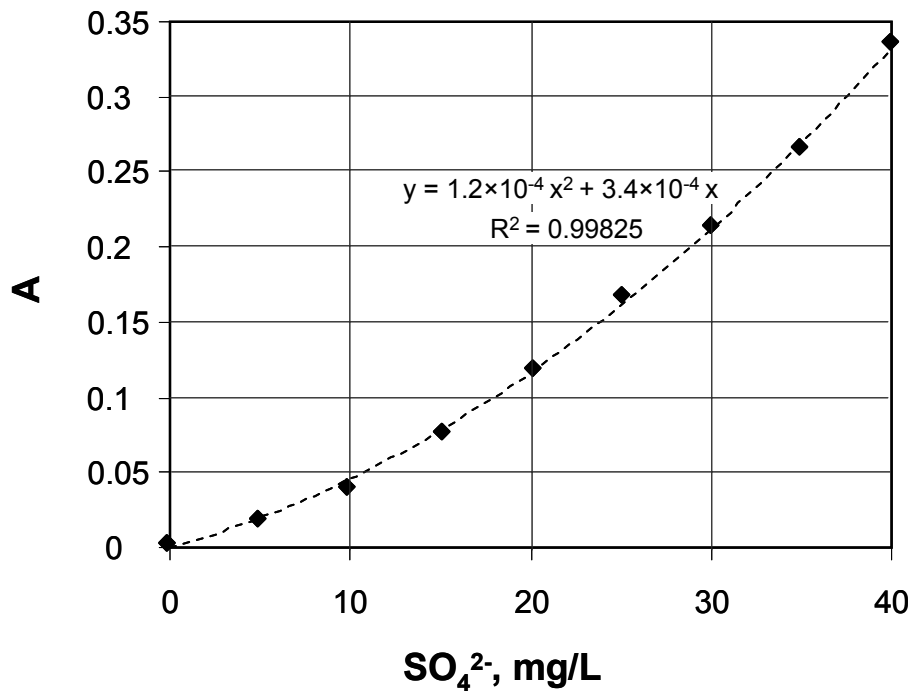


Figure A-4.1 – Calibration curve for determining sulphate concentration

A-4.2. Analysis of chloride: argentometric titration

Apparatus

- Erlenmeyer flask
- Buret

Reagents

- Potassium chromate indicator solution: dissolve 50 g K_2CrO_4 (Aldrich) in a little distilled water. Add $AgNO_3$ (A&C American Chemicals) solution until a definite red precipitate is formed. Let stand for 12 hr and dilute to 1 L with distilled water.
- Silver nitrate titrant. Dissolve 2.395 g $AgNO_3$ in distilled water and dilute to 1 L. Standardize against 0.0141 N NaCl.
- Standard sodium chloride. Dissolve 0.824 g NaCl (dried at $140^\circ C$) in distilled water and dilute to 1 L (1 mL is equal to 500 μg Cl^-).

Procedure

- Sample preparation: Use a 100 mL-sample or a suitable portion diluted to 100 mL. If the sample is highly coloured, add 3 mL $Al(OH)_3$ suspension, mix and let settle. If sulphide, sulphate or thiosulphate is present, add 1 mL H_2O_2 and stir for 1 min.
- Titration: Directly titrate samples in the pH range 7-10. Adjust sample pH to 7-10 with H_2SO_4 or NaOH if it is not in this range. Add 1 mL $KCrO_4$ indicator solution. Titrate with standard $AgNO_3$ titrant to a pinkish yellow end point. Be consistent in end point recognition.
- Standardize $AgNO_3$ titrant and establish reagent blank value by titration method outlined above. A blank of 0.2 to 0.3 mL is usual.

Calculation

$$mg \text{ } Cl^- / L = \frac{(A - B) \times N \times 35450}{mL \text{ sample}} \quad A-4.1$$

Where:

A = mL titration for sample

B = mL titration for blank

N = Normality of $AgNO_3$ titrant

Blank (distilled water)

Reference

Standard Methods for the Examination of Water and Wastewater (1981). American Public Health Association, American Water Works Association, Water Pollution Control Federation. A.E. Greenberg, J.J. Connors, D. Jenkins, M.A.H. Franson (Eds.) Washington, D.C., USA

Appendix 5: Contact angle measurement

Contact angle developed in the aqueous solution/mineral/air interface was calculated by the image analysis of photographic images using basic trigonometric functions.

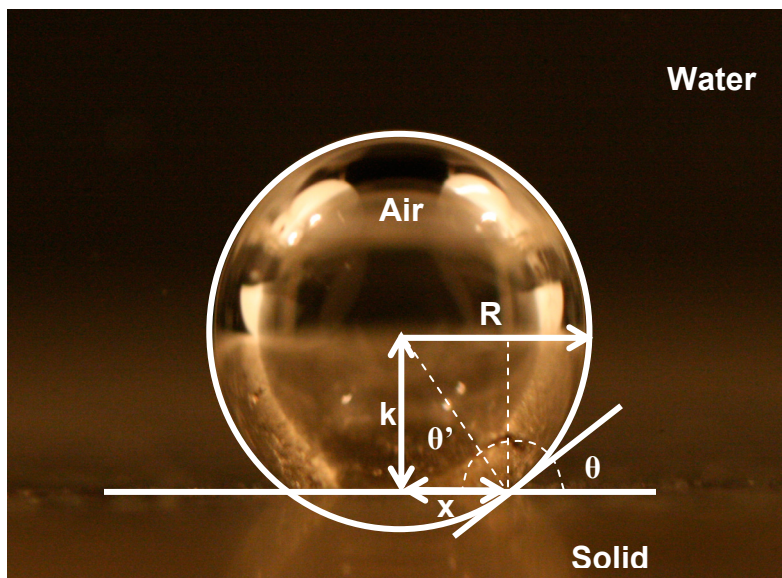


Figure A-5.1 – A bubble on a hydrophobic surface

Figure A-5.1 shows a typical image. To calculate the contact angle, θ , a circle is drawn around the bubble to intersect a line at the mineral surface. The radius of the bubble (R) and the distance from the centre to the mineral surface (k) are obtained from the picture. The distance x (the solid-water-air point) is obtained from Pythagoras' theorem:

$$x = \sqrt{R^2 - k^2} \quad \text{A-5.1}$$

The angle θ' is calculated by using:

$$\theta' = \arctan\left(\frac{k}{x}\right)\left(\frac{180}{\pi}\right) \quad \text{A-5.2}$$

Consequently, the contact angle is:

$$\theta = 90 - \theta' \quad \text{A-5.3}$$